



Poznan University of Medical Sciences
Poland

JMS *Journal of Medical Science*

previously *Nowiny Lekarskie*

Founded in 1889

2023
Vol. 92, No. 1

QUARTERLY

Indexed in:

DOAJ, Crossref, Google Scholar,
Polish Medical Bibliography, Index Copernicus,
Ministry of Education and Science

eISSN 2353-9801
ISSN 2353-9798
DOI: 10.20883/ISSN.2353-9798

www.jms.ump.edu.pl

EDITOR-IN-CHIEF

Jarosław Walkowiak

EDITORIAL BOARD

David Adamkin, USA
Sofio Bakhtadze, Georgia
Adrian Baranchuk, Canada
Paolo Castiglioni, Italy
Ewelina Chawłowska, Poland
Agata Czajka-Jakubowska, Poland
Jan Domaradzki, Poland
Piotr Eder, Poland
Michael Gekle, Germany
Krzysztof Greberski, Poland
Karl-Heinz Herzig, Finland
Mihai Ionac, Romania
Paweł P. Jagodziński, Poland
Jerzy Jankun, USA
Lucian Petru Jiga, Germany
Nataliya Kashirskaya, Russia
Berthold Koletzko, Germany
Stan Kutcher, Canada
Tadeusz Malinski, USA
Piotr Myśliwiec, Poland
Talgat Nurgozhin, Kazakhstan
Marcos A. Sanchez-Gonzalez, USA
Georg Schmidt, Germany
Mitsuko Seki, Japan
Puneet Sindhvani, USA
Elżbieta Skorupska, Poland
Rafał Staszewski, Poland
Tomasz Szczapa, Poland
Jerzy P. Szaflarski, USA
Sebastian Szubert, Poland
Tomasz Torliński, United Kingdom
Natallia Tsikhan, Belarus
Dariusz Walkowiak, Poland
Przemysław Zalewski, Poland
Ewa Zasadzka, Poland

ASSOCIATE EDITORS

Agnieszka Bienert
Ewa Mojs
Adrianna Mostowska
Nadia Sawicka-Gutaj

SECTION EDITORS

Jaromir Budzianowski – Pharmaceutical Sciences
Paweł P. Jagodziński – Basic Sciences
Joanna Twarowska-Hauser – Clinical Sciences

LANGUAGE EDITORS

Margarita Lianeri, Canada
Jacek Żywiczka, Poland

STATISTICAL EDITOR

Magdalena Roszak, Poland

SECRETARIAT ADDRESS

27/33 Szpitalna Street, 60-572 Poznań, Poland
phone: +48 618491432, fax: +48 618472685
e-mail: jms@ump.edu.pl
www.jms.ump.edu.pl

DISTRIBUTION AND SUBSCRIPTIONS

70 Bukowska Street, 60-812 Poznań, Poland
phone/fax: +48 618547414
e-mail: sprzedazwydawnictw@ump.edu.pl

PUBLISHER

Poznan University of Medical Sciences
10 Fredry Street, 61-701 Poznań, Poland
phone: +48 618546000, fax: +4861852 04 55
www.ump.edu.pl

© 2023 by respective Author(s). Production and hosting
by Journal of Medical Science (JMS)

This is an open access journal distributed under
the terms and conditions of the Creative Commons
Attribution (CC BY-NC) licence

eISSN 2353-9801

ISSN 2353-9798

DOI: 10.20883/ISSN.2353-9798

Publishing Manager: Grażyna Dromirecka

Technical Editor: Bartłomiej Wąsiel



WYDAWNICTWO NAUKOWE
UNIWERSYTETU MEDYCZNEGO
IM. KAROLA MARCINKOWSKIEGO
W POZNANIU

60-812 Poznań, ul. Bukowska 70
tel./fax: +48 618547151
www.wydawnictwo.ump.edu.pl

Ark. wyd. 9,5. Ark. druk. 10,0.
Zam. nr 187/23.

The Editorial Board kindly informs that since 2014 *Nowiny Lekarskie* has been renamed to *Journal of Medical Science*.

The renaming was caused by using English as the language of publications and by a wide range of other organisational changes. They were necessary to follow dynamic transformations on the publishing market. The Editors also wanted to improve the factual and publishing standard of the journal. We wish to assure our readers that we will continue the good tradition of *Nowiny Lekarskie*.

You are welcome to publish your basic, medical and pharmaceutical science articles in *Journal of Medical Science*.

Ethical guidelines

The Journal of Medical Science applies the ethical principles and procedures recommended by COPE (Committee on Conduct Ethics), contained in the Code of Conduct and Best Practice Guidelines for Journal Editors, Peer Reviewers and Authors available on the COPE website: <https://publicationethics.org/resources/guidelines>

CONTENTS

ORIGINAL PAPERS

Klaudia Gutowska, Zuzanna Wojdyńska, Sebastian Szewczyk, Justyna Milczarek-Banach, Piotr Miśkiewicz
Increased heart rhythm in response to high-dose intravenous methylprednisolone pulse therapy of moderate-to-severe Graves' orbitopathy. 7

Justyna Alicja Ber, Agnieszka Bienert, Paweł Sobczyński, Małgorzata Nowicka, Łukasz Żurański, Marcin Hołysz, Edmund Grześkowiak, Paweł Wiczling
Population pharmacokinetic-pharmacodynamic model of dexmedetomidine in elderly patients undergoing sedation after abdominal aortic surgery 15

Leonardo Campanelli
A simple model of human walking. 32

Krishna Kumar, Harison Gopalan, Jayalakshmi Jayaprakash
Formulation of a radiological scoring system to prognosticate patients with primary intracerebral haemorrhage 44

Kinga Skoracka, Ewelina Swora-Cwynar, Aleksandra Królczyk, Małgorzata Kałużna, Katarzyna Ziemnicka, Marek Ruchała, Agnieszka Dobrowolska, Iwona Krela-Kaźmierczak
Assessment of dietary habits among Polish women with Hashimoto's disease 52

Stefanos Chatzidakis, Demetris Lamnisos, Vasilis Constantinides, Angelos Kyriacou, Aliko Economides, Panayiotis A. Economides
Impact of autoimmune thyroiditis on primary hyperparathyroidism 63

Gina James Keorges
PD-L1 expression in Triple Negative Breast Cancer: a study of an Iraqi population 69

THOUSAND WORDS ABOUT...

Jacob van der Veer, Szymon Rzepczyk, Czesław Żaba
Keep an eye on the crime – a new look at the forensic use of post-mortem eye examination to estimate time of death 74

Instructions for Authors 79

Increased heart rhythm in response to high-dose intravenous methylprednisolone pulse therapy of moderate-to-severe Graves' orbitopathy

Klaudia Gutowska

Student's Scientific Circle "Endocrinus", Department of Internal Medicine and Endocrinology, Medical University of Warsaw, Warsaw, Poland

<https://orcid.org/0000-0002-1291-0920>

Zuzanna Wojdyńska

Student's Scientific Circle "Endocrinus", Department of Internal Medicine and Endocrinology, Medical University of Warsaw, Warsaw, Poland

<https://orcid.org/0000-0003-2034-7397>

Sebastian Szewczyk

Student's Scientific Circle "Endocrinus", Department of Internal Medicine and Endocrinology, Medical University of Warsaw, Warsaw, Poland

<https://orcid.org/0000-0001-5511-5823>

Justyna Milczarek-Banach

Department of Internal Medicine and Endocrinology, Medical University of Warsaw, Warsaw, Poland

<https://orcid.org/0000-0001-6548-6118>

Piotr Miśkiewicz

Department of Internal Medicine and Endocrinology, Medical University of Warsaw, Warsaw, Poland

<https://orcid.org/0000-0003-4015-6491>

Corresponding author: piotr.miskiewicz@wum.edu.pl

DOI: <https://doi.org/10.20883/medical.e774>

Keywords: Graves' ophthalmopathy, Graves' disease, glucocorticoids, heart rate

Received: 2022-11-16

Accepted: 2022-12-23

Published: 2023-02-09

How to Cite: Gutowska K, Wojdyńska Z, Szewczyk S, Milczarek-Banach J, Miśkiewicz P. Increased heart rhythm in response to high-dose intravenous methylprednisolone pulse therapy of moderate-to-severe Graves' orbitopathy. *Journal of Medical Science*. 2023;92(1):e774. doi:10.20883/medical.e774



© 2023 by the author(s). This is an open access article distributed under the terms and conditions of the Creative Commons Attribution (CC BY-NC) license. Published by Poznan University of Medical Sciences

ABSTRACT

Background. Intravenous glucocorticoids pulses administration is the main therapeutic option in the treatment of Graves' orbitopathy. Such therapy could relate to the multiple adverse effects. The aim of the study is evaluation the influence of intravenous methylprednisolone (IVMP) pulse therapy on the heart rhythm (HR) changes in patients with active, moderate-to-severe Graves' Orbitopathy (GO).

Methods. We studied 20 patients with moderate-to-severe GO. All patients received 12 IVMP pulses (6 x 500 mg plus 6 x 250 mg) at equal time intervals in a weekly schedule. We performed Holter ECG monitoring for 3 consecutive days (the day before, the day of IVMP and day after IVMP) to monitor HR and arrhythmias. We compared changes in HR between these 3 days and set time interval when the alteration was significant. This evaluation was performed during the 1st, 6th and 12th IVMP pulse.

Results. Increased HR, in comparison with the day before, was registered on the day of IVMP administration. The most significant increase in HR started 5 hours (h) after a pulse administration and lasted 12 h. There were no significant differences in HR between the day before and the day after IVMP. We did not notice any major adverse cardiac events including severe arrhythmias.

Conclusions. IVMP therapy is associated with increased HR, that occurs a few hours after infusion, lasts several hours and is transient.

Introduction

High doses of intravenous glucocorticoids (GCs) are commonly used as a treatment for many autoimmune and inflammatory disorders. According to the European Group on Graves' Orbitopathy (EUGOGO) guidelines, intravenous methylprednisolone (IVMP) is an accepted first-line agent for active, moderate-to-severe and very severe Graves' orbitopathy (GO) [1]. This treatment is proven to be more efficient and safer than oral GCs. For active, moderate-to-severe GO it is recommended to treat patients with twenty IVMP pulses once weekly for 12 weeks. In the first 6 pulses, the dose is 0.5 g IVMP and for the next 6 weeks, it is reduced to 0.25 g IVMP.

However, some patients may experience adverse cardiovascular effects during the administration of iv. GCs, which in rare cases may even be fatal. There are limited data, mostly obtained from case reports, reporting the occurrence of venous thromboembolism, cardiac arrhythmias, acute myocardial infarction or acute heart failure [2]. Increased heart rhythm (HR) has drawn our attention as a possible adverse effect correlated with IVMP [3, 4]. During this study, we performed 72-hours of Holter monitoring to evaluate the impact of IVMP on patients with moderate-to-severe GO, concerning HR changes and arrhythmias.

Material and Methods

Study population

This observational study was conducted at the Department of Internal Medicine and Endocrinology at the Medical University of Warsaw between 2011 and 2015. 20 consecutive patients (14 women and 6 men) with active, moderate-to-severe GO treated with IVMP pulse therapy following EUGOGO, were enrolled in the study. The inclusion criteria were: (1) age \geq 18 years; (2) euthyroidism (patients with hyperthyroidism treated with antithyroid drugs, after radiotherapy/surgical treatment on levothyroxine (L-T4) therapy, if necessary, with euthyroid Graves' disease, or with Hashimoto's disease on L-T4 therapy; and (3) completion of 12 IVMP pulses. Patients with previous GCs treatment in the last 6 months were excluded from the research. Clinical characteristics of patients are shown in **Table 1**.

Ethical statements

This research was approved by the bioethics committee at the Medical University of Warsaw, Poland. Each patient submitted written consent before the study.

Table 1. Clinical characteristics of the patient population.

| | |
|-----------------------------------|----------------|
| Male, n (%) | 6 (30) |
| Female, n (%) | 14 (70) |
| Age, years (mean \pm SD) | 51 \pm 11 |
| Etiology of GO | |
| Graves' disease, n (%) | 15 (75) |
| Hashimoto's disease, n (%) | 5 (25) |
| Smoking | |
| Current smokers, n (%) | 10 (50) |
| Past smokers, n (%) | 7 (35) |
| Non-smokers, n (%) | 3 (15) |
| Comorbidities | |
| Hypertension, n (%) | 9 (45) |
| Medications | |
| Beta-blockers, n (%) | 7 (35) |
| ACEI, n (%) | 6 (30) |
| ARB, n (%) | 1 (5) |
| Calcium-blockers, n (%) | 5 (25) |
| Statins, n (%) | 5 (25) |
| Diuretics, n (%) | 1 (5) |
| L-thyroxine, n (%) | 14 (70) |
| Antithyroid drugs, n (%) | 7 (35) |
| Laboratory measurements | |
| TSH, (range: 0.27–4.2 μ U/mL) | 2.2 \pm 1.5 |
| ft4, (range: 12–22 pmol/L) | 16.6 \pm 3.7 |
| TBII, (N < 1.73 IU/L) | 5.9 \pm 4.7 |

GO – Graves' Orbitopathy; AITD – Autoimmune Thyroid Disorder; ACEI – Angiotensin Converting Enzyme Inhibitors; ARB – Angiotensin Receptor Blockers; TSH – thyreotropin; ft4 – free thyroxine; TBII – thyreotropin binding inhibitor immunoglobulin; Laboratory tests (TSH, ft4, TBII) are shown as a mean value \pm standard deviation (SD).

Study design and 24-hour Holter ECG monitoring

All participants received IVMP pulses following EUGOGO recommendations (cumulative dose of methylprednisolone 4.5 g, treatment duration 12 weeks in once-weekly iv. pulses, each pulse in the first 6 weeks 0.5 g MP and next 6 weeks 0.25 g MP). Each pulse was administered at the same time interval (10–12 a.m.). The clinical status of patients was evaluated before each pulse, including blood pressure monitoring, glucose level monitoring and symptoms of infection.

A 24-hour Holter ECG monitoring was carried out with EXCEL 2 by Medilog Oxford and ROZINN by Margot Medical. HR was measured hourly for 3 consecutive days (the day before, the day of IVMP and the day after IVMP) during 1st, 6th and 12th

IVMP pulse. For every pulse, we performed 3 analyses comparing mean, minimal and maximal circadian HR between (1) the day before and the day of IVMP, (2) the day of IVMP and the day after IVMP, (3) the day before and the day after IVMP. To define the exact time of the most significant difference between HR we compared mean, minimal and maximal HR from corresponding hours between the day before and the day of IVMP. We set the time interval of the first and the last hour of the day when a significant difference in HR between compared days was observed. For this period, the average HR for each patient was calculated. We performed a statistical analysis comparing average HR between the day before IVMP and the day of IVMP, for the defined time interval. Lastly, we searched for severe arrhythmias in 24-hour Holter ECG monitoring.

Statistical Analysis

Statistical analysis was performed using version 13.3 Statistica software. Continuous variables were demonstrated as mean \pm standard deviation (SD) or median values (lower quartile-upper quartile). Categorical data were presented as numbers (n) or percentages (%). Comparisons between mean, maximal and minimal circadian HR were assessed before and after selected IVMP pulses using a non-parametric Wilcoxon signed-rank test. Results including p-value <0.05 were considered statistically significant.

Results

Increase in mean, minimal and maximal circadian HR on the day of IVMP administration compared to the day before was found in all analyzed pulses ($p < 0.001$ for 1st, $p < 0.001$ for 6th, $p < 0.005$ for 12th) (see **Table 2**). There were no statistically significant differences observed in mean, minimal and maximal circadian HR, including all pulses between the day before and the day after IVMP infusion. Mean HR from corresponding hours was compared between the day before and the day of IVMP. Significant increase in HR, concomitantly in all pulses, was noticed for the first time at 5 p.m. This significant change in HR, between the day before and the day of IVMP was recurrent at every hour until 5 a.m. On this basis, precise timeline representing a significant change in heart rate starts on the day of IVMP at 5 p.m. and lasts for 12-h, until 5 a.m. the following day. During this period, a significant increase in mean, minimal and maximal HR was found between the day before and the day of IVMP administration (see **Table 3**). This increase in median HR was 18% for 1st and 6th pulse and 17% for 12th pulse. In the group with beta-blockers (35% of patients) we observed the same trend of changes in HR. None of our patients developed major adverse cardiovascular events or serious heart rhythm disturbances. However, we observed some mild and transient arrhyth-

Table 2. Changes in mean, maximal and minimal circadian heart rhythm on the day before, the day with and the day after intravenous methylprednisolone (IVMP) administration during 1st, 6th, 12th pulse.

| IVMP Pulse (circadian) | Day Before Pulse Median (Q1-Q3, n/min) | Day With Pulse Median (Q1-Q3, n/min) | Day After Pulse Median (Q1-Q3, n/min) |
|------------------------|--|--------------------------------------|---------------------------------------|
| Mean HR | | | |
| 1st | 77 (69-80) | 82 (80-88) | 78 (70-86) |
| 6th | 76 (68-77) | 86 (80-88) | 81 (74-87) |
| 12th | 80 (73-83) | 85 (79-88) | 76 (70-83) |
| Maximal HR | | | |
| 1st | 90 (82-94) | 96 (92-102) | 93 (82-100) |
| 6th | 89 (82-91) | 99 (93-103) | 94 (84-99) |
| 12th | 93 (83-96) | 98 (91-102) | 89 (82-97) |
| Minimal HR | | | |
| 1st | 62 (57-66) | 69 (67-72) | 65 (56-72) |
| 6th | 62 (56-64) | 70 (67-75) | 69 (61-74) |
| 12th | 67 (61-70) | 70 (67-74) | 65 (58-70) |

HR: average heart rhythm [n/min], Q1: lower quartile, Q3: upper quartile.

mias during ECG monitoring, such as: supraventricular extrasystoles, ventricular extrasystoles, supraventricular tachycardia, supraventricular and ventricular pairs. None of patients suffered

from atrial fibrillation. Some of patients reported feeling of tachycardia after IVMP infusion which was without any additional side effect, and they described as a mild disorder.

Table 3. Changes in mean heart rhythm during 12-h time interval (5 p.m.–5 a.m.) on the day before and the day with intravenous methylprednisolone (IVMP) during 1st, 6th, 12th pulse. P-value was assessed using a non-parametric Wilcoxon signed-rank test.

| IVMP Pulse (5 p.m.–5 a.m.) | Day Before Pulse Median (Q1–Q3, n/min) | Day With Pulse Median (Q1–Q3, n/min) | p-value |
|-------------------------------|---|---|---------|
| Mean HR | | | |
| 1st | 69 (66–76) | 82 (79–88) | <0.001 |
| 6th | 69 (66–75) | 82 (79–90) | <0.001 |
| 12th | 73 (68–80) | 83 (78–88) | <0.002 |
| Maximal HR | | | |
| 1st | 82 (77–90) | 96 (91–101) | <0.001 |
| 6th | 83 (76–88) | 97 (93–103) | <0.001 |
| 12th | 83 (77–92) | 96 (90–102) | <0.005 |
| Minimal HR | | | |
| 1st | 57 (56–63) | 70 (67–75) | <0.001 |
| 6th | 57 (56–62) | 68 (67–76) | <0.001 |
| 12th | 64 (60–68) | 70 (65–75) | <0.002 |

HR: average heart rhythm [n/min], Q1: lower quartile, Q3: upper quartile

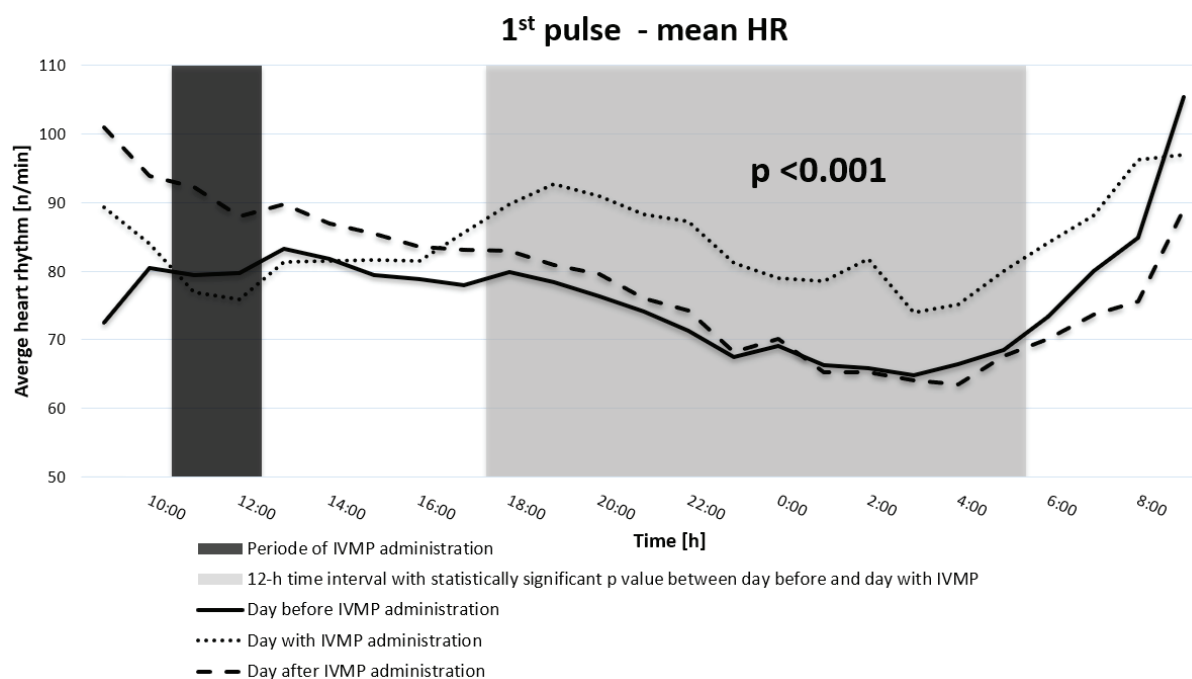


Figure 1. Average HR variabilities within the day before, the day of IVMP and the day after 1st IMVP administration. P-value shows mean HR comparison for a 12-h time interval (5 p.m.–5 a.m.) between the day before and the day of drug infusion. P-value was assessed using a non-parametric Wilcoxon signed-rank test.

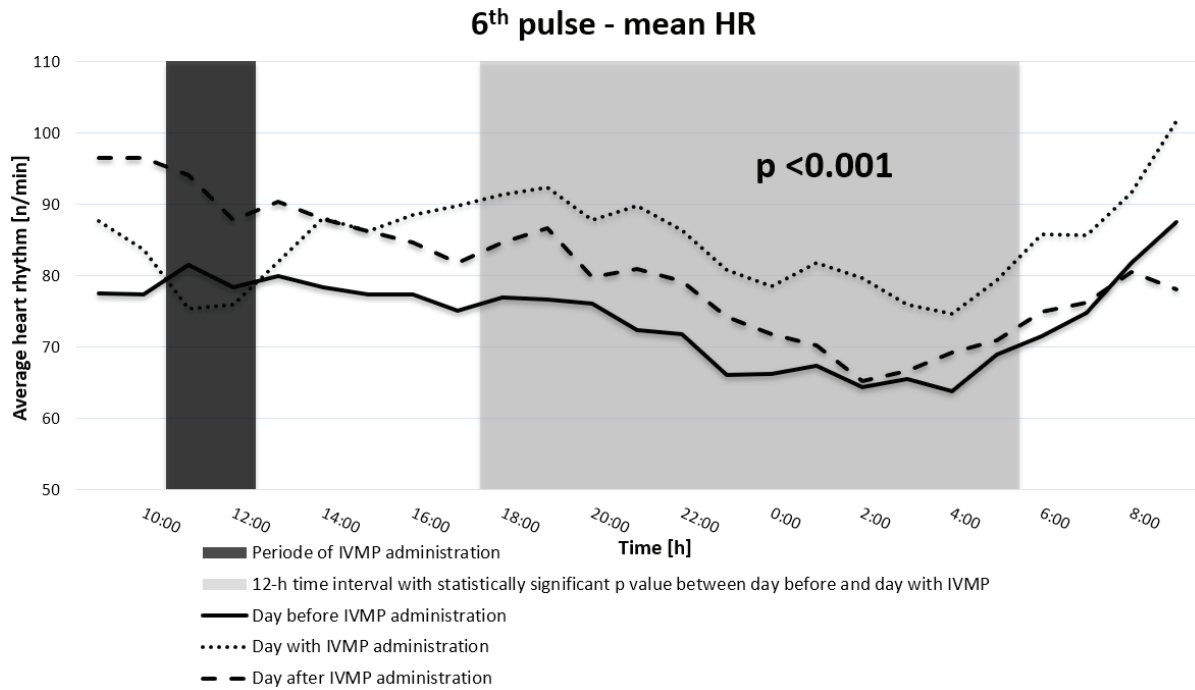


Figure 2. Average HR variabilities within the day before, the day of IVMP and the day after 6th IMVP administration. P-value shows mean HR comparison for a 12-h time interval (5 p.m. – 5 a.m.) between the day before and the day of drug infusion. P-value was assessed using a non-parametric Wilcoxon signed-rank test.

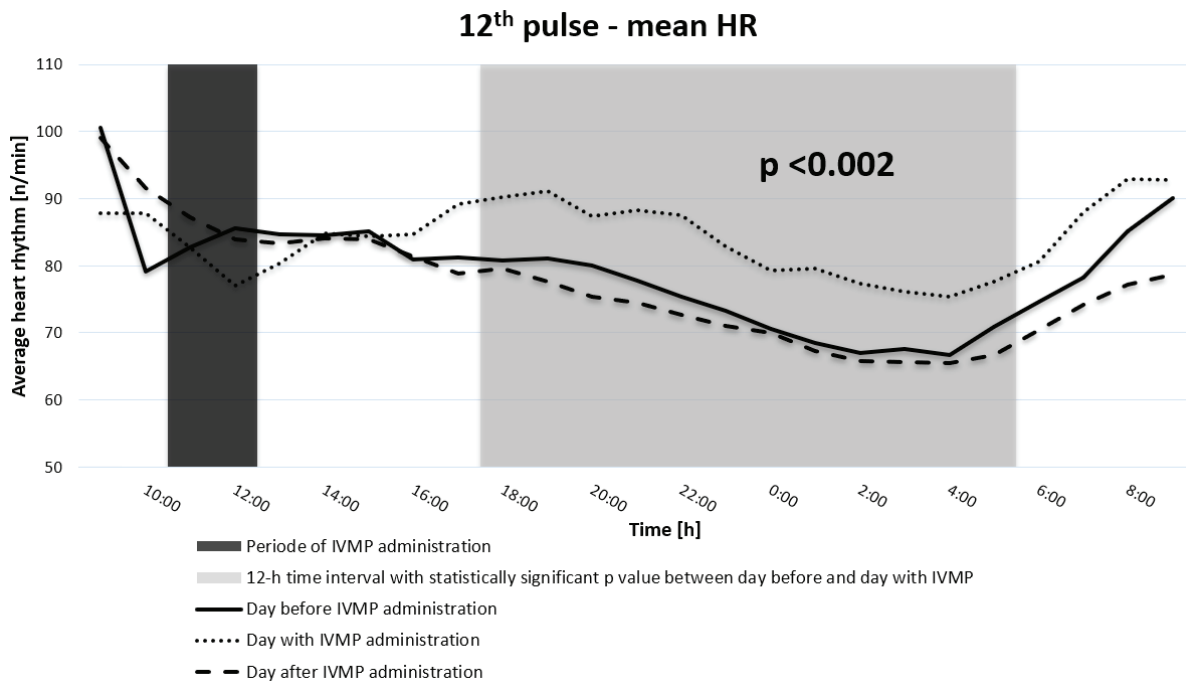


Figure 3. Average HR variabilities within the day before, the day of IVMP and the day after 12th IMVP administration. P-value shows mean HR comparison for a 12-h time interval (5 p.m. – 5 a.m.) between the day before and the day of drug infusion. P-value was assessed using a non-parametric Wilcoxon signed-rank test.

Discussion

GO is the main extrathyroidal manifestation of Graves' disease, though severe forms are rare [1]. IVMP is a well-established first-line treatment for moderate-to-severe active GO with better response rate and tolerance than oral GCs. However, there are reports of serious adverse effects associated with this therapy [2, 5], Cardiovascular disorders and various arrhythmias after corticosteroid pulse therapy have been observed in several diseases [2, 5–7].

Most commonly, cardiac arrhythmias described as related to IVMP were ventricular tachycardia [8], bradycardia [9] and atrial fibrillation [10–12]. However, there were also described cases of cardiovascular collapse [13], cardio-circulatory arrest [14] and sudden death [15]. A range of these serious cardiac arrhythmias can be observed shortly after methylprednisolone (MP) infusion [3] as well as during late hours after treatment [8, 9]. Although it seems that proarrhythmic impact of IVMP depends on the dose and the type of used drug, the mechanism remains unclear.

In Miśkiewicz et al. [16] study the impact of IVMP on blood pressure (BP) and N-terminal pro-brain natriuretic peptide level was investigated. Increase in maximal systolic BP and mean nocturnal BP was observed with a higher prevalence of non-dipping BP profile. The results suggested a cumulative effect of IVMP on BP with compensatory higher brain natriuretic peptide.

In the presented study, HR was significantly higher on the day of IVMP administration in comparison to the day before and the day after infusion. Besides, the change of HR was significantly greater 5-h after IVMP infusion, in the 12-h time interval (5 p.m.–5 a.m.) with an average increase of 20% for all pulses. Our results are consistent with previous reports by M. Pishgahi et al. [3] and Fujimoto et al. [4] in which significant increase in HR after pulse therapy was detected, including ventricular tachycardia in the second study. However, ECG monitoring could not accurately elucidate changes in cardiac rhythm. Both authors suggested that these dysrhythmias might be an effect of acute shift of potassium across the cell's membrane. Glucocorticoids, like methylprednisolone, can alter electrolyte levels, particularly potassium and sodium, through their

activation of the mineralocorticoid receptor (MR). This leads to changes in sodium reabsorption and potassium excretion, which help regulate salt concentration in the body. While methylprednisolone has minimal mineralocorticoid activity, high doses of the drug may bind to the mineralocorticoid receptor in the collecting duct and increase these effects [17]. Low potassium levels (hypokalemia) can affect the resting membrane potential of heart cells and reduce repolarization reserve, increasing the risk of tachyarrhythmias such as Torsade's de pointes and polymorphic VT, which can progress to ventricular fibrillation and sudden cardiac death [18]. Although the blood levels of sodium and potassium were not measured in the study, an increase in heart rate observed in the study supports the hypothesis that the intravenous use of methylprednisolone may be contributing to these effects through its hypokalemic effects.

Bradyarrhythmias were not observed in our study. Our findings are inconsistent with results obtained by Tvede et al. [9], who noted a one-week decline in heart rhythm in all 5 patients after they received MP. Similar report by Yong et al. [19] presented significant decrease in mean HR during the 1.5-h time interval after IVMP administration with no cumulative effect. What is also important in our study, 35% of analyzed patients were exposed to beta-blockers. This group was not statistically different in the HR changes and incidence of cardiac arrhythmias.

Our report indicates that IVMP therapy is associated with increased HR after each pulse. The change in HR is transient and last only on the day of IVMP infusion. None of our patients developed major cardiovascular adverse events or serious heart rhythm disturbances. Most of the patients reported feeling of tachycardia after IVMP infusion but was described as a mild side effect. However, elderly or obese patients with cardiovascular comorbidities may have a higher risk of developing cardiac adverse events [6]. We did not observe difference between group with and without betablockers, but our patients were without severe cardiac diseases. In the group of patients with higher risk of cardiac exacerbation, routine betablocker therapy should be considered with cardiac rhythm monitoring. The mechanism of influence of IVMP is not clear and needs further investigation.

Limitations

This study has some limitations. There was a small group of patients and our trial did not investigate the underlying cause of the increased heart rhythm after IVMP.

Conclusions

Therapy with IVMP is associated with increased HR which occurs a few hours after infusion. Changes in heart rate (about 20%) last several hours, are transient and do not lead to any adverse cardiovascular events. Future research needs to be performed to provide greater insight into the correlation between IVMP and HR.

Acknowledgements

Conflict of interest statement

The authors declare no conflict of interest.

Funding sources

There are no sources of funding to declare.

Data availability statement

The data that support the findings of this study are available from the corresponding author upon reasonable request.

References

1. Bartalena L, Kahaly GJ, Baldeschi L, Dayan CM, Eckstein A, Marcocci C, Marinò M, Vaidya B, Wiersinga WM; EUGOGO †. The 2021 European Group on Graves' orbitopathy (EUGOGO) clinical practice guidelines for the medical management of Graves' orbitopathy. *Eur J Endocrinol*. 2021 Aug 27;185(4):G43-G67. doi: 10.1530/EJE-21-0479. PMID: 34297684.
2. Miśkiewicz P, Kryczka A, Ambroziak U, Rutkowska B, Głównyńska R, Opolski G, Kahaly G, Bednarczuk T. Is high dose intravenous methylprednisolone pulse therapy in patients with Graves' orbitopathy safe? *Endokrynol Pol*. 2014;65(5):402-13. doi: 10.5603/EP.2014.0056. PMID: 25301492.
3. Pishgahi M, Dadkhahfar S, Robati RM, Kheradmand Z, Shahidi-Dadras M, Zargari O, Elpern DJ. Electrocardiographic changes after high-dose corticosteroid pulse therapy in pemphigus patients. *J Dermatolog Treat*. 2018 Dec;29(8):802-805. doi: 10.1080/09546634.2018.1466980. Epub. 2018 May 7. PMID: 29668335.
4. Fujimoto S, Kondoh H, Yamamoto Y, Hisanaga S, Tanaka K. Holter electrocardiogram monitoring in nephrotic patients during methylprednisolone pulse therapy. *Am J Nephrol*. 1990;10(3):231-6. doi: 10.1159/000168087. PMID: 1696428.
5. Marcocci C, Watt T, Altea MA, Rasmussen AK, Feldt-Rasmussen U, Orgiazzi J, Bartalena L; European Group of Graves' Orbitopathy. Fatal and non-fatal adverse events of glucocorticoid therapy for Graves' orbitopathy: a questionnaire survey among members of the European Thyroid Association. *Eur J Endocrinol*. 2012 Feb;166(2):247-53. doi: 10.1530/EJE-11-0779. Epub. 2011 Nov 4. PMID: 22058081.
6. Vasheghani-Farahani A, Sahraian MA, Darabi L, Aghsaie A, Minagar A. Incidence of various cardiac arrhythmias and conduction disturbances due to high dose intravenous methylprednisolone in patients with multiple sclerosis. *J Neurol Sci*. 2011 Oct 15;309(1-2):75-8. doi: 10.1016/j.jns.2011.07.018. Epub. 2011 Aug 9. PMID: 21831398.
7. Belmonte MA, Cequiere A, Roig-Escofet D. Severe ventricular arrhythmia after methylprednisolone pulse therapy in rheumatoid arthritis. *J Rheumatol [Internet]*. 1986 Apr;13(2):477-9. Available from: <http://www.ncbi.nlm.nih.gov/pubmed/3723518>.
8. Kumari R, Uppal SS. First report of supraventricular tachycardia after intravenous pulse methylprednisolone therapy, with a brief review of the literature. *Rheumatol Int*. 2005 Nov;26(1):70-3. doi: 10.1007/s00296-005-0589-7. Epub. 2005 Feb 23. PMID: 15726372.
9. Tvede N, Nielsen LP, Andersen V. Bradycardia after high-dose intravenous methylprednisolone therapy. *Scand J Rheumatol*. 1986;15(3):302-4. doi: 10.3109/03009748609092597. PMID: 3798047.
10. McLuckie AE, Savage RW. Atrial fibrillation following pulse methylprednisolone therapy in an adult. *Chest*. 1993 Aug;104(2):622-3. doi: 10.1378/chest.104.2.622. PMID: 8339660.
11. Reddy V, Taha W, Kundumadam S, Khan M. Atrial fibrillation and hyperthyroidism: A literature review. *Indian Heart J*. 2017 Jul-Aug;69(4):545-550. doi: 10.1016/j.ihj.2017.07.004. Epub. 2017 Jul 5. PMID: 28822529; PMCID: PMC5560908.
12. Yamamura K, Ohga S, Nishiyama K, Doi T, Tsutsumi Y, Ikeda K, Fujishima A, Takada H, Hara T. Recurrent atrial fibrillation after high-dose methylprednisolone therapy in a girl with lupus-associated hemophagocytic syndrome. *Lupus*. 2011 Jul;20(8):871-5. doi: 10.1177/0961203310392429. Epub. 2011 Mar 17. PMID: 21415254.
13. Cohen IJ. Cardiovascular collapse after high dose methylprednisolone. *Pediatr Hematol Oncol*. 1993 Jul-Sep;10(3):v-vii. doi: 10.3109/08880019309029486. PMID: 8217535.
14. Schult M, Löhmann D, Knitsch W, Kuse ER, Nashan B. Recurrent cardiocirculatory arrest after kidney transplantation related to intravenous methylprednisolone bolus therapy. *Transplantation*. 1999 Jun 15;67(11):1497-8. doi: 10.1097/00007890-199906150-00022. PMID: 10385096.
15. Bocanegra TS, Castañeda MO, Espinoza LR, Vasey FB, Germain BF. Sudden death after methylprednisolone pulse therapy. *Ann Intern Med*. 1981 Jul;95(1):122. doi: 10.7326/0003-4819-95-1-122_1. PMID: 7247116.
16. Miskiewicz P, Milczarek-Banach J, Bednarczuk T, Opolski G, Głównyńska R. Blood Pressure Profile and N-Terminal-proBNP Dynamics in Response to

- Intravenous Methylprednisolone Pulse Therapy of Severe Graves' Orbitopathy. *Int J Mol Sci.* 2018 Sep 26;19(10):2918. doi: 10.3390/ijms19102918. PMID: 30261581; PMCID: PMC6213036.
17. Liu D, Ahmet A, Ward L, Krishnamoorthy P, Mandelcorn ED, Leigh R, Brown JP, Cohen A, Kim H. A practical guide to the monitoring and management of the complications of systemic corticosteroid therapy. *Allergy Asthma Clin Immunol.* 2013 Aug 15;9(1):30. doi: 10.1186/1710-1492-9-30. PMID: 23947590; PMCID: PMC3765115.
18. Weiss JN, Qu Z, Shivkumar K. Electrophysiology of Hypokalemia and Hyperkalemia. *Circ Arrhythm Electrophysiol.* 2017 Mar;10(3):e004667. doi: 10.1161/CIRCEP.116.004667. PMID: 28314851; PMCID: PMC5399982.
19. Young SM, Lim AYN, Lang SS, Lee KO, Sundar G. Efficacy and safety of pulsed intravenous methylprednisolone in early active thyroid eye disease. *Orbit.* 2019 Oct;38(5):362-369. doi: 10.1080/01676830.2018.1553189. Epub. 2018 Dec 12. PMID: 30540214.

Population pharmacokinetic-pharmacodynamic model of dexmedetomidine in elderly patients undergoing sedation after abdominal aortic surgery

Justyna Alicja Ber

Department of Clinical Pharmacy and Biopharmacy,
Poznan University of Medical Sciences, Poland

 <https://orcid.org/0000-0003-2270-4386>

Corresponding author: justyna.ber@ump.edu.pl

Agnieszka Bienert

Department of Clinical Pharmacy and Biopharmacy,
Poznan University of Medical Sciences, Poland

 <https://orcid.org/0000-0001-7272-5738>

Paweł Sobczyński

Department of Anaesthetics and Intensive Therapy,
The Lord's Transfiguration University Hospital,
Poznan University of Medical Sciences, Poland

 <https://orcid.org/0000-0002-6447-8615>

Małgorzata Nowicka

Department of Anaesthetics and Intensive Therapy,
The Lord's Transfiguration University Hospital,
Poznan University of Medical Sciences, Poland

 —

Łukasz Żurański

Department of Anaesthetics and Intensive Therapy,
The Lord's Transfiguration University Hospital,
Poznan University of Medical Sciences, Poland

 <https://orcid.org/0000-0003-3343-8765>

Marcin Hołysz

Department of Biochemistry and Molecular Biology,
Poznan University of Medical Sciences, Poland

 <https://orcid.org/0000-0003-2505-3582>

Edmund Grześkowiak

Department of Clinical Pharmacy and Biopharmacy,
Poznan University of Medical Sciences, Poland

 <https://orcid.org/0000-0002-9938-6729>

Paweł Wiczling

Department of Biopharmacy and Pharmacodynamics,
Medical University of Gdańsk, Poland

 <https://orcid.org/0000-0002-2878-3161>

 DOI: <https://doi.org/10.20883/medical.e770>

Keywords: pharmacodynamics,
dexmedetomidine, intensive care units,
geriatrics, analgesedation

Received: 2022-11-04

Accepted: 2022-12-28

Published: 2023-02-20

How to Cite: Ber JA, Bienert A, Sobczyński P, Nowicka M, Żurański Łukasz, Hołysz M, Grześkowiak E, Wiczling P. Population pharmacokinetic-pharmacodynamic model of dexmedetomidine in elderly patients undergoing sedation after abdominal aortic surgery. Journal of Medical Science. 2023;92(1):e770. doi:10.20883/medical.e770



© 2023 by the author(s). This is an open access article distributed under the terms and conditions of the Creative Commons Attribution (CC BY-NC) license. Published by Poznan University of Medical Sciences

ABSTRACT

Background. Dexmedetomidine (DEX) is a widely used sedative agent for treating post-surgery patients. It also acts on hemodynamic parameters like heart rate or cardiac output. This study aimed to develop a pharmacokinetic-pharmacodynamic (PK/PD) model of DEX using bispectral index (BIS) and cardiac output (CO) as a response.

Methodology and results. 21 mechanically ventilated elderly cardiac patients undergoing abdominal aortic surgery were enrolled in the study. DEX was given to maintain moderate or deep sedation. Genotypes

of *ADR2A'55* were identified using real-time PCR-HRM. Data were analyzed using nonlinear mixed-effect modelling. A two-compartment model described DEX pharmacokinetics. The sigmoid E_{max} and linear models were used to describe BIS and CO measurements. The typical value of EC_{50} for DEX effects on BIS was 3.62 ng/ml, and the slope between CO and DEX concentrations was 0.819 (L/min)/(ng/ml). We were unable to show the effects of considered covariates on DEX pharmacodynamics.

Conclusions. We proposed the PK/PD model of DEX to understand better the BIS and CO changes observed after surgery. The measured CI values were in the reference range showing that the used doses of DEX ensured stable cardiac function in the studied patients.

Introduction

Dexmedetomidine (DEX) is a highly selective α_2 -agonist with anxiolytic, analgesic, and sedative effects [1]. It binds to α_{2A} -adrenergic receptors in locus coeruleus that causes sedation similar to natural sleep [2]. DEX is used in all age groups in perioperative, procedural and ICU sedation, premedication, withdrawal syndrome treatment, delirium, or as an adjuvant to anaesthesia [3]. It is also recommended to achieve minimal and moderate sedation whenever a patient state does not require deep sedation [4]. Its use is also associated with an analgesic-sparing effect [5]. DEX causes a dose-dependent decrease in heart rate (HR), cardiac output (CO), systolic (SBP), and diastolic blood pressure (DBP) [6]. However, a high dose and a quick application of DEX can increase blood pressure [7]. DEX does not cause respiratory depression in an approved dosage range ($0.2\text{--}1.4\ \mu\text{g}\cdot\text{kg}^{-1}\cdot\text{h}^{-1}$) contrary to other sedative drugs [8]. Another advantage of this drug is the possibility of contact with a patient during drug administration, which is compatible with current guidelines [9].

DEX, for the first time, was approved for sedation for continuous infusion not exceeding 24 hours, in the range of $0.2\text{--}0.7\ \mu\text{g}\cdot\text{kg}^{-1}\cdot\text{h}^{-1}$ (Precedex[®]). The producer specified a therapeutic concentration of this drug as the range of 0.4 to 1.2 ng/ml for the registered dosage [10]. Over time, new science reports were published, and EMA registered DEX (Dexdor[®]) in Europe for sedation for up to 14 days with the range of $0.2\text{--}1.4\ \mu\text{g}\cdot\text{kg}^{-1}\cdot\text{h}^{-1}$. The therapeutic concentration has been assessed up to 2.4 ng/ml [8]. A concentration higher than 1.9 ng/ml causes loss of consciousness [11]. Consequently, DEX concentration should be kept below 1.9 ng/ml to achieve minimal to moderate sedation.

DEX is widely used in elderly patients. It decreases the number of postoperative cognitive dysfunction and delirium incidences, particularly vulnerable in geriatric patients [12, 13]. Perioperative use of DEX decreases in-hospital and operative mortality and reduces incidences of postoperative stroke in elderly patients following cardiac surgery [14]. It improves sleep quality and decreases the administration and risk of side effects of opioids [15].

The patient's age, body mass index, cardiac output, serum albumin levels, and liver and kidney function were identified as covariates influencing DEX pharmacokinetics [16]. Also, genetic polymorphism of α_2 -adrenergic receptor (2A subtype) was identified to affect pharmacological response after DEX administration, e.g. rs1800544 or rs553668 [17, 18]. However, the influence of this polymorphism on the sedative effect of DEX is yet to be fully established.

The present study aims to characterize the pharmacokinetics and pharmacodynamics of DEX in cardiac patients after abdominal aortic surgeries. The secondary aim of this work was to identify potential factors explaining inter-individual variability in PK/PD parameters, including age, body weight, and polymorphism of the α_{2A} -adrenergic gene.

Materials and methods

Patients and genotype identification

All procedures performed on human participants were under the ethical standards of the institutional research committee and the 1964 Helsinki declaration and its later amendments or comparable ethical standards. The institutional Bioethical Committee approved the study protocol with permission numbers 213/13 and 572/16.

It was an observational study on elderly surgical patients from Anaesthetics and Critical Care Department (University Hospital of Lord's Transfiguration, Poznan University of Medical Sciences) sedated with DEX after abdominal aortic surgery. General anaesthesia was started with induction by a single dose of propofol and continued with sevoflurane. DEX administration was initiated immediately after arrival in the ICU (< 1h). Patients were mechanically ventilated during analgo-sedation. Patients were excluded if they had bradycardia, significant hemodynamic instability, and confirmed allergies to DEX.

Dexmedetomidine hydrochloride (Dexdor, Orion Pharma Poland sp. z.o.o.) infusion was initiated at a rate of $0.7 \mu\text{g}\cdot\text{kg}^{-1}\cdot\text{h}^{-1}$ without a loading dose and followed by continuous infusion at a rate ranging from 0.08 to $1.39 \mu\text{g}\cdot\text{kg}^{-1}\cdot\text{h}^{-1}$. The drug was given to obtain moderate or deep sedation [9, 19, 20] in monotherapy (four patients additionally received a single dose of propofol/midazolam, and one patient obtained a continuous infusion of propofol with ketamine). The administration of DEX was combined with analgesics (oxycodone, acetaminophen, tramadol, or metamizole). It was discontinued when there was significant hemodynamic instability, after patient extubation, or at the physician's discretion. DEX doses and co-administration of other drugs depended on the patient's health status, sedation scale, vital parameters, cardiovascular function, and implemented procedures. Clinical adverse hemodynamic instability was bradycardia (heart rate <50 beats per minute) and/or hypotension (systolic blood pressure <90 mmHg or mean arterial pressure <65 mmHg).

The depth of sedation was assessed using the bispectral index (BIS), which was monitored by IntelliVue MX800 (Philips, Netherlands). BIS values were kept between 50 and 80 to maintain moderate to deep sedation [9, 19, 20]. Cardiac index, a hemodynamic parameter related to cardiac output, was measured by FloTrac System (Edwards Lifesciences, USA). In addition, the following vital parameters were also monitored: heart rate, stroke variation volume (SVV), and systolic, diastolic, and mean arterial pressure (SBP, DBP, MAP). All parameters were measured and recorded in the study protocol immediately before (baseline values), during the infusion, and after its cessation.

The Supplementary Material describes genotype identification.

Pharmacokinetic-pharmacodynamic model

A pharmacokinetic model was built in the first step and described in our previous publication together with the analytical method [21].

The population nonlinear mixed-effect modeling was done using NONMEM (Version 7.2.0, Icon Development Solutions, Ellicott City, MD, USA) and the Fortran compiler 9.0. NONMEM runs were executed using Wings for NONMEM (WFN720, <http://wfn.sourceforge.net>). The FOCE estimation method with the interaction option in NONMEM was applied. The minimum value of the NONMEM objective function (OFV), typical goodness of fit diagnostic plots, and evaluation of the precision of the PK/PD parameters and variability estimates were used to discriminate between various models during the model-building process. The NONMEM data processing, simulations, and plots were carried out using Matlab® Software version 7.0 (The MathWorks, Inc., Natick, MA, USA).

A two-compartment model with parameters fixed to the previously estimated values was used to describe DEX PK [21]. The BIS values were linked to DEX concentrations (C_{DEX}) and hypothetical concentration (C_X) of drugs administered prior to DEX administration (propofol and sevoflurane) through the following E_{max} model:

$$BIS = BIS_0 \left(1 - \frac{E_{max} \left(\frac{C_{DEX}}{EC_{50,DEX}} + \frac{C_X}{EC_{50,X}} \right)}{1 + \frac{C_{DEX}}{EC_{50,DEX}} + \frac{C_X}{EC_{50,X}}} \right) \quad (1)$$

This equation was further rearranged, assuming C_X decreases mono-exponentially with a rate k . It leads to the following equation assuming an additive interaction between all the drugs:

$$BIS(P_i, t_j) = BIS_{0,i} \cdot \left(1 - \frac{C(t_j) + X_{0,i} \cdot \exp(-k_i \cdot t_j)}{C(t_j) + X_{0,i} \cdot \exp(-k_i \cdot t_j) + EC_{50,DEX}} \right) \quad (2)$$

In Eq. 2, denotes the baseline $C_{X,0}$ multiplied by the ratio of EC_{50} of DEX and EC_{50} of propofol and sevoflurane, BIS_0 denotes the baseline BIS score

(fully awake), E_{max} is the maximal effect fixed to 1 (BIS value of zero at sufficiently high concentrations of DEX), EC_{50} is the drug concentration leading to half-maximal effects.

The cardiac output was finally described using the following linear model:

$$CO(P_i, t_j) = CO_{0,i} \cdot (1 - SL_i \cdot C(t_j)) \quad (3)$$

where CO_0 denotes the baseline CO, and SL denotes the change in CO per unit change in DEX concentrations.

Inter-individual variability (IIV) for all PD parameters was modelled assuming log-normal distribution:

$$P_i = \theta_p \exp(\eta_{P,i}) \quad (4)$$

where P_i is the set of PK/PD parameters for i^{th} individual, θ_p is the population estimate of PK parameters, $\eta_{P,i}$ is a random effect for a particular parameter with mean 0 and variance ω_p^2 .

Any j^{th} observation of BIS and CO measured at time t_j , as defined by the following equation:

$$BIS_{Obs,ij} = BIS(P_i, t_j) + \varepsilon_{BIS,ij} \quad (5)$$

$$CO_{Obs,ij} = CO(P_i, t_j) + \varepsilon_{CO,ij} \quad (6)$$

CO and BIS denote the basic structural population model (Eq. 2 and 3). P_i is a pharmacokinetic parameter for the i^{th} individual, and ε_{COij} and ε_{BISij} represent the proportional residual intra-individual random error. We assumed that ε was symmetrically distributed around a mean of 0, with variance denoted by σ^2 .

Covariance Analysis

The covariate search was performed by plotting individual (post-hoc) estimates of the PK parameters against covariates (weight, age) to identify their potential effects. The categorical covariates (i.e. noradrenaline use, polymorphism) were included in the model based on indicator variables. The difference in the minimum NONMEM OFV obtained for the two hierarchical models (likelihood ratio) is approximately χ^2 distributed. During the covariate search, the effect of each

covariate was examined by adding an appropriate equation to the base model. When the difference in OFV between the models amounted to 3.84 for one degree of freedom, it was considered statistically significant (at $p < 0.05$) for the covariate to be included in the base model. This process was repeated until all significant covariates were added. Then backward elimination was performed by removing one covariate at a time. The least important covariate was dropped from the model according to the OFV unless that difference in OFV was more significant than 6.63 (corresponding to $p < 0.01$). The final model was established when no more covariates could be excluded.

Model evaluation

The model performance was assessed using Visual Predictive Check (VPC). The VPC calculation was based on 1000 datasets simulated with the final parameter estimates. This study used the 10th, 50th, and 90th percentile to summarize the data and VPC prediction. The VPC compares the confidence intervals obtained from prediction with the observed data over time. If the corresponding percentile from the observed data falls outside the 95% confidence interval derived from predictions, it indicates the model misspecification. Since PD data deviated from nominal times to some extent, binning across time was done.

Evaluation of model robustness was based on the non-parametric bootstrapping with 1000 replicates. From the bootstrap empirical posterior distribution, 90% confidence intervals (5th–95th percentile) were obtained for the parameters described by Parke et al. [22].

Results

Patients and genotype identification

Twenty one elderly patients were enrolled in the study (eighteen male and three female) from the Anaesthetics and Critical Care Department (University Hospital of Lord's Transfiguration, Poznan University of Medical Sciences). The patient's age and weight were 68 (IQR = 9) and 75 (IQR = 13) kg. DEX was given to maintain moderate ($n = 13$) or deep ($n = 7$) sedation after abdominal aortic surgery in mechanically ventilated patients. DEX administration was initiated 38.9 (± 20.0) min-

utes after the end of anaesthesia with an infusion rate of $0.7 \mu\text{g}\cdot\text{kg}^{-1}\cdot\text{h}^{-1}$. The infusion was continued with a rate ranging from 0.08 to $1.39 \mu\text{g}\cdot\text{kg}^{-1}\cdot\text{h}^{-1}$ and lasted 295 (IQR = 156) minutes (four patients received DEX for >24 hours). The cumulative dose equalled 331.47 (IQR = 186.53) μg .

Genotypes of *ADR2A*55* were identified for all patients except patient number 1003. Eighteen had a wild type (G|G), and two people were heterozygous (A|G, ID: 1008 and 10016). According to the Ensembl database [23], genotype distribution in the European population is 0.702, 0.276, and 0.022 for G|G, A|G, and A|A, respectively. The corresponding values in this study are 0.90 (G|G) and 0.10 (A|G), and 0.0 (A|A).

Pharmacodynamic and hemodynamic data

PD parameters included depth of sedation (bispectral index, BIS) and cardiac output (cardiac index converted to cardiac output). For two patients (ID = 1002 and 1005), the CO and for one patient (1002), the BIS measurements were missing. The observed time profiles of BIS and CO are presented in **Figure 1**. Baseline and mean (over the infusion duration) values of hemodynamic parameters are presented in **Table S1**, along with PD data.

Observed median (range) values of PD parameters during DEX infusion were 65.7 (40.4–80.4) for BIS, 2.69 (1.96 – 3.86) $\text{L}\cdot\text{min}^{-1}\cdot\text{m}^{-2}$ for CI, 6.60 (3.00 – 15.25) % for SVV, 66.5 (59.5 – 94.7) beats/min for HR, 120.00 (83.67 – 167.50) mmHg for SBP, 58.57 (44.67 –

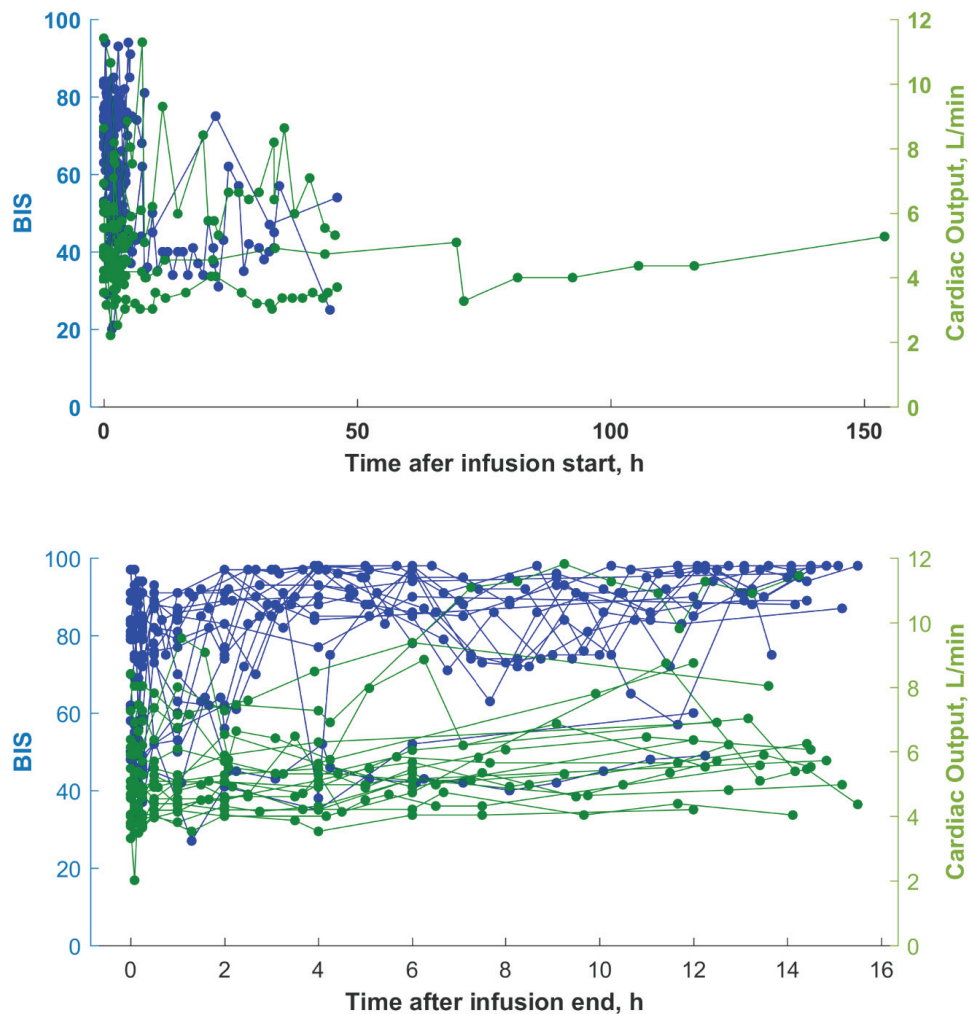


Figure 1. The observed time profiles of bispectral index and cardiac output. Straight lines connect dots representing measurements.

78.50) mmHg for DBP, and 79.94 (66.71–110.00) mmHg for MAP. All values were lower during the infusion period when compared to the baseline.

One hundred fifty-one heart rate measurements (from 805) were below 60. Incidences of bradycardia recurred in 6 patients (1002, 1008, 10015, 10018, 10020, and 10021). We noticed 48 (from 933) SBP values below 90 and 80 (from 830) MAP values below 65. Incidences of hypotension recurred in 6 patients (1007, 10012, 10013, 10014, 10018, and 10021).

PK/PD model parameters and simulations

The previously described pharmacokinetic model was built for 70 patients, including the studied group [21]. The individual PK parameters were used as a driving force of PD responses. The typical values of PK parameters were estimated at

22.5 L for the volume of the central compartment, 86.1 L for the volume of the peripheral compartment, 34.7 L/h (for a typical patient) for systemic clearance, and 40.8 L/h for the distribution clearance. These values are consistent with the literature findings [24, 25]. The sigmoid E_{max} model was used to describe the BIS effect and the linear model for the CO effect.

Table 1 provides the final parameter estimates and bootstrap results. All parameters and inter-subject and residual error variances were estimated with low (<50%) coefficients of variation (%CV). The shrinkage was small for baseline cardiac output and bispectral index and moderated for other parameters. The inter-individual variability (IIV) was estimated for all parameters, except k . It was moderate (<60%) for the CO_0 and BIS_0 and high (60–99%) for other parameters.

Table 1. The parameter estimates of the final PK/PD model of DEX. The bootstrap estimates are given for comparison. 1 out of 1000 bootstrap runs terminated early. RSE denotes relative standard errors whereas CV coefficient of variation.

| Parameter [unit] | Description | θ , Estimate (%RSE) [Shrinkage] | Estimate, Bootstrap Median [5 th –95 th CI] |
|------------------------------------|--|--|---|
| $\theta_{CO,0}$ [L/min] | Baseline cardiac output | 5.79 (6) | 5.81 [5.28–6.43] |
| θ_{SL} [(L/min)/(ng/ml)] | Slope between CO and DEX concentrations | 0.819 (31.9) | 0.845 [0.461–1.31] |
| $\theta_{BIS,0}$ | Baseline BIS | 87.9 (4.5) | 88.6 [81.1–93.9] |
| θ_{X_0} [ng/ml] | Hypothetical concentrations of other than DEX at the infusion start | 0.923 (34.6) | 0.951 [0.518–2.01] |
| θ_{EC50} [ng/ml] | EC_{50} of DEX | 3.62 (25.1) | 3.66 [2.42–6.21] |
| θ_k [1/h] | Elimination rate constant of drugs given prior to DEX administration | 0.299 (15.4) | 0.291 [0.217–0.371] |
| Between Subject Variability | | | |
| $\omega^2_{CO,0}$ [%CV] | Inter-individual variability of CO_0 | 24.1 (18.2) [8.4] | 23.3 [14.7–30.4] |
| ω^2_{SL} [%CV] | Inter-individual variability of SL | 88.5 (27.0) [27.6] | 83.7 [37.6–129] |
| $\omega^2_{BIS,0}$ [%CV] | Inter-individual variability of BIS_0 | 17.0 (4.5) [7.8] | 16.1 [1.4–25.6] |
| $\omega^2_{X_0}$ [%CV] | Inter-individual variability of X_0 | 92.5 (22.7) [24.2] | 87.3 [9–120] |
| ω^2_{EC50} [%CV] | Inter-individual variability of $EC50$ | 77.7 (18.0) [17.4] | 73.8 [36.6–96.7] |
| Residual Error Model | | | |
| σ^2 | Additive residual error variability for BIS | 9.66 (6.4) [5] | 9.72 [8.7–10.8] |
| σ^2 [L/min] | Additive residual error variability for CO | 0.874 (12.8) [4.2] | 0.873 [0.681–1.05] |

The typical values of EC_{50} for DEX effects on BIS were estimated at 3.62 ng/ml, and the slope between CO and DEX concentrations in the linear model for CO was estimated at 0.819 (L/min)/(ng/ml). Baseline values of CO and BIS were 5.79 L/min and 87.9, respectively. The following covariates that potentially impact DEX pharmacodynamics were analyzed during the model-building

process: age, body weight, noradrenaline use, and single nucleotide polymorphism of *ADRA2A*. **Figures 2** and **3** present the results. None of the analyzed covariates has an impact on DEX PD. However, since only two patients had a mutation of *ADRA2A**55 and four patients received noradrenaline, these results should be treated as exploratory.

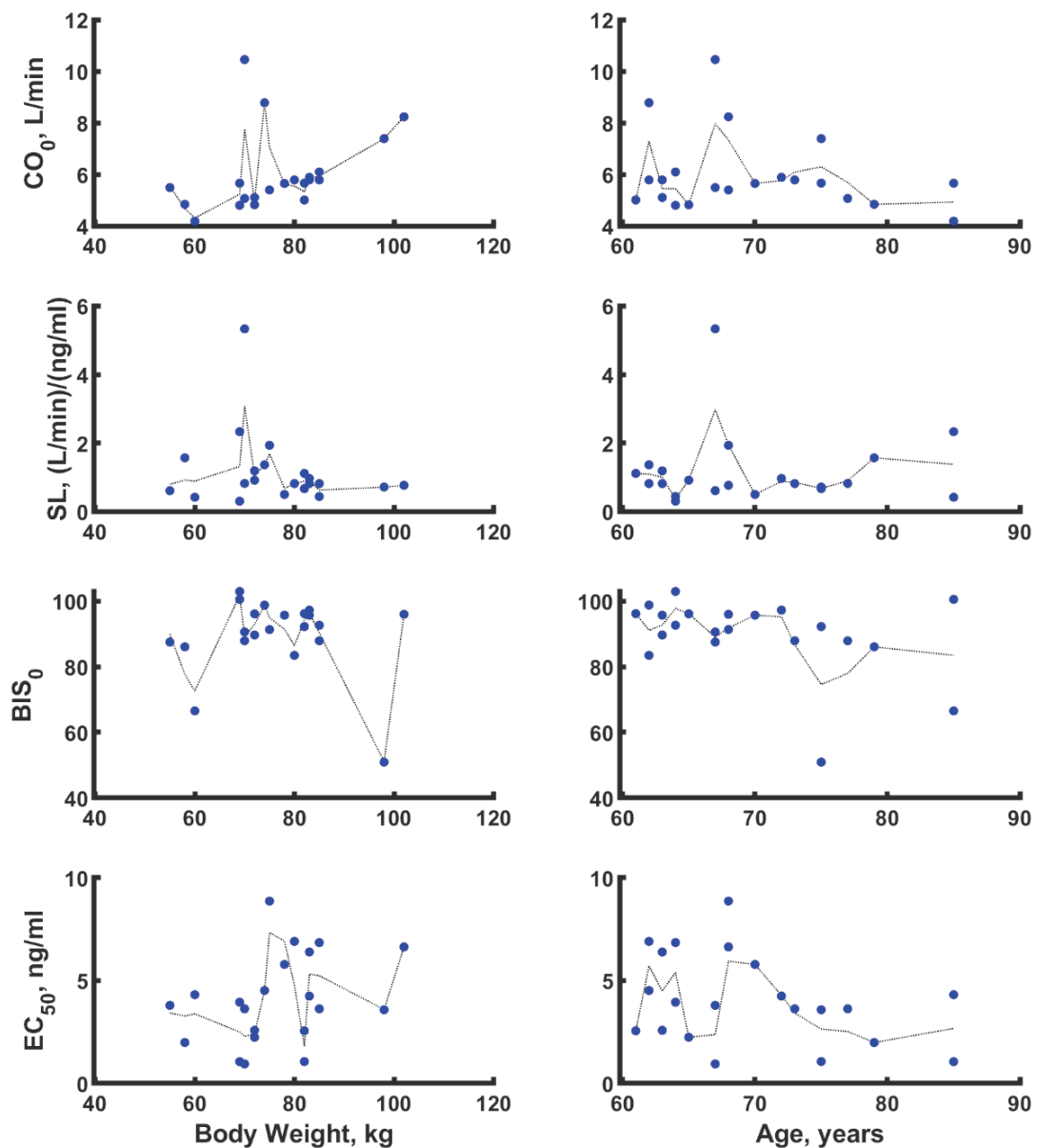


Figure 2. The relationship between individual values of PD parameters and subject body weight or age.

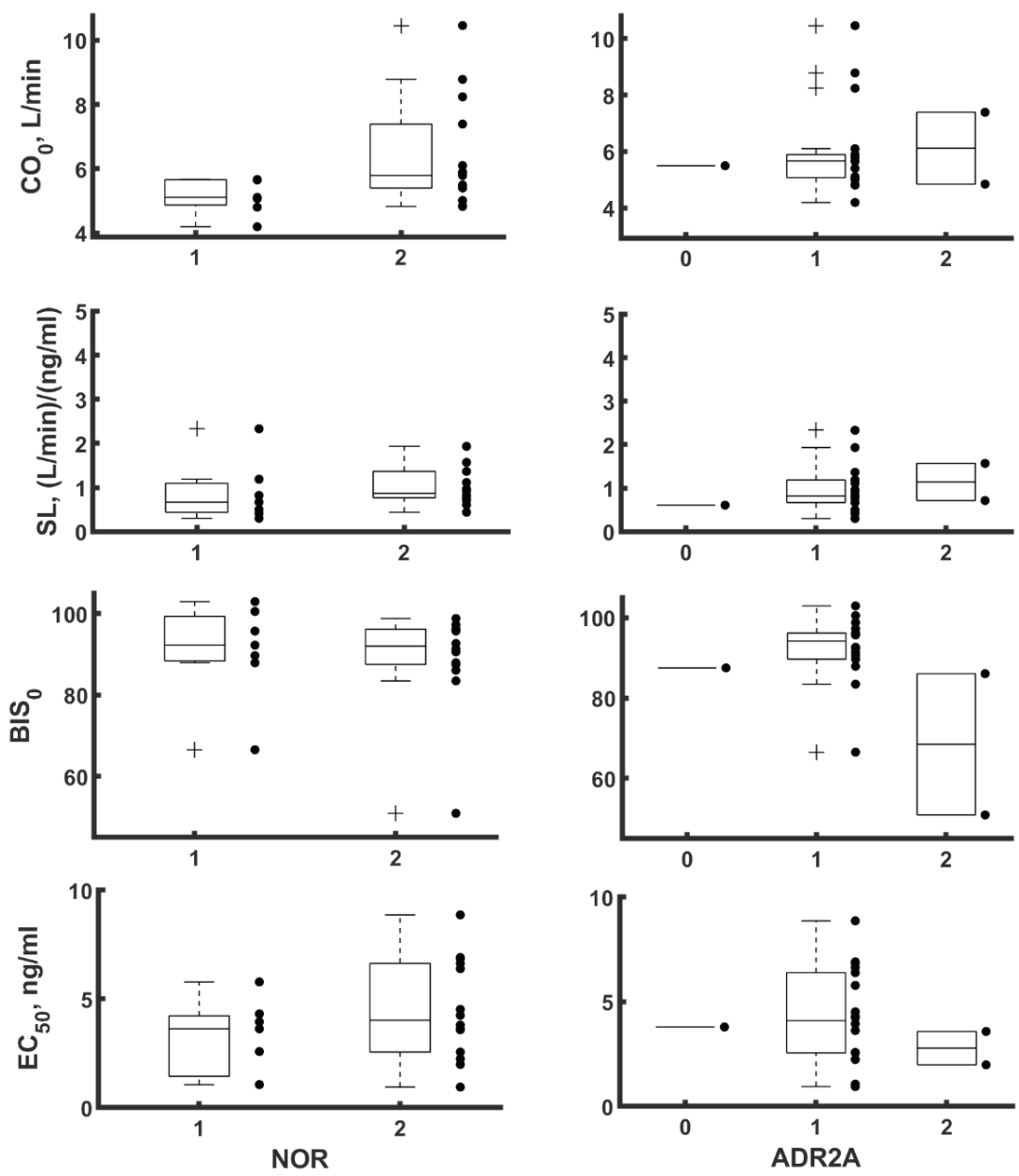


Figure 3. Relationship between PD parameters versus noradrenaline use (NOR, 1 – yes, 2 – no) and polymorphism of ADR2A (0 – patients with missing information on genetic polymorphism, 1 – G/G, 2 – A/G).

Figure 4 shows goodness-of-fit plots for the final model. The individual predictions are close to the experimental data with no significant systematic bias, indicating the model's good performance. Other goodness-of-fit plots also confirmed this performance. Finally, a visual predictive check

(VPC) for DEX PD was used to assess the simulation properties of the model. **Figures 5** (for CO) and **6** (for BIS) depict the results. VPC plots did not show any major misspecifications as both the central tendency of the data and the variability at a particular sampling time are adequately recaptured well.

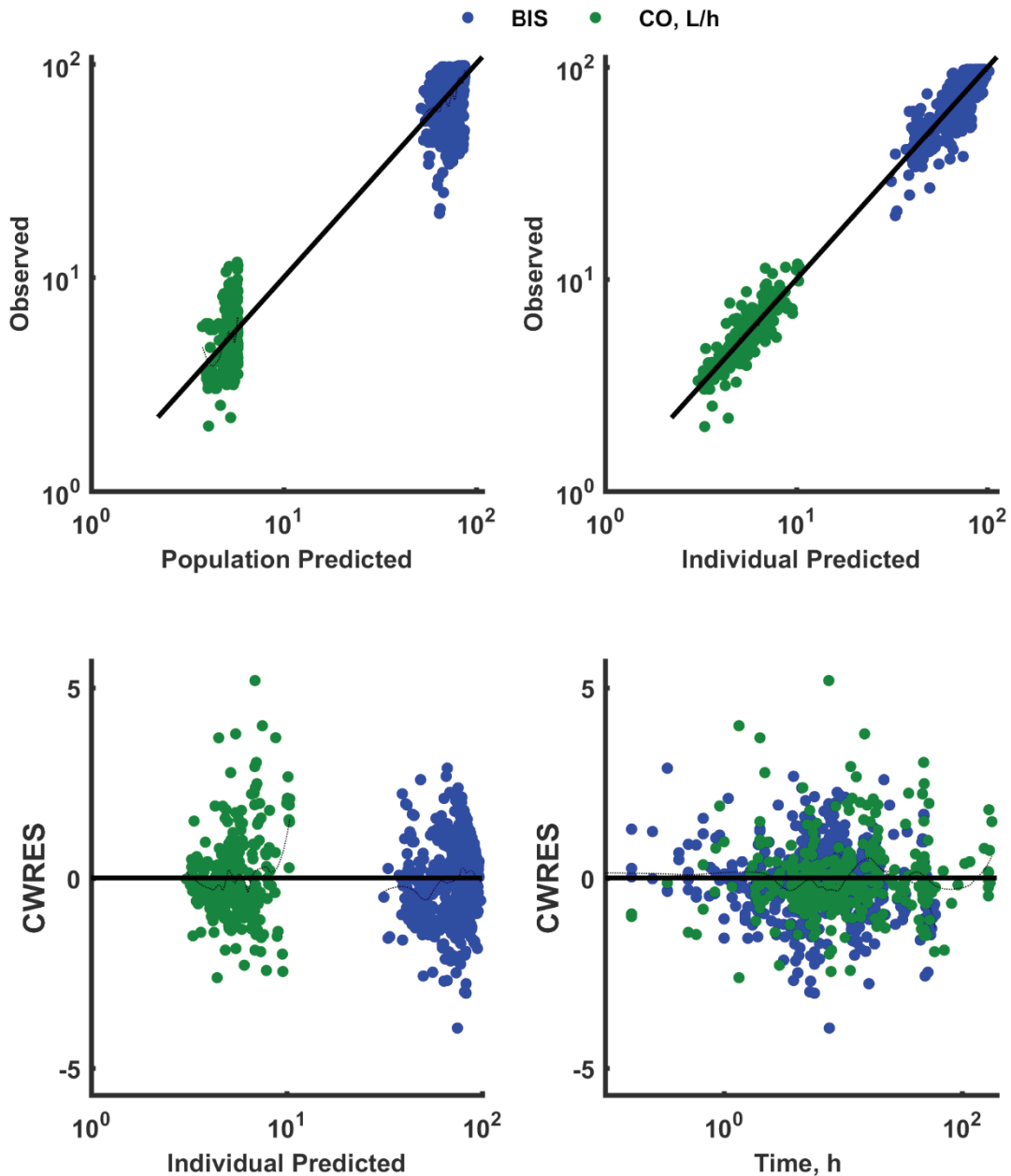


Figure 4. Goodness-of-fit plots for the final PK/PD model: the observed versus the population predicted responses, the observed versus the individual predicted responses, the conditional weighted residuals (CWRES) versus the individual predicted responses and the CWRES versus time.

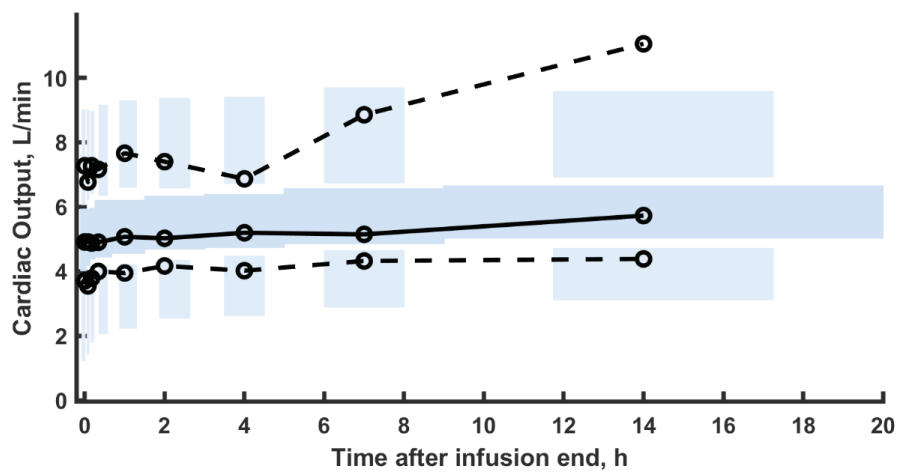
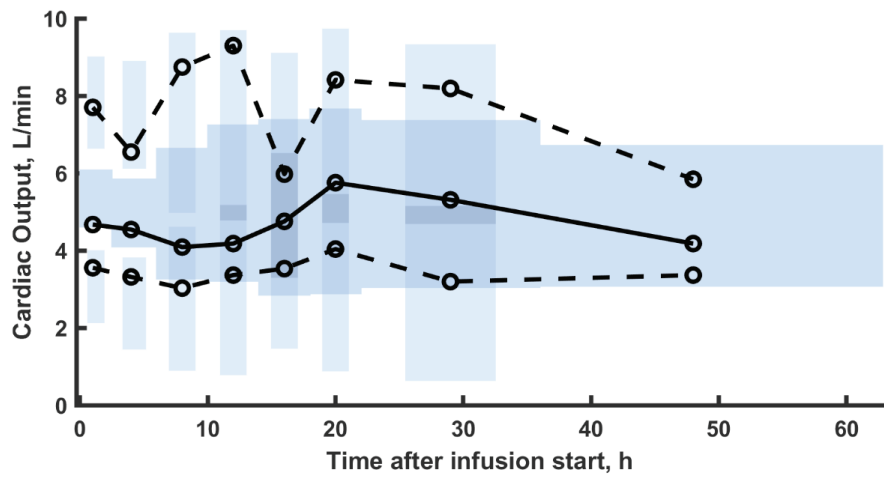


Figure 5. The VPC plots for dexmedetomidine PD (cardiac output). The VPC plots show the simulation-based 90% confidence intervals around the 10th, 50th, and 90th percentiles of the PD data in the form of blue (50th) and grey (10th and 90th) areas. The corresponding percentiles from the observed data are plotted in black colour.

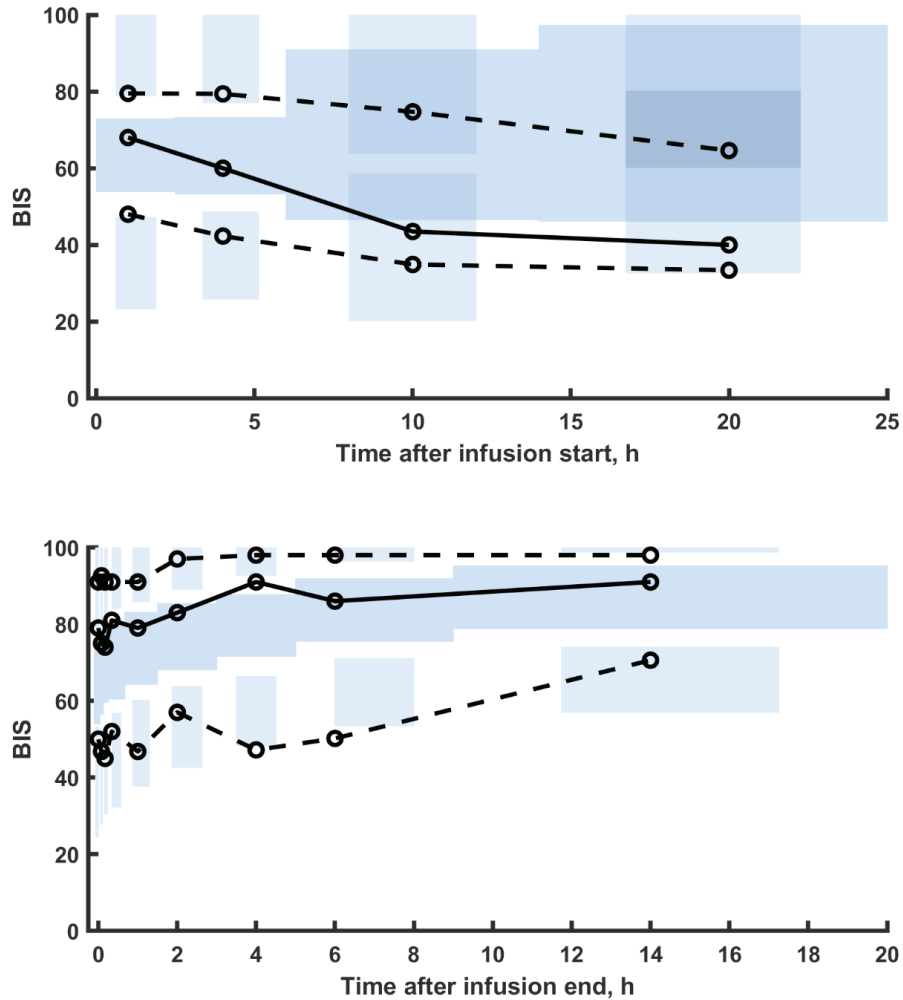


Figure 6. The VPC plots for dexmedetomidine PD (BIS). The VPC plots show the simulation-based 90% confidence intervals around the 10th, 50th, and 90th percentiles of the PD data in the form of blue (50th) and grey (10th and 90th) areas. The corresponding percentiles from the observed data are plotted in black colour.

Discussion

The present study aimed to perform a population PK/PD analysis of DEX in elderly patients after abdominal aortic surgery.

The DEX concentrations were measured in all subjects. According to the earlier findings, the therapeutic range (0.4–2.4 ng/ml) was achieved in 18 patients, and all concentrations were in the range of 0.4–1.9 ng/ml. The plasma concentrations <0.4 ng/ml were noted in patients 1005 and 10016. Patient no 1001 had two measured concentrations >2.4 ng/ml, and the mean BIS value during analgosedation was 54.17 (deep

sedation). Nevertheless, the mean BIS values in patients 1005 and 10016 were 51.86 (deep sedation) and 77.00 (moderate sedation), respectively. Five patients had a mean BIS value <60 (deep sedation), whereas drug concentrations were <1.2 ng/ml during infusion. Our findings show high inter-individual variability in drug response in this homogeneous group of patients.

The bispectral index was chosen to estimate the sedative effect of DEX based on the sigmoidal E_{max} model. The E_{max} model was also used to describe bispectral index as a pharmacodynamic effect of other drugs, e.g. propofol [26, 27], sevoflurane [28], or propofol with fentanyl [29]. DEX

infusion was initiated on average 38.9 min after the end of anaesthesia. Thus, patients were still under the influence of drugs used in anaesthesia (mainly propofol and sevoflurane) and the estimated baseline BIS values were 87.9 (the value for minimal sedation and anxiolysis). Drug concentrations at the start of DEX infusion (X_0) were incorporated into the model to consider this. The estimated EC_{50} was 3.62 ng/ml. Colin et al. [30] developed a PK/PD model of DEX in healthy volunteers (9 females and 9 males aged: 18–72 years). They observed a relationship between C_{50} (an effect-site concentration necessary to reach half of the maximal effect) and BIS values. The estimated C_{50} was 2.63 ng/ml in healthy volunteers with a baseline BIS value of 96.8 and 4.78 ng/ml in healthy volunteers with a baseline BIS value of 89.7. The second group had similar BIS and slightly higher EC_{50} than our patients. Furthermore, older adults enrolled on the study are likely to present sensitivity to many drugs [31]. Additionally, Colin et al. examined healthy volunteers, whereas we researched surgical patients. Wang et al. [32] showed that the DEX dose should be decreased with the increasing age of the patient. Acceptable sedation using DEX was achieved in patients aged 65–74 and 75–85 years when the drug dose was 0.57 and 0.38 $\mu\text{g}/\text{kg}$, respectively. Because of few scientific reports about DEX PD models (using BIS as a response), comparing our results with other research is challenging. The differences in side effects of DEX related to patient's age were observed by Shehabi et al. [33], who conducted SPICE III randomized controlled trial and noticed that the early use of DEX in ventilated critically ill patients is likely beneficial in patients older than 65 years regardless of diagnostic categories and illness severity. They observed a high probability of reduced 90-day mortality in this group of patients. On the other hand, the study showed that early DEX-based sedation in younger patients appears likely to increase 90-day mortality, particularly in non-operative critically ill patients with high severity of illness [33]. They reported that bradycardia and hypotension were more frequently occurring side effects in patients with DEX-based sedation than in another group [34]. We did not observe bradycardia episodes among elderly ICU patients included in our previous study, which was not the case for hypotension episodes. We concluded that DEX could be safely used in geriatric population, but hemodynamic parameters need

careful monitoring during DEX administration [35]. The European Medicine Agency based on SPICE III warned about increased mortality risk in intensive care unit patients ≤ 65 years [36].

Yoo et al. [37] focused on noradrenaline decrease due to the DEX effect and described this relationship using an indirect response model. They related noradrenaline concentrations to BIS, BP or HR. DEX effect on the bispectral index was described using a sigmoidal E_{max} model controlled by noradrenaline in an effect compartment. They estimated EC_{50} at 3.9 nmol/L (noradrenaline). Unfortunately, they did not estimate EC_{50} for DEX concentrations. Li et al. [38] developed the PD model of DEX, but they used the Ramsay score to evaluate the sedation effect of the drug. Moreover, DEX was administered as a single intranasal dose to healthy volunteers.

PD model for cardiac function

Cardiac output was monitored in the studied subjects as a pharmacodynamic response to DEX [39, 40]. The hemodynamic effect was described by a linear model. E_{max} model was also tested, but EC_{50} tended to large values implying a linear relationship between CO and DEX. A linear relationship between the drug effects on cardiac output was also described for other drugs, e.g. dobutamine [41], dopamine [42], and ketamine [43]. Occasionally an E_{max} model was used, e.g. for propofol [44]. Cardiac output (converted to cardiac index) was monitored in 19 patients (17 of them were measured baseline value). Baseline CI was 2.9 (2.1–6.0) $\text{L}\cdot\text{min}^{-1}\cdot\text{m}^{-2}$ whereas the average value during DEX infusion was 2.69 (1.96–3.86) $\text{L}\cdot\text{min}^{-1}\cdot\text{m}^{-2}$. It is worth remembering that parameters baseline values were measured after anaesthesia when patients were still under anaesthetic drugs. Drug concentrations were inversely proportional to cardiac output. All measured CI values were in the reference range for the elderly (>60 years) – 1.88–4.71 $\text{L}\cdot\text{min}^{-1}\cdot\text{m}^{-2}$ [45]. That confirms DEX's influence on cardiac output and shows safe use doses. There were only a few incidents when the values were below the recommended threshold (patient 1001). Furthermore, there were noted high plasma concentrations in patient 1001, whereas the infusion rate was 0.13–0.80 $\mu\text{g}\cdot\text{kg}^{-1}\cdot\text{h}^{-1}$. Cardiac output influenced DEX clearance which could be a reason for high plasma drug concentrations [46].

Covariate testing

This work assessed the effect of single nucleotide polymorphisms of the *ADR2A* gene (*ADR2A*55*, rs553668) on clearance. There is a higher gene expression level in mutated forms than in wild types. A mutant allele variant increases the risk of hypertension, childhood attention-deficit hyperactivity disorder, increased platelet-induced platelet aggregation, increased heart rate in response to lower-body negative pressure, and lower levels of haemoglobin A_{1c} and total cholesterol [47]. Kurnik et al. [18] proved that mutation in one position (rs553668) affects DEX pharmacodynamics, causes a more robust drug response, and also more considerable differences in blood pressure than in patients with wild-type genotype. Among the researched group, two patients had a mutated form of the examined polymorphism – A|G. Nobody was mutated homozygous (A|A). *ADR2A*55* genotype was tested as a covariate during the model-building process, and we could not find any relationship. We see the need to expand the researched group to re-examine this effect with more mutated forms.

Four patients received noradrenaline during DEX infusion (10015, 10018, 100116, 10021). Noradrenaline influences cardiovascular functions, e.g. increases mean arterial pressure. However, its effect on cardiac output is ambiguous. It causes both an increase and a decrease in cardiac output. Maas et al. [48] examined cardiac output changes in cardiosurgical patients that received noradrenaline. They found that stroke volume variation could predict this catecholamine effect on cardiac output. They observed that a high SVV baseline value (14.4 ± 4.2) provoked a rise in cardiac output after noradrenaline, whereas low values (9.1 ± 2.4) – a decrease in CO. In three researched patients that received noradrenaline baseline SVV value was ≤ 5 , in one case – 12 (Table S2). Two cases followed Maas' results. It is 50% of the analyzed group. We could not draw a definitive conclusion about the relationship between SVV and CO in patients who obtained noradrenaline.

We are aware that our research has some limitations. The study is small, with 21 patients, of which only two people had the mutation in the *ADRA2A* gene (*ADR2A*55*) and only four patients received noradrenaline. Therefore, we could not prove the influence of mutation and noradrena-

line use on DEX pharmacodynamics. Patients were under the impact of anaesthetic drugs at the beginning of DEX infusion, which affected the PD responses. We did not have sufficient data to evaluate the effect of anaesthetics on PD DEX. Other drugs presenting an effect on CO were not assessed. We measured only DEX concentrations. We did not undertake to assess a DEX influence on hemodynamic parameters, e.g. SBP, DBP, HR, because the administration of the drugs affects blood pressure and heart rate. We should have also taken into account fluid management. However, the study provided a model describing DEX PD in patients with low BIS values at baseline. The results indicate that the DEX dose depends on the BIS value at baseline. The finding is a clinically significant example of drug interactions at the pharmacodynamic level. It also indicates that measuring the concentration of all drugs affecting BIS is necessary to understand DEX pharmacodynamics in real clinical scenarios fully.

Conclusions

The PK/PD model of DEX was built based on data from 21 patients treated in ICU. Cardiac output was described using a linear model, whereas BIS was with the *E_{max}* model. The measured CI values were in the reference range showing that the used doses of the drug ensured stable cardiac function in the examined elderly patients group.

Acknowledgements

The model was partly developed during the 9th annual Uppsala Pharmacometrics Summer School (UPSS) – Covariate Model Building + PKPD Modeling of Continuous and Categorical Data in Uppsala Universitet. We thank all scientists who participated in this course, especially Professor Mats Karlsson, for all the helpful and thought-provoking suggestions.

Conflict of interest statement

The authors declare no conflict of interest.

Funding sources

Funding sources: This research was supported by a grant (2015/17/B/NZ7/03032) from the Polish National Science Centre.

Data Sharing: The data supporting the findings of this study may be shared on request from the corresponding author, Justyna Ber, at justyna.ber@ump.edu.pl.

References

1. Scheinin H, Karhuvaara S, Olkkola KT, Kallio A, Anttila M, Vuorilehto L, Scheinin M. Pharmacodynamics and pharmacokinetics of intramuscular dexmedetomidine. *Clin Pharmacol Ther.* 1992 Nov;52(5):537-46. doi: 10.1038/clpt.1992.182. PMID: 1358496.
2. Correa-Sales C, Rabin BC, Maze M. A hypnotic response to dexmedetomidine, an alpha 2 agonist, is mediated in the locus coeruleus in rats. *Anesthesiology.* 1992 Jun;76(6):948-52. doi: 10.1097/00000542-199206000-00013. PMID: 1350889.
3. Kaur M, Singh PM. Current role of dexmedetomidine in clinical anesthesia and intensive care. *Anesth Essays Res.* 2011 Jul-Dec;5(2):128-33. doi: 10.4103/0259-1162.94750. PMID: 25885374; PMCID: PMC4173414.
4. Vincent JL, Shehabi Y, Walsh TS, Pandharipande PP, Ball JA, Spronk P, Longrois D, Strøm T, Conti G, Funk GC, Badenes R, Mantz J, Spies C, Takala J. Comfort and patient-centred care without excessive sedation: the eCASH concept. *Intensive Care Med.* 2016 Jun;42(6):962-71. doi: 10.1007/s00134-016-4297-4. Epub. 2016 Apr 13. PMID: 27075762; PMCID: PMC4846689.
5. Zhang X, Bai X. New therapeutic uses for an alpha2 adrenergic receptor agonist--dexmedetomidine in pain management. *Neurosci Lett.* 2014 Feb 21;561:7-12. doi: 10.1016/j.neulet.2013.12.039. Epub. 2013 Dec 25. PMID: 24373989.
6. Bloor BC, Ward DS, Belleville JP, Maze M. Effects of intravenous dexmedetomidine in humans. II. Hemodynamic changes. *Anesthesiology.* 1992 Dec;77(6):1134-42. doi: 10.1097/00000542-199212000-00014. PMID: 1361311.
7. Talke P, Anderson BJ. Pharmacokinetics and pharmacodynamics of dexmedetomidine-induced vasoconstriction in healthy volunteers. *Br J Clin Pharmacol.* 2018 Jun;84(6):1364-1372. doi: 10.1111/bcp.13571. Epub. 2018 Apr 2. PMID: 29495085; PMCID: PMC5980451.
8. Weerink MAS, Struys MMRF, Hannivoort LN, Barends CRM, Absalom AR, Colin P. Clinical Pharmacokinetics and Pharmacodynamics of Dexmedetomidine. *Clin Pharmacokinet.* 2017 Aug;56(8):893-913. doi: 10.1007/s40262-017-0507-7. PMID: 28105598; PMCID: PMC5511603.
9. The American Society of Anesthesiologists. Committee on Quality Management and Departmental Administration. Continuum of Depth of Sedation: Definition of General Anesthesia and Levels of Sedation/Analgesia. <https://www.asahq.org/~media/Sites/ASAHQ/Files/Public/Resources/standards-guidelines/continuum-of-depth-of-sedation-definition-of-general-anesthesia-and-levels-of-sedation-analgesia.pdf> (date accessed: 20.01.2020).
10. Snapir A, Posti J, Kentala E, Koskenvuo J, Sundell J, Tuunanen H, Hakala K, Scheinin H, Knuuti J, Scheinin M. Effects of low and high plasma concentrations of dexmedetomidine on myocardial perfusion and cardiac function in healthy male subjects. *Anesthesiology.* 2006 Nov;105(5):902-10; quiz. 1069-70. doi: 10.1097/00000542-200611000-00010. PMID: 17065883.
11. Ebert TJ, Hall JE, Barney JA, Uhrich TD, Colincio MD. The effects of increasing plasma concentrations of dexmedetomidine in humans. *Anesthesiology.* 2000 Aug;93(2):382-94. doi: 10.1097/00000542-200008000-00016. PMID: 10910487.
12. Zhou C, Zhu Y, Liu Z, Ruan L. Effect of dexmedetomidine on postoperative cognitive dysfunction in elderly patients after general anaesthesia: A meta-analysis. *J Int Med Res.* 2016 Dec;44(6):1182-1190. doi: 10.1177/0300060516671623. Epub. 2016 Dec 7. PMID: 27913743; PMCID: PMC5536774.
13. Su X, Meng ZT, Wu XH, Cui F, Li HL, Wang DX, Zhu X, Zhu SN, Maze M, Ma D. Dexmedetomidine for prevention of delirium in elderly patients after non-cardiac surgery: a randomised, double-blind, placebo-controlled trial. *Lancet.* 2016 Oct 15;388(10054):1893-1902. doi: 10.1016/S0140-6736(16)30580-3. Epub. 2016 Aug 16. PMID: 27542303.
14. Cheng H, Li Z, Young N, Boyd D, Atkins Z, Ji F, Liu H. The Effect of Dexmedetomidine on Outcomes of Cardiac Surgery in Elderly Patients. *J Cardiothorac Vasc Anesth.* 2016 Dec;30(6):1502-1508. doi: 10.1053/j.jvca.2016.02.026. Epub. 2016 Mar 3. PMID: 27435836; PMCID: PMC5010787.
15. Li HJ, Li CJ, Wei XN, Hu J, Mu DL, Wang DX. Dexmedetomidine in combination with morphine improves postoperative analgesia and sleep quality in elderly patients after open abdominal surgery: A pilot randomized control trial. *PLoS One.* 2018 Aug 14;13(8):e0202008. doi: 10.1371/journal.pone.0202008. PMID: 30106963; PMCID: PMC6091958.
16. Tellor BR, Arnold HM, Micek ST, Kollef MH. Occurrence and predictors of dexmedetomidine infusion intolerance and failure. *Hosp Pract (1995).* 2012 Feb;40(1):186-92. doi: 10.3810/hp.2012.02.959. PMID: 22406894.
17. Yağar S, Yavaş S, Karahalil B. The role of the ADRA2A C1291G genetic polymorphism in response to dexmedetomidine on patients undergoing coronary artery surgery. *Mol Biol Rep.* 2011 Jun;38(5):3383-9. doi: 10.1007/s11033-010-0446-y. Epub. 2010 Nov 23. PMID: 21104443.
18. Kurnik D, Muszkat M, Li C, Sofowora GG, Friedman EA, Scheinin M, Wood AJ, Stein CM. Genetic variations in the $\alpha(2A)$ -adrenoreceptor are associated with blood pressure response to the agonist dexmedetomidine. *Circ Cardiovasc Genet.* 2011 Apr;4(2):179-87. doi: 10.1161/CIRCGENETICS.110.957662. Epub. 2011 Feb 15. PMID: 21325151; PMCID: PMC3080459.
19. Ball J. How useful is the bispectral index in the management of ICU patients? *Minerva Anesthesiol.* 2002 Apr;68(4):248-51. PMID: 12024092.
20. Tasaka CL, DUBY JJ, Pandya K, Wilson MD, A Hardin K. Inadequate Sedation During Therapeutic Paralysis: Use of Bispectral Index in Critically Ill Patients. *Drugs Real World Outcomes.* 2016 May 28;3(2):201-208. doi: 10.1007/s40801-016-0076-3. PMID: 27398299; PMCID: PMC4914538.
21. Ber J, Wiczling P, Hołysz M, Klupczyńska A, Bartkowska-Śniatkowska A, Bieda K, Smuszkiewicz P, Nowicka M, Żurański Ł, Sobczyński P, Maty-

- siak J, Grześkowiak E, Bienert A. Population Pharmacokinetic Model of Dexmedetomidine in a Heterogeneous Group of Patients. *J Clin Pharmacol*. 2020 Nov;60(11):1461-1473. doi: 10.1002/jcph.1647. Epub. 2020 Jun 5. PMID: 32500578.
22. Parke J, Holford NH, Charles BG. A procedure for generating bootstrap samples for the validation of nonlinear mixed-effects population models. *Comput Methods Programs Biomed*. 1999 Apr;59(1):19-29. doi: 10.1016/s0169-2607(98)00098-4. PMID: 10215174.
 23. Internet: <https://www.ensembl.org/index.html>.
 24. Väitalo PA, Ahtola-Sätälä T, Wighton A, Sarapohja T, Pohjanjousi P, Garratt C. Population pharmacokinetics of dexmedetomidine in critically ill patients. *Clin Drug Investig*. 2013 Aug;33(8):579-87. doi: 10.1007/s40261-013-0101-1. PMID: 23839483; PMCID: PMC3717151.
 25. Smuszkiewicz P, Wiczling P, Ber J, Warzybok J, Małkiewicz T, Matysiak J, Klupczyńska A, Trojanowska I, Kokot Z, Grześkowiak E, Krzyżanski W, Bienert A. Pharmacokinetics of dexmedetomidine during analgosedation in ICU patients. *J Pharmacokinetic Pharmacodyn*. 2018 Apr;45(2):277-284. doi: 10.1007/s10928-017-9564-7. Epub. 2017 Dec 30. PMID: 29290034; PMCID: PMC5845053.
 26. Chidambaran V, Venkatasubramanian R, Sadhasivam S, Esslinger H, Cox S, Diepstraten J, Fukuda T, Inge T, Knibbe CAJ, Vinks AA. Population pharmacokinetic-pharmacodynamic modeling and dosing simulation of propofol maintenance anesthesia in severely obese adolescents. *Paediatr Anaesth*. 2015 Sep;25(9):911-923. doi: 10.1111/pan.12684. Epub. 2015 May 13. PMID: 25975390; PMCID: PMC4516654.
 27. Wiczling P, Bienert A, Sobczyński P, Hartmann-Sobczyńska R, Bieda K, Marcinkowska A, Malatyńska M, Kaliszczan R, Grześkowiak E. Pharmacokinetics and pharmacodynamics of propofol in patients undergoing abdominal aortic surgery. *Pharmacol Rep*. 2012;64(1):113-22. doi: 10.1016/s1734-1140(12)70737-5. PMID: 22580527.
 28. Cortínez LI, Trocóniz IF, Fuentes R, Gambús P, Hsu YW, Altermatt F, Muñoz HR. The influence of age on the dynamic relationship between end-tidal sevoflurane concentrations and bispectral index. *Anesth Analg*. 2008 Nov;107(5):1566-72. doi: 10.1213/ane.0b013e318181f013. PMID: 18931213.
 29. Wiczling P, Bieda K, Przybyłowski K, Hartmann-Sobczyńska R, Borsuk A, Matysiak J, Kokot ZJ, Sobczyński P, Grześkowiak E, Bienert A. Pharmacokinetics and pharmacodynamics of propofol and fentanyl in patients undergoing abdominal aortic surgery – a study of pharmacodynamic drug-drug interactions. *Biopharm Drug Dispos*. 2016 Jul;37(5):252-63. doi: 10.1002/bdd.2009. PMID: 26990035.
 30. Colin PJ, Hannivoort LN, Eleveld DJ, Reyntjens KMEM, Absalom AR, Vereecke HEM, Struys MMRF. Dexmedetomidine pharmacokinetic-pharmacodynamic modelling in healthy volunteers: 1. Influence of arousal on bispectral index and sedation. *Br J Anaesth*. 2017 Aug 1;119(2):200-210. doi: 10.1093/bja/aex085. PMID: 28854538.
 31. Akhtar S. Pharmacological considerations in the elderly. *Curr Opin Anaesthesiol*. 2018 Feb;31(1):11-18. doi: 10.1097/ACO.0000000000000544. PMID: 29189287.
 32. Wang C, Zhang H, Fu Q. Effective dose of dexmedetomidine as an adjuvant sedative to peripheral nerve blockade in elderly patients. *Acta Anaesthesiol Scand*. 2018 Jul;62(6):848-856. doi: 10.1111/aas.13087. Epub. 2018 Feb 9. PMID: 29424059.
 33. Shehabi Y, Serpa Neto A, Howe BD, Bellomo R, Arabi YM, Bailey M, Bass FE, Kadiman SB, McArthur CJ, Reade MC, Seppelt IM, Takala J, Wise MP, Webb SA; SPICE III Study Investigators. Early sedation with dexmedetomidine in ventilated critically ill patients and heterogeneity of treatment effect in the SPICE III randomised controlled trial. *Intensive Care Med*. 2021 Apr;47(4):455-466. doi: 10.1007/s00134-021-06356-8. Epub. 2021 Mar 8. PMID: 33686482.
 34. Shehabi Y, Howe BD, Bellomo R, Arabi YM, Bailey M, Bass FE et al. Early sedation with dexmedetomidine in critically ill patients. *New England Journal of Medicine*. 2019 Jun 27;380(26):2506-2517. Doi: 10.1056/NEJMoa1904710.
 35. Ber JA, Malec M, Bienert A, Nowicka M, Żurański Łukasz, Grześkowiak E, Hartmann-Sobczyńska R, Sobczyński P. The pharmacodynamics of dexmedetomidine in elderly cardiac patients undergoing analgosedation in the ICU. *JMS [Internet]*. 2018 Mar. 12 [cited. 2022 Dec. 12];86(4):265-71. Available from: <https://jms.ump.edu.pl/index.php/JMS/article/view/264>.
 36. European Medicine Agency. Direct healthcare professional communications (DHPC): Dexmedetomidine: Increased risk of mortality in intensive care unit (ICU) patients ≤65 years. Accessed: 9.12.2022 r.
 37. Yoo H, Iirola T, Vilo S, Manner T, Aantaa R, Lahtinen M, Scheinin M, Olkkola KT, Jusko WJ. Mechanism-based population pharmacokinetic and pharmacodynamic modeling of intravenous and intranasal dexmedetomidine in healthy subjects. *Eur J Clin Pharmacol*. 2015 Oct;71(10):1197-207. doi: 10.1007/s00228-015-1913-0. Epub. 2015 Aug 2. PMID: 26233335; PMCID: PMC7167593.
 38. Li A, Yuen VM, Goulay-Dufaj S, Sheng Y, Standing JF, Kwok PCL, Leung MKM, Leung AS, Wong ICK, Irwin MG. Pharmacokinetic and pharmacodynamic study of intranasal and intravenous dexmedetomidine. *Br J Anaesth*. 2018 May;120(5):960-968. doi: 10.1016/j.bja.2017.11.100. Epub. 2018 Feb 2. Erratum in: *Br J Anaesth*. 2018 Sep;121(3):687. PMID: 29661413.
 39. Chang YF, Chao A, Shih PY, Hsu YC, Lee CT, Tien YW, Yeh YC, Chen LW; NTUH Center of Microcirculation Medical Research (NCMMR). Comparison of dexmedetomidine versus propofol on hemodynamics in surgical critically ill patients. *J Surg Res*. 2018 Aug;228:194-200. doi: 10.1016/j.jss.2018.03.040. Epub. 2018 Apr 11. PMID: 29907211.
 40. El Mourad MB, Shaaban AE, El Sharkawy SI, Afandy ME. Effects of Propofol, Dexmedetomidine, or Ketofol on Respiratory and Hemodynamic Profiles in Cardiac Patients Undergoing Transesophageal Echocar-

- diography: A Prospective Randomized Study. *J Cardiothorac Vasc Anesth*. 2021 Sep;35(9):2743-2750. doi: 10.1053/j.jvca.2020.11.013. Epub. 2020 Nov 10. PMID: 33262033.
41. Dubin A, Lattanzio B, Gatti L. The spectrum of cardiovascular effects of dobutamine – from healthy subjects to septic shock patients. *Rev Bras Ter Intensiva*. 2017 Oct-Dec;29(4):490-498. doi: 10.5935/0103-507-X.20170068. PMID: 29340539; PMCID: PMC5764562.
 42. DeWitt ES, Black KJ, Thiagarajan RR, DiNardo JA, Colan SD, McGowan FX, Kheir JN. Effects of commonly used inotropes on myocardial function and oxygen consumption under constant ventricular loading conditions. *J Appl Physiol* (1985). 2016 Jul 1;121(1):7-14. doi: 10.1152/jappphysiol.00058.2016. Epub. 2016 May 5. PMID: 27150829; PMCID: PMC5504386.
 43. Olofsen E, Sigtermans M, Noppers I, Niesters M, Mooren R, Bauer M, Aarts L, Sarton E, Dahan A. The dose-dependent effect of S(+)-ketamine on cardiac output in healthy volunteers and complex regional pain syndrome type 1 chronic pain patients. *Anesth Analg*. 2012 Sep;115(3):536-46. doi: 10.1213/ANE.0b013e31825496f6. Epub. 2012 May 10. PMID: 22575567.
 44. Wu Z, Li J, Wang C, Yang J, Chen X, Yang W, Xiong Z, Peng X. Characterization of cardiovascular depression effect for propofol during anesthesia induction period on morbidly obese patients. *Biomed Pharmacother*. 2018 Oct;106:618-623. doi: 10.1016/j.biopha.2018.06.158. Epub. 2018 Jul 11. PMID: 29990851.
 45. Cattermole GN, Leung PY, Ho GY, Lau PW, Chan CP, Chan SS, Smith BE, Graham CA, Rainer TH. The normal ranges of cardiovascular parameters measured using the ultrasonic cardiac output monitor. *Physiol Rep*. 2017 Mar;5(6):e13195. doi: 10.14814/phy2.13195. PMID: 28320891; PMCID: PMC5371563.
 46. Dutta S, Lal R, Karol MD, Cohen T, Ebert T. Influence of cardiac output on dexmedetomidine pharmacokinetics. *J Pharm Sci*. 2000 Apr;89(4):519-27. doi: 10.1002/(SICI)1520-6017(200004)89:4<519::AID-JPS9>3.0.CO;2-U. PMID: 10737913.
 47. Kurnik D, Muszkat M, Li C, Sofowora GG, Solus J, Xie HG, et al. Variations in the α 2A -adrenergic receptor gene and their functional effects. *Clin Pharmacol Ther*. 2006;79(3):173–85. doi: 10.1016/j.clpt.2005.12.049.
 48. Maas JJ, Pinsky MR, de Wilde RB, de Jonge E, Jansen JR. Cardiac output response to norepinephrine in postoperative cardiac surgery patients: interpretation with venous return and cardiac function curves. *Crit Care Med*. 2013 Jan;41(1):143-50. doi: 10.1097/CCM.0b013e318265ea64. PMID: 23128382.

Supplementary material

Genetic method

As a first step, DNA was isolated from frozen anti-coagulated whole blood using an E.Z.N.A.® Blood DNA Kit (Omega Bio-Tek). The DNA purification procedure was carried out according to the manufacturer's instruction [1]. The isolated DNA was stored at 20°C.

Genotype identification was carried out by real-time polymerase chain reaction with high-resolution melting analysis (real-time PCR-HRM) using a LightCycler® 480 II system (Roche® Diagnostic GmbH, Mannheim, Germany). One single nucleotide polymorphism (SNP) of an α 2-adrenergic receptor gene was selected for the study – *ADR2A*55* (rs553668). A primer pair was designed for a PCR amplification reaction using Oligo 7.6 software (Primer Analysis Software, Colorado, USA) and is presented below.

F: 5' GCTGCCCTTAGCATTTTTCTT 3'
R: 5' GCTAATCCCCTTCCATTCC 3'

The optimal annealing temperature (50°C) was evaluated by real-time PCR amplification with a gradient of annealing temperature using LightCycler® 96 (Roche® Diagnostic GmbH, Mannheim, German. Software: LightCycler® 96 1.1.0.1320, 2011, Roche Diagnostic International Ltd.). LightCycler® 480 High Resolution Melting Master kit was used to perform real-time PCR. The reaction was performed according to the manufacturer's instruction [2]. The amplification products were analyzed by high resolution melting curve analysis. The obtained data were evaluated using LightCycler® 480 Gene Scanning Software.

References

1. Omega BIO-TEK. D3392 E.Z.N.A.® DNA Mini Kit Protocol. <https://www.omegabiotek.com/product/e-z-n-a-blood-dna-mini-kit/> (date accessed: 29.12.2020).
2. Roche. LightCycler® 480 High Resolution Melting Master – Instruction for Use Version 7. <https://pim-eservices.roche.com/LifeScience/Document/7fbff181-4394-e611-6a9e-00215a9b3428> (date accessed: 29.12.2020).

Table S1. The hemodynamic and pharmacodynamic parameters monitored before and during dexmedetomidine infusion.

| Patient's symbol | Baseline values | | | | | Mean values | | | | | | | | |
|------------------|-----------------|----------------------------|----------|----------------|------------|-------------|------------|-----------|----------------------------|------------|----------------|--------------|-------------|--------------|
| | BIS | CI [L/min/m ²] | SVV [%] | HR [beats/min] | SBP [mmHg] | DBP [mmHg] | MAP [mmHg] | BIS | CI [L/min/m ²] | SVV [%] | HR [beats/min] | SBP [mmHg] | DBP [mmHg] | MAP [mmHg] |
| 1001 | 71 | 2.1 | 17.0 | 91 | 161 | 85 | 107 | 54.17 | 2.01 | 13.08 | 75.80 | 128.44 | 65.02 | 79.17 |
| 1002 | - | - | - | 94 | 187 | 87 | 120 | - | - | - | 59.79 | 146.33 | 67.85 | 108.63 |
| 1003 | 53 | 2.4 | 9.0 | - | 80 | 38 | 53 | 77.00 | 3.45 | 9.75 | 60.00 | 105.37 | 45.62 | 73.67 |
| 1004 | 70 | - | - | 125 | 153 | 74 | 101 | 66.40 | 3.45 | 7.25 | 72.80 | 167.50 | 78.50 | 110.00 |
| 1005 | 67 | - | - | - | 190 | 82 | 116 | 74.25 | - | - | 62.50 | 154.00 | 75.75 | 98.12 |
| 1006 | 77 | 2.9 | 7.0 | 81 | 128 | 81 | 102 | 72.83 | 2.70 | 6.00 | 72.71 | 102.87 | 55.00 | 73.12 |
| 1007 | 63 | 2.4 | 10.0 | 73 | 120 | 73 | 76 | 66.50 | 2.69 | 8.00 | 74.00 | 83.67 | 52.89 | 66.71 |
| 1008 | 39 | 3.9 | 9.0 | 72 | 172 | 61 | 86 | 40.40 | 3.11 | 5.81 | 62.74 | 151.90 | 57.82 | 85.24 |
| 1009 | 52 | 6 | 11.0 | - | 158 | 64 | 91 | 53.37 | 3.86 | 6.60 | 94.67 | 106.20 | 57.40 | 74.90 |
| 10010 | 83 | 3.2 | 3.0 | 86 | 137 | 63 | 94 | 80.40 | 3.10 | 3.90 | 72.50 | 122.60 | 51.80 | 73.00 |
| 10011 | 71 | 2.9 | 8.0 | - | 139 | 75 | 100 | 65.00 | 2.25 | 9.50 | 66.50 | 103.43 | 58.57 | 75.57 |
| 10012 | 75 | 2.6 | 7.0 | 83 | 190 | 106 | 140 | 80.20 | 2.07 | 15.25 | 71.86 | 119.50 | 64.37 | 91.00 |
| 10013 | 77 | 3.0 | 5.6 | 73 | 185 | 63 | 109 | 55.00 | 3.67 | 6.25 | 60.17 | 137.50 | 44.67 | 70.33 |
| 10014 | 74 | 2.7 | 14.0 | 106 | 115 | 70 | 85 | 70.00 | 2.48 | 7.33 | 80.75 | 89.44 | 55.87 | 69.13 |
| 10015 | 70 | 2.6 | 4.0 | 65 | 142 | 79 | 103 | 62.50 | 2.17 | 3.00 | 59.47 | 135.23 | 74.47 | 95.06 |
| 10016 | 53 | 3.0 | 3.8 | 75 | 166 | 80 | 119 | 50.86 | 1.96 | 10.60 | 70.17 | 114.12 | 66.50 | 84.75 |
| 10017 | 70 | 2.3 | 2.0 | 60 | 107 | 53 | 72 | 76.29 | 2.56 | 3.75 | 63.33 | 119.00 | 54.25 | 72.50 |
| 10018 | 84 | 3.8 | 4.0 | - | 194 | 68 | 106 | 55.14 | 2.37 | 5.75 | 59.92 | 139.93 | 62.36 | 86.21 |
| 10020 | 75 | - | - | 88 | 155 | 78 | 110 | 78.29 | 3.50 | 6.00 | 64.73 | 113.82 | 58.82 | 79.94 |
| 100116 | 77 | 3.2 | 7.0 | 65 | 142 | 60 | 90 | 51.86 | 2.93 | 9.17 | 64.79 | 132.29 | 58.57 | 83.64 |
| 10021 | 56 | 2.2 | 5.0 | 68 | 122 | 58 | 83 | 63.32 | 2.42 | 5.62 | 71.41 | 120.33 | 56.14 | 79.97 |
| median | 70.5 | 2.9 | 7.0 | 78 | 153 | 73 | 101 | 65.70 | 2.69 | 6.60 | 66.50 | 120.00 | 58.57 | 79.94 |
| range | 39-84 | 2.1-6.0 | 2.0-17.0 | 60-125 | 80-194 | 38-108 | 53-140 | 40.4-80.4 | 1.96-3.86 | 3.00-15.25 | 59.50-94.70 | 83.67-167.50 | 44.67-78.50 | 66.71-110.00 |

Table S2. Changes in cardiac output and stroke volume variation baseline value in patients received noradrenaline.

| Patient's symbol | Baseline value | Cardiac index [Lmin ⁻¹ m ⁻²] | | Stroke volume variation [%] |
|------------------|----------------|---|--|-----------------------------|
| | | Mean value during dexmedetomidine infusion | | |
| 10015 | 2.6 | 2.1 | | 4 |
| 10018 | 3.8 | 2.0 | | 4 |
| 100116 | 3.2 | 2.6 | | 12 |
| 10021 | 2.2 | 2.4 | | 5 |

A simple model of human walking

Leonardo Campanelli

All Saints University School of Medicine, Toronto, Canada



Corresponding author: leonardo.s.campanelli@gmail.com

Received: 2023-02-10

Accepted: 2023-03-01

Published: 2023-03-01

How to Cite: Campanelli L. A simple model of human walking. *Journal of Medical Science*. 2023;92(1);e568. doi:10.20883/medical.e817

DOI: <https://doi.org/10.20883/medical.e817>

Keywords: human locomotion, gait, inverted pendulum model, modelling



© 2023 by the author(s). This is an open access article distributed under the terms and conditions of the Creative Commons Attribution (CC BY-NC) licence. Published by Poznan University of Medical Sciences

ABSTRACT

Aim. We investigate Alexander's inverted pendulum model, the simplest mathematical model of human walking. Although it successfully explains some kinematic features of human walking, such as the velocity of the body's centre of mass, it does not account for others, like the vertical reaction force and the maximum walking speed. This paper aims to minimally extend Alexander's model in such a way as to make it a viable and quantitative model of human walking for clinical biomechanics.

Material and methods. In order to compare the predictions of Alexander's model with experimental data on walking, we incorporate in it a robust phenomenological relation between stride frequency and stride length derived in the literature, and we introduce a step-angle dependent muscle force along the pendulum. We then analytically solve the pendulum's motion equation and find the corresponding analytical expression for the average walking speed.

Results. The values of the average walking speed for different heights predicted by our model are in excellent agreement with the ones obtained in treadmill experiments. Moreover, it successfully predicts the observed walking-running transition speed, which occurs when the stride length equals the height of an individual. Finally, our extended model satisfactorily reproduces the experimentally observed ground reaction forces in the midstance and terminal stance phases. Consequently, the predicted value of the (height-dependent) maximum walking speed is in reasonable agreement with the one obtained in more sophisticated models of human walking.

Conclusions. Augmented with our minimal extensions, Alexander's model becomes an effective and realistic model of human walking applicable in clinical investigations of the human gait.

1. Introduction

The physics and mathematics of animal locomotion are fundamental in several disciplines. For example, biomechanical models can allow paleobiologists to deduce the main characteristics of the locomotion of extinct animals from their fossilized remains (see [1]). In athletics, mathematical models of human locomotion can attempt to

determine the theoretical optimum performance in certain events such as race walking (see [2]). However, medical engineers and clinical biomechanists are instead concerned with animal locomotion because of its relevance to determining limb and joint forces, which play a crucial role in rehabilitation from either injury or disease (see [3]).

Human walking is one of the simplest gaits of terrestrial locomotion among legged animals. Nevertheless, a clear and definitive understanding of the energetics, stability, and kinematics still needs to be included (for a review of analytical modelling and experimental studies of human walking, see [4]).

Theoretical and experimental works on human walking have focussed on energetics and stability or kinematics. In the former case, mechanical energy principles are applied to relate the mass-specific metabolic energetic cost and mechanical cost of transport to the dynamical properties of gait (see [5–7]). In the latter case, which is more relevant to clinical biomechanics, Newtonian dynamical equations applied to simple inertial models of jointed rigid bodies are used to determine the motion of the components during walking (see [8]).

The simplest model of human walking is the two-dimensional “Alexander’s inverted pendulum (IP) model” [9], which consists of a simple inverted pendulum where the whole body mass concentrates in a single particle. It was introduced in the late 70s, although probably, the first indirect references to an inverted pendulum as a model of human walking date back to 1953 [10]. In recent years, a great variety of two-dimensional kinetic models based on the IP model have been developed to mimic better and understand the pattern of human walking.. These models include springs [11–16], dampers [17], and additional segments and joints, or either additional segments or joints [18, 19] (for other works based on the IP model, see [20–24]).

The apparent limitation of two-dimensional models of human walking is that they are unable to describe the lateral dynamics of the gait. Such dynamics can only be studied by more sophisticated three-dimensional models, like those constructed in [25–29]. In particular, the vertical, horizontal, and lateral ground reaction forces (GRF) predicted by the recent three-dimensional bipedal model by Liang et al. [30] agree with experimental data.

Since the introduction of the IP model by Alexander, the level of complexity of walking models has increased, as the number of parameters needed to reproduce quantitatively and in a satisfactory way the characteristics of the human gait. Moreover, Alexander’s model cannot describe the

lateral motion and the transition from one step to another. On the other hand, its simplicity has attracted many authors’ attention over the years (see [2, 18, 31, 32]) as the kinematics and dynamics of walking during the double support phase (where the transition from one step to another occurs) are not as crucial for clinical biomechanics as the kinematics and dynamics of walking in the single support phase. Also, the importance of lateral motion in clinical application is subdominant, at least at first approximation, for the vertical and horizontal ones. While Anderson and Pandy [31] briefly described the GRF in the IP model, Buczek et al. [32] performed a more detailed analysis and compared the prediction of the model about GRF and velocity of the center of mass with gait data for regular walking. This work was extended by McGrath et al. [18] by including fast and slow walking speeds, which are essential for clinical considerations (the inclusion of an actuated hip joint to the IP model, although engaging in that it reproduced the experimentally measured hip moment curve, did not result in significant changes in the kinematics of the centre of mass and ground reaction forces). These studies conclude that that, while the horizontal and vertical velocities of the centre of mass and the horizontal GRF in the midstance and terminal stance phases agree reasonably well with experimental data, the vertical component of the GRF does not, especially for fast walking.

One of the goals of this paper is to extend these works by including a step-angle-dependent muscle force along the IP in such a way as to reproduce the experimentally observed vertical GRFs in the single support phase. Also, we will show that Alexander’s model successfully predicts the observed walking-running transition speed.

2. Methods and Results

2.1. The inverted pendulum model: Generalities

The human body, while walking, can be represented as an inverted pendulum with variable moment of inertia concerning the instantaneous axis of rotation subject to different (natural) forces and torques. Alternatively, one can assume a constant moment of inertia and regard the telescopic actions of the body (principally due to the

swinging limbs) as generating inertial forces and torques.

In this latter case, the scalar projection along the instantaneous axis of rotation of the equation of motion $\dot{\mathbf{L}} = \boldsymbol{\tau}_{\text{net}}^{(\text{ext})}$, \mathbf{L} is the angular momentum, reads

$$I\ddot{\theta}(t) = \tau_{\text{net}}^{(\text{ext})}. \quad (1)$$

Here, I is the constant moment of inertia concerning the instantaneous axis of rotation y (see **Figure 1**),

$$\tau_{\text{net}}^{(\text{ext})} = \tau_g + \tau_{\text{int}} \quad (2)$$

is the net external torque, τ_g is the gravitational torque, and τ_{int} is the body-ground interaction torque generated by the muscle forces and includes all telescopic actions. Also, a dot denotes differentiation regarding time, and θ is the angle formed by the pendulum and the vertical (the z -axis in **Figure 1**). Notice that θ is measured starting from the vertical and is negative (positive) on the left (right) of the z -axis.

In order to solve the above equation of motion, one has to know the exact expression of the

(time-dependent) torques generated by the body muscles during the entire gait cycle.

It is important to observe, however, that the kinematics (horizontal and vertical velocities of the centre of mass) and dynamics (ground reaction forces) of walking are experimentally symmetrical concerning the vertical, at least in the first approximation [4] and especially for slow and regular walking allowing us to focus our analysis on the phase of the gait cycle that goes from the double-support phase to the vertical. Moreover, roughly speaking, the effect of the first part of the propulsion force is impulsive, with the propulsion force provided by the gluteus maximus of the supporting leg and by the swinging of the opposite leg. In contrast, the second part of the propulsion spreads out more temporally and is provided essentially by the gastrocnemius [33]. However, the centre of mass of the gastrocnemius, and then the point of application of the force generated by it, is situated below the knee so that its contribution to the interaction torque is reduced concerning that given by the gluteus maximus, whose point of application is near to the centre of mass of the body. In the first approximation, the interaction torque generated by the gastrocnemius can be neglected. Accordingly, the gluteus maximus and the swing-

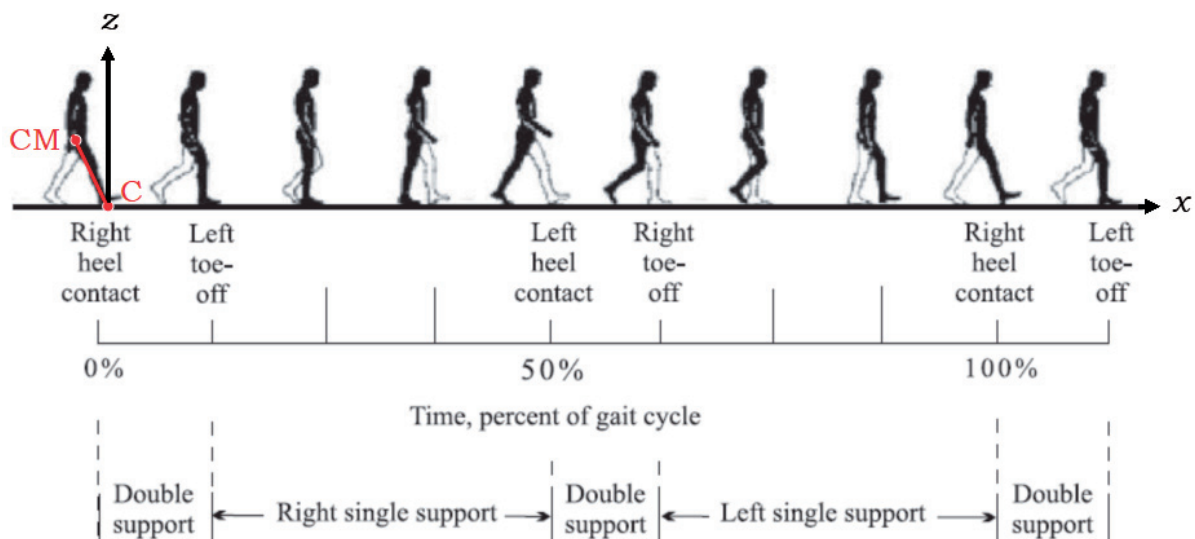


Figure 1. Schematic view of human walking during a gait cycle (adapted from [4]). In the stiff-leg approximation, the trajectory of the centre of mass of the walker (point CM) is an arc of a circle whose centre is the point of contact body-ground (point C). The angle between the (stiff) leg and the vertical axis is the "step angle" θ . In the inverted pendulum model of human walking, θ coincides with the angle formed by the z -axis and the line connecting CM and the fixed point C. In the model discussed below, the muscle force F_{muscle} is directed along the leg. Notice that in the text and following [18], we will assume the duration of the double support phase to be 10% of the gait cycle and that the supporting leg reaches the vertical position at 30% of the gait cycle.

ing of the opposite leg, principally during the second part of the double support phase, provide the only propulsion force.

As already noticed, Alexander's model cannot describe the transition from one step to another during the double support phase. Thus, its application must be limited to the single support phase. In this phase, which is the most important one in clinical studies, the interaction torque is negligible, and the gravitational force ultimately determines the dynamics of the inverted pendulum.

Referring to **Figure 1**, the gravitational torque is given by

$$\tau_g = -mgr_{\text{cm}} \sin \theta \quad (3)$$

where m is the mass of the body, $g = 9.8\text{m/s}^2$ is the acceleration of gravity, r_{cm} is the distance between the fixed point and the centre of mass of the body, and \mathbf{j} is the unit vector along the y -axis (the body is moving in the positive x -direction).

The solution of Eq. (1) in the single support phase will be discussed in Sec. 2.4. In the rest of this section, we introduce some physical quantities significant for the following discussions about the kinematics and dynamics of Alexander's model.

The moment of inertia I can be written as

$$I = \delta mr_{\text{cm}}^2 \quad (4)$$

where δ is a dimensionless parameter. The value $\delta = 1$, which will be used throughout this paper, corresponds to the simple case where all the body mass concentrates in the centre of mass (simple inverted pendulum). Moreover, we write

$$r_{\text{cm}} = \sigma h \quad (5)$$

where σ is a dimensionless parameter and h is the body height. Henceforth, we will use the value $\sigma = 0.56$, corresponding to an erect person with arms at the side [34]. The period of the IP oscillation (equal to the stride time) can be written as

$$t_s = 2\pi \sqrt{\frac{h}{\xi g}}, \quad (6)$$

where ξ is a dimensionless parameter that generally depends on the initial step angle θ_0 .

2.2. Average speed of walking

Two fundamental parameters in human gait are the stride frequency $f_s = 1/t_s$ and stride length L_s . Although it has been shown that they have distinct effects on gait variability, a strong positive linear correlation has been found between them in free walking [35],

$$L_s = af_s + b, \quad (7)$$

where $a \simeq 1.7$ and $b \simeq -0.30$. The analysis in [35] was performed on individuals of an average height of $h = 1.65\text{m}$. Inserting Eq. (7) into Eq. (6) and solving for ξ , we find

$$\xi = \frac{1}{g} \left(\frac{2\pi}{a}\right)^2 (4\sigma h \sin|\theta_0| - b)^2, \quad (8)$$

where we used Eqs. (5) and (6). As a working hypothesis, let us assume ξ to be independent of the height of a person (this *ansatz* is justified *a posteriori* in that the speed of walking predicted by the IP model agrees well, as we will show, with the experimental data from individuals of very different heights). In this case, a and b scale as $a \propto h^{3/2}$ and $b \propto h$, respectively. Writing $a = a_0 h^{3/2}$ and $b = b_0 h$, we then have

$$\xi = \frac{1}{g} \left(\frac{2\pi}{a_0}\right)^2 (4\sigma \sin|\theta_0| - b_0)^2, \quad (9)$$

where $a_0 = 0.80$ and $b_0 = -0.18$, or

$$\xi(s) = 0.207 + 2.28s + 6.26s^2, \quad (10)$$

where we have defined

$$s = \frac{L_s}{h} = 4\sigma \sin|\theta_0|. \quad (11)$$

Let us now calculate the average walking speed, defined as the horizontal component of the velocity of the centre of mass, averaged over the stride time. In our case, this corresponds to $\bar{v}_x = L_s/t_s$, so that

$$\bar{v}_x = \frac{s}{2\pi} \sqrt{\xi(s)gh}. \quad (12)$$

Notice that the results in [35] are valid for walking speeds between 0.75m/s and 1.80m/s for a height of 1.65m, which means that the expression for $\xi(s)$ can be trusted when the initial step angle is in the interval $0.27 \lesssim |\theta_0| \lesssim 0.45$ (this

Table 1. Physical characteristics (h , h_{leg} , and L_s/h), walking speed ($\overline{v_x}$), and Froude number (Fr) of the four stature-age groups analyzed in [5]. An asterisk indicates the prediction of the inverted pendulum model.

| Group | h (m) | h_{leg} (m) | L_s/h | $\overline{v_x}$ (m/s) | $\overline{v_x^*}$ (m/s) | Fr | Fr* |
|-------|-------------|----------------------|-------------|------------------------|--------------------------|-------------|-------------|
| A | 1.14 ± 0.02 | 0.58 ± 0.02 | 0.76 ± 0.03 | 0.96 ± 0.04 | 0.95 ± 0.07 | 0.16 ± 0.01 | 0.16 ± 0.02 |
| B | 1.42 ± 0.02 | 0.77 ± 0.02 | 0.76 ± 0.02 | 1.03 ± 0.03 | 1.06 ± 0.06 | 0.14 ± 0.01 | 0.15 ± 0.01 |
| C | 1.62 ± 0.01 | 0.86 ± 0.01 | 0.78 ± 0.02 | 1.13 ± 0.04 | 1.19 ± 0.06 | 0.15 ± 0.01 | 0.17 ± 0.02 |
| D | 1.77 ± 0.01 | 0.94 ± 0.01 | 0.76 ± 0.02 | 1.21 ± 0.04 | 1.19 ± 0.07 | 0.16 ± 0.01 | 0.15 ± 0.01 |

implies that Eq. (12) is valid for velocities between 0.78m/s and 1.88m/s for a height of 1.80m).

The step length is about 38% of a person's height during regular walking [5] ($s \approx 0.76$), corresponding to a step angle of about $|\theta_0| \approx 0.35$ (20°). For an "average individual" of height $h = 1.80\text{m}$, then, the average speed for regular walking is predicted to be around 1.2m/s (4.3km/h), in agreement with the experimental result of [5]. Equation (12) also returns walking speeds in good agreement with the ones experimentally measured in [5] and shown in **Table 1**. Here, h is the height, h_{leg} is the leg length, L_s/h is the ratio of the stride length to the height, $\overline{v_x}$ is the walking speed at the minimum measured metabolic cost of transport, and Fr is the Froude number for four different stature-age groups (named A, B, C, and D in [5]). In the sixth and eighth columns, we report the values of the average walking speed, $\overline{v_x^*}$, and Froude number, Fr*, as predicted by the inverted pendulum model.

Interestingly, the average walking speed is well approximated by the expression

$$\overline{v_x} \approx 1.21 \left(\frac{|\theta_0|}{20^\circ} \right)^{1.72} \left(\frac{h}{1.80\text{m}} \right)^{1/2} \text{m/s}. \quad (13)$$

Notice that the maximum percentage deviation of the above-approximated expression from the exact one is less than 0.62% for $0.20 \leq |\theta_0| \leq 0.61$, namely well below the typical statistical error of about 4% in [5]. From Eq. (13), it follows that the average walking speed (given that a person's height is a fixed parameter) is controlled, in regular walking, only by the value of the initial step angle.

2.3. Walking-running transition

A spontaneous transition from walking to running is expected in humans at sufficiently high speeds (see [36–39]). Although in the past, such a transition was believed to occur in order to minimize the energetic cost of locomotion, it is now

widely accepted that the ultimate reason for it has a physiological/kinematic origin: fatigue and discomfort in the tibialis anterior and other dorsiflexor muscles of the ankle are the triggers for the transition [40].

The walking-running transition can be kinematically described by the so-called Froude number $\text{Fr} = v^2/gL$, where v and L are the typical speed and height of the hip joint from the ground of a moving animal, respectively [36]. In our case, we can define the Froude number as

$$\text{Fr} = \frac{\overline{v_x}^2}{gh_{\text{leg}}}, \quad (14)$$

where h_{leg} is the leg length. From Eq. (12), and writing

$$h_{\text{leg}} = \frac{h}{\rho}, \quad (15)$$

we find

$$\text{Fr} = \frac{\rho}{4\pi^2} s^2 \xi(s). \quad (16)$$

For regular walking ($s \approx 0.76$) and taking $\rho = 1.9$ [5], we find $\text{Fr} \approx 0.15$, a value independent of an individual's height. This result agrees with the value experimentally determined in [5] for four different stature-age groups, as shown in **Table 1**.

It is believed that the preferred transition speed from walking to running takes place at a Froude number of about 0.5 [36]. In our model with $\rho = 1.9$, this value of Fr corresponds to $s = 1.0$ (and in turn to $|\theta_0| \approx 0.46$ or $|\theta_0| \approx 26.5^\circ$), i.e. the walking-running transition takes place, approximately, when the stride length equals the height of the individual. For $s = 1$, the average walking speed at the walking-running transition is about $\overline{v_x} \approx 1.9\text{m/s}$ (6.9km/h) for a height of $h = 1.70\text{m}$, which is in excellent agreement with the results of Hreljac et al. [41] who found $\overline{v_x} = 1.88 \pm 0.11\text{m/s}$ for 11 individuals with $h = 1.70 \pm 0.08\text{m}$.

2.4. Kinematics: Horizontal and vertical velocities

Equation (1) describes the body's motion during the entire gait cycle. However, as discussed in Sec. 2.1, the interaction torque should be addressed during the single support phase. In this phase, then, the equation of motion reads

$$\theta'' = \sin\theta, \quad (17)$$

where we used Eqs. (2) and (3). Here, a prime denotes differentiation regarding t/t_0 and

$$t_0 = \sqrt{\frac{I}{mr_{cm}g}} = \sqrt{\frac{\sigma\delta h}{g}}. \quad (18)$$

The solution of Eq. (17) with Dirichlet boundary conditions $\theta(0) = \theta_0$ and $\theta(t_s/t_0) = 0$ is easily found,

$$\theta(t) = -2\text{am}(u|\mu), \quad (19)$$

where $\text{am}(u|\mu)$ is the Jacobi amplitude for the Jacobi elliptic functions. Here,

$$u = \chi\left(1 - \frac{4t}{t_s}\right), \mu = -\frac{\pi^2}{4\sigma\delta\xi\chi^2}, \quad (20)$$

and x is implicitly defined by

$$\chi = F\left(-\frac{\theta_0}{2}|\mu\right), \quad (21)$$

where $F(\phi|\mu)$ is the elliptic integral of the first kind [42]. A graph of x as a function of $|\theta_0|$ for $\delta = 1$ and $\sigma = 0.56$ is given in **Figure 2**.

The angular speed $\omega(t) = \dot{\theta}(t)$ is

$$\omega(t) = \omega_f \text{dn}(u|\mu), \quad (22)$$

where $\text{dn}(u|\mu)$ is the Jacobi elliptic function of dn type and $\omega_f = \omega(t_s/4)$ is the angular speed at the vertical,

$$\omega_f = \frac{8\chi}{t_s}. \quad (23)$$

The horizontal and vertical components of the velocity of the centre of mass, v_x and v_z , are

$$v_x(t) = \omega \cos\theta, v_z(t) = -\omega \sin\theta. \quad (24)$$

They are shown in **Figure 3** as a function of time (expressed as a percentage of the gait cycle) for three different walking speeds. Following [18], we present data and our results for half of the gait cycle, from the middle of one double support phase (at 5% of the gait cycle) to the middle of the next (at 55% of the gait cycle). The dashed lines are the one-standard-deviation experimental data from Winter [43, 44], which refer to a person of height $h = 1.80\text{m}$. In contrast, the continuous ones are the predictions of the inverted pendulum model. Finally, **Table 2** describes the best-fit values for the fitted parameter θ_0 and the corresponding average speeds of walking. The left vertical continuous line indicates the end of one double support phase at 10% of the gait cycle, while the right one is the beginning of the next double support phase at 50%.

As it is clear from the figure, the horizontal velocities predicted by the IP model fit very well the experimental data, from slow to fast walking and on the entire gait cycle. The vertical ones, however, agree only in the midstance and terminal stance phases, whose boundaries are indicated by the two dotted vertical lines. Roughly speaking, the start of the midstance is at 15% of

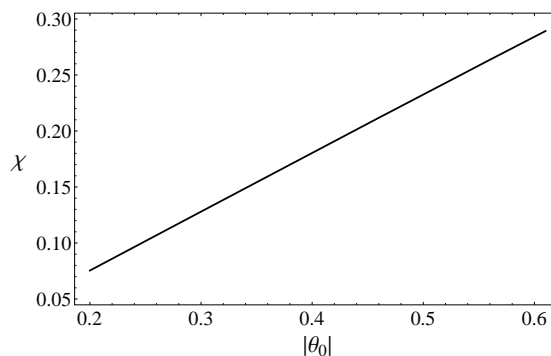


Figure 2. The function $x(\theta_0)$, implicitly defined by Eq. (21), for $\delta = 1$ and $\sigma = 0.56$.

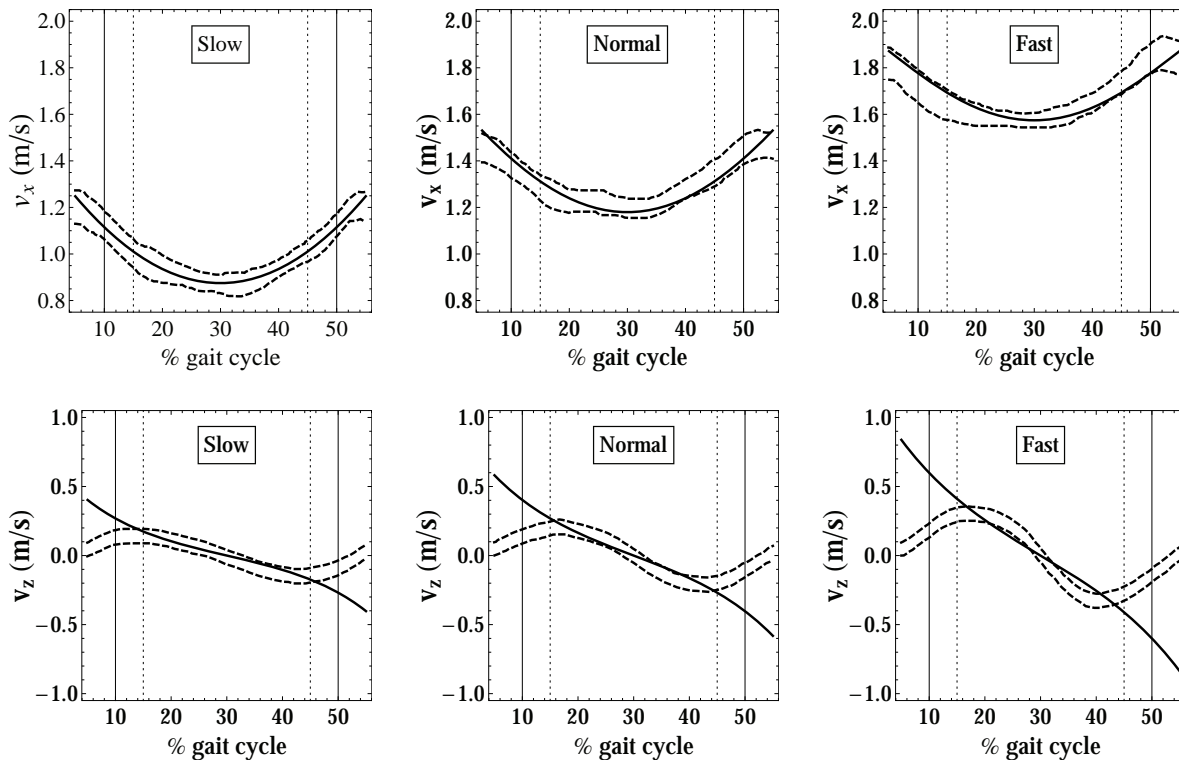


Figure 3. The horizontal (v_x) and vertical (v_z) components of the velocity of the centre of mass in the inverted pendulum model of human walking as a function of time (expressed as a percentage of the gait cycle) for three different walking speeds from the middle of one double support phase (at 5% of the gait cycle) to the middle of the next (at 55% of the gait cycle). The dashed lines are the one-standard-deviation experimental data from Winter [43, 44], while the continuous ones are the (best-fit) predictions of the inverted pendulum model. The left dotted vertical line indicates the end of one double support phase at 10% of the gait cycle, while the right one is the beginning of the next double support phase at 50%. The midstance phase extends from 15% of the gait cycle (left dotted vertical line) to the vertical (30% of the gait cycle). The terminal stance phase starts at the vertical and ends at 45% of the gait cycle (right dotted vertical line).

Table 2. Best-fit values of the initial step angle θ_0 for the three gaits depicted in Figure 3 and the corresponding average walking speeds. Also indicated are the best-fit values of the coefficients a_n of the quartic polynomial in Eq. (28).

| Gait | $ \theta_0 $ | \bar{v}_x (m/s) | a_0 | a_1 | a_2 | a_3 | a_4 |
|--------|--------------|-------------------|---------|---------|-------|--------|-------|
| Slow | 0.312 | 1.00 | -0.0559 | 0.286 | 9.63 | -6.73 | -122 |
| Normal | 0.363 | 1.30 | -0.126 | 0.00350 | 13.9 | -0.303 | -102 |
| Fast | 0.421 | 1.68 | -0.193 | 0.0102 | 17.6 | -2.82 | -86.8 |

the gait cycle (left dotted vertical line), and the end of the terminal stance is at 45% (right dotted vertical line) [4].

2.5. Dynamics: Ground reaction forces

In Alexander's IP model of human walking, the vertical (F_z) and horizontal (F_x) ground reaction forces are

$$\frac{F_z}{mg} = (\cos\theta - t_0^2 \omega^2) \cos\theta \quad (25)$$

and

$$F_x = F_z \tan\theta, \quad (26)$$

respectively. As a function of time and normalized to the body weight, these forces are shown in Figure 4 by dot-dashed (grey) lines (the other notations are as in Figure 3).

As it is clear from the figure, while the predicted horizontal GRFs agree with the observed ones (especially in the single support phase), the vertical ones are not. The simple IP model cannot reproduce the characteristic "M" shape of the vertical GRF. Moreover, in the midstance and ter-

minimal stance phases, the concavity of F_z is opposite to the one experimentally observed. Finally, Alexander's model predicts a maximum reaction at the vertical instead of the experimentally observed minimum.

The fact that the IP model does not account for the vertical force–time history can be explained by the omission, in the model, of the muscle forces (natural and inertial) generated by the body during the entire gait cycle, as explained in Sec. 2.1. On the other hand, the profile of the horizontal and vertical velocities of the centre of mass is well predicted by the model in the mid-stance and terminal stance phases, suggesting that in the single support phase, although active, they do indeed produce a little torque.

For this reason, and as a working hypothesis, let us introduce a time-dependent muscle force, F_{muscle} , directed along the pendulum (positive if pointing towards the fixed point, negative otherwise). The vertical reaction force becomes

$$\frac{F_z}{mg} = \left(\cos \theta - t_0^2 \omega^2 + \frac{F_{\text{muscle}}}{mg} \right) \cos \theta, \quad (27)$$

while the horizontal one is the same as in Eq. (26), with F_z replaced by the new expression (27).

Since the angle θ is generally small, we can expand F_{muscle} in terms of the step angle as

$$\frac{F_{\text{muscle}}}{mg} = \sum_{n=0}^N a_n \theta^n, \quad (28)$$

where the coefficients a_n are, in general, functions of the initial step angle θ_0 (we will neglect a possible dependence of a_n on δ , σ , m , and h).

The continuous lines in **Figure 4** are the vertical and horizontal ground reaction forces when the muscle force is included. They were obtained by fitting the experimental data on the vertical reaction force by using Eq. (27). We found a good agreement with the data by truncating the expansion (28) to the fourth order (the inclusion of higher order terms did not improve the fit appreciably). **Table 2** depicts the values of the fitted parameters a_0 , a_1 , a_2 , a_3 and a_4 .

As it is clear from the figure, the introduction of a muscle force along the IP reproduces well

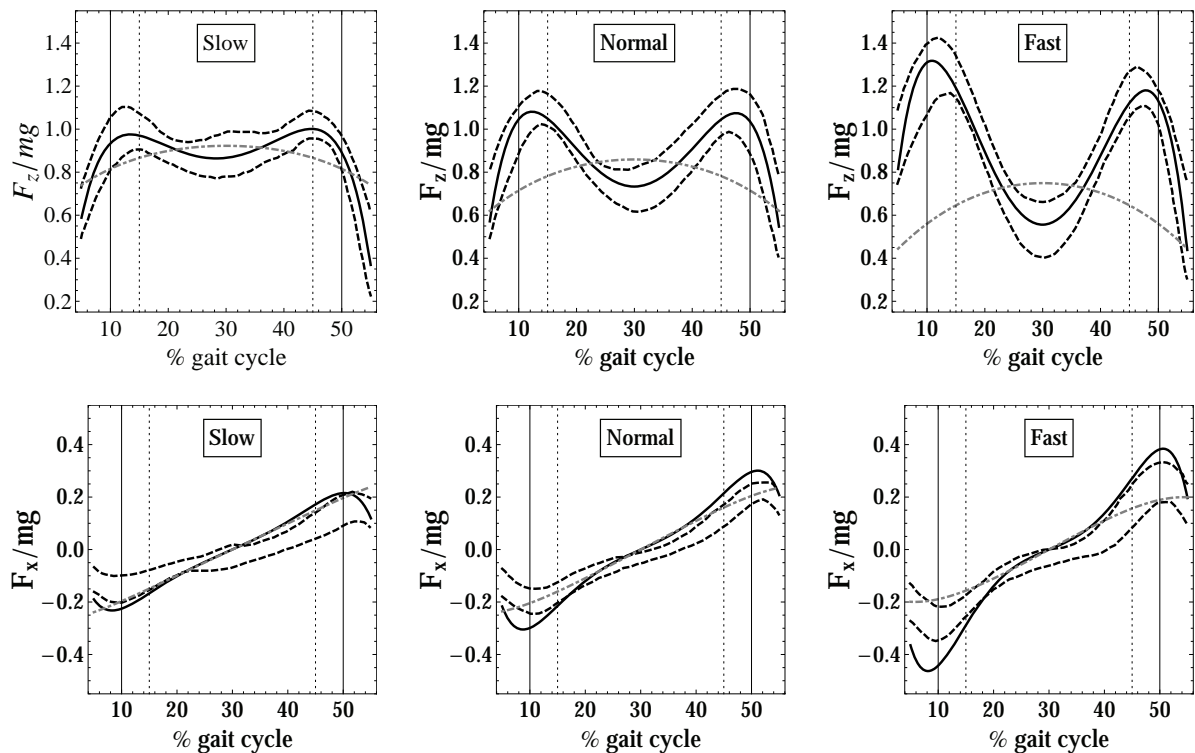


Figure 4. The horizontal (F_x) and vertical (F_z) ground reaction forces (normalized to the body weight mg) as a function of time (expressed as a percentage of the gait cycle) for three different walking speeds (the same of Figure 3). The dashed lines are the 1 standard-deviation experimental data from Winter [43, 44], while the dot-dashed (gray) lines are the prediction of the Alexander's IP model (with no muscle forces). The continuous lines are the (best-fit) predictions of the IP model with the inclusion of the muscle force (28). Vertical lines are as in **Figure 3**.

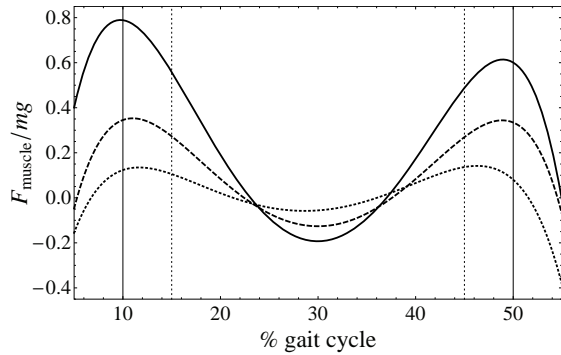


Figure 5. The muscle force in Eq. (28) (normalized to the body weight mg and for $N = 4$) as a function of time (expressed as a percentage of the gait cycle) for three different walking speeds: slow (dotted line), regular (dashed line), and fast (continuous line). The values of the expansion coefficients a_n and the corresponding average walking speeds for the three gaits are given in Table 2. Vertical lines are as in Figure 3.

the vertical GRFs from slow to fast walking and in the entire gait cycle. The horizontal GRFs are satisfactorily reproduced only in the midstance and terminal stance phases.

Figure 5 shows the muscle force (28) that the body must generate to produce the ground reaction forces in Figure 4 as a function of time. As discussed in Sec. 2.1, this force includes telescopic actions that could be, in principle, determined in more realistic and sophisticated models of human walking. However, it is plausible to assume that inertial forces are subdominant around the vertical compared to the ones generated by the gastrocnemius and the soleus [33]. These strong propulsive forces lift the heel and then are principally directed upward along the supporting leg, thus explaining the negative valley in the force-time diagram of Figure 5. The magnitude of these forces is crucial for the determination of the maximum speed of walking, as discussed in the next section.

2.6. Maximum speed of walking

In our simplified walking model, two conditions must be met to walk (for a general discussion of physical constraints during walking, see [45]). They are the condition of “no sliding” and the condition of “no-fly”, the latter being violated when dynamical effects cause a “lifting” of the supporting foot (the point of contact body-ground). Assuming that the coefficient of static friction between the ground and the fixed point is suffi-

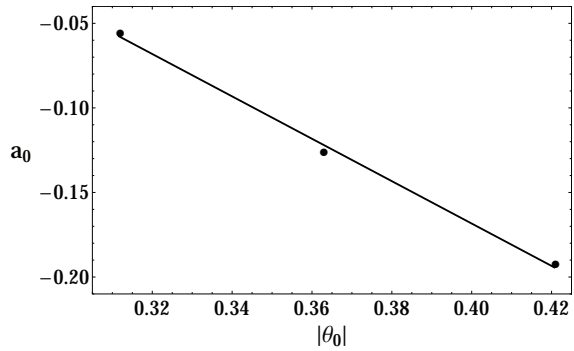


Figure 6. The parameter a_0 in Eq. (28) and Table 2 as a function of $|\theta_0|$. The continuous line is the best-fitting line.

ciently large to prevent sliding, the no-fly condition, $F_z > 0$, gives the value of the maximum initial step angle as the solution of the equation

$$t_0 \omega_f = 1 + a_0. \quad (29)$$

The above equation can be solved if the explicit expression of a_0 as a function of the initial step angle is known (notice that a_0 is equal to the value of the muscle force per unit body weight at the vertical). An approximate expression for a_0 can be obtained by interpolating the three values of a_0 in Table 2 for slow, regular, and fast walking. These values are shown in Figure 6 together with the line of best-fit,

$$a_0 = 0.333 - 1.25|\theta_0|. \quad (30)$$

Inserting the above equation in Eq. (29) and solving for θ_0 , we find the maximum initial step angle $|\theta_0|^{(\max)} = 0.61$ (35°). This value is both outside the interpolation range (see Table. 2) and outside the range of θ_0 where the expression of $\xi(s)$ can be safely trusted (see discussion in Sec. 2.2). Interestingly enough, however, the corresponding value of the maximum speed of walking for a height of $h = 1.75\text{m}$, $\bar{v}_x^{(\max)} \simeq 3.1\text{m/s}$ (11km/h), agrees with the result of Marshall who found, by using a more sophisticated model of human walking, a maximal velocity between 2.7m/s and 3.3m/s (depending on the magnitude of the pelvic rotation).

3. Discussion

Alexander's model is the simplest model of human walking. If, on the one hand, its mathematical simplicity has attracted the attention of biomechanists, on the other hand, it results in two ineradicable limitations:

- (i) It cannot describe the transition from one step to another, and, as for any two-dimensional model of human walking,
- (ii) it cannot describe the lateral dynamics of the gait.

Moreover, it does not account for the temporal shape of the vertical reaction force and the maximum walking speed.

However, the mechanics of walking during the double support phase (where the transition from one step to another takes place) and the lateral motion are less important for clinical applications than the properties of the horizontal and vertical motions in the single support phase. For this reason, we added two new features to Alexander's model to make its predictions compatible with the observed vertical reaction force and the maximum walking speed.

First, we incorporated into the model a phenomenological relation between the stride frequency and stride length as determined in treadmill experiments. Second, we introduced a step-angle dependent force along the pendulum to simulate the effects generated during the single support phase by telescopic actions and propulsive muscle forces.

These minimal modifications make Alexander's model more physiologically representative and provide insight into the role of muscle forces during walking. In particular, we found that

- (i) the experimental vertical reaction forces are fully reproduced by the extended model, as it is clear from the upper panels of **Figure 4**;
- (ii) the muscle force at the vertical, primarily generated by the gastrocnemius and the soleus, critically contributes to the determination of the maximum speed of walking [see Eq. (29)];
- (iii) the average speed of walking (see **Table 1**) and the walking-running transition speed (see the end of Sec. 2.3) agree with the ones found experimentally.

Finally, our extended Alexander's model is entirely solvable; indeed, we have provided an exact analytical solution to its equation of motion,

which differs from the other extensions mentioned in the Introduction based on multiple pendulums, including springs and dampers. Unfortunately, in this case, the mechanics must be simplified to be analyzed analytically, and numerical methods must be used, resulting in a consequent loss of simplicity.

4. Conclusions

We have considered the two-dimensional inverted pendulum model of human walking, where the human body while walking, is approximated by a simple inverted pendulum. During a gait cycle and in the second part of the double support phase, propulsion torques are generated, which start the rotation of the inverted pendulum. Braking forces terminate such a rotation in the first part of the next double support phase. Although the pendulum model cannot describe such phases, it can reproduce the main characteristics of human gait in the single limb support phase, particularly in the midstance and terminal stance phases. To simplify our analysis, we have assumed that no propulsion/braking torques are active during the single limb support phase.

The main results of our paper are as follows.

- (i) Using a phenomenological relation between stride frequency and stride length based on the literature, we have found an analytical expression for the average walking speed. The average speed is a function of only an individual's initial step angle and height. The predicted values of the average speed for different heights are in excellent agreement with the ones obtained in treadmill experiments.

Moreover, our expression for the average walking speed successfully predicts the observed walking-running transition speed, which, according to our results, occurs when the stride length equals the height of an individual.

- (ii) We have found an exact analytical solution to the equation of motion of the two-dimensional inverted simple pendulum. Together with the phenomenological stride frequency-stride length relation, such a solution fits the experimentally observed horizontal and vertical velocities of the body's centre of mass as a function of time in the midstance and ter-

minal stance phases for different gaits, from slow to fast walking.

- (iii) The classical Alexander's model of human walking, which consists of a free inverted pendulum, does not reproduce the experimentally observed vertical ground reaction forces. On the other hand, we have shown that the introduction of quartic step-angle dependent muscle force along the pendulum allows the "forced" IP model to fit, rather well, the observed ground reaction forces in the mid-stance and terminal stance phases in slow, regular, and fast walking.
- (iv) Finally, we have shown that the forced inverted pendulum model, when the muscle force values are extrapolated above the walking-running transition, gives a value of the height-dependent maximum walking speed, which is compatible with the one obtained in more sophisticated three-dimensional models of human walking.

Acknowledgements

The author would like to thank the editor and two anonymous referees for constructive suggestions and comments on an earlier version of this paper.

Conflict of interest statement

The authors declare no conflict of interest.

Funding sources

There are no sources of funding to declare.

References

1. Nyakatura JA, Melo K, Horvat T, Karakasiliotis K, Allen VR, Andikfar A, Andrada E, Arnold P, Lauströer J, Hutchinson JR, Fischer MS, Ijspeert AJ. Reverse-engineering the locomotion of a stem amniote. *Nature*. 2019;351:351-355.
2. Harrison AJ, Molloy PG, Furlong LAM. Does the McNeill Alexander model accurately predict maximum walking speed in novice and experienced race walkers? *J Sport Health Sci*. 2018;7:372-377.
3. Lu TW, Chang CF. Biomechanics of human movement and its clinical applications. *Kaohsiung J Med Sci*. 2012;28:S13-S25.
4. Racic V, Pavic A, Brownjohn JMW. Experimental identification and analytical modelling of human walking forces: Literature review. *J Sound Vib*. 2009;326:1-49.
5. Weyand PG, Smith BR, Puyau MR, Butte NF. The mass-specific energy cost of human walking is set by stature. *J Exp Biol*. 2010;213:3972-3979.
6. Massaad F, Lejeune TM, Detrembleur C. The up and down bobbing of human walking: a compromise between muscle work and efficiency. *J Physiol*. 2007;582(2): 789-799.
7. Faraji S, Wu AR, Ijspeert AJ. A simple model of mechanical effects to estimate metabolic cost of human walking. *Sci Rep*. 2018;8:10998.
8. Marshall AE. A Dynamical Model for the Stride in Human Walking. *Math Model*. 1983;4:391-415.
9. Alexander R McN. Mechanics and Scaling of Terrestrial Locomotion. In *Scale Effects in Animal Locomotion*, Pedley TJ, ed., pp. 93-110, Academic Press, London; 1977.
10. Saunders J, Inman V, Eberhart H. The major determinants in normal and pathological gait. *J Bone Jt Surg*. 1953;35A:543-58.
11. Geyer H, Seyfarth A, Blickhan R. Compliant leg behaviour explains basic dynamics of walking and running. *Proceedings of the Royal Society B: Biological Sciences*. 2006;273(1603):2861-2867.
12. Whittington BR, Thelen DG. A simple mass-spring model with roller feet can induce the ground reactions observed in human walking. *J Biomech Eng*. 2009;131(1):011013.
13. Lee M, Kim S, Park S. Resonance-based oscillations could describe human gait mechanics under various loading conditions. *J Biomech*. 2014;44(1):319-322.
14. Martin AE, Schmiedeler JP. Predicting human walking gaits with a simple planar model. *J Biomech*. 2014;47(6):1416-1421.
15. Li T, Li Q, Liu T. An actuated dissipative spring-mass walking model: predicting human-like ground reaction forces and the effects of model parameters. *J Biomech*. 2019;90:58-64.
16. Antoniak G, Biswas T, Cortes N, Sikdar S, Chun C, Bhandawat V. Spring-loaded inverted pendulum goes through two contraction-extension cycles during the single support phase of walking. *Biol Open*. 2019;8(6):bio043695.
17. Kim S, Park S. Leg stiffness increases with speed to modulate gait frequency and propulsion energy. *J Biomech*. 2011;44:1253-8.
18. McGrath M, Howard D, Baker R. The strengths and weaknesses of inverted pendulum models of human walking. *Gait Posture*. 2015;41(2):389-94.
19. Lim H, Park S. Kinematics of lower limbs during walking are emulated by springy walking model with a compliantly connected, off-centered curvy foot. *J Biomech*. 2018;71:119-126.
20. Kuo AD. The six determinants of gait and the inverted pendulum analogy: A dynamic walking perspective. *Human Movement Science*. 2007;26:617-56.
21. Donelan JM, Kram R, Kuo AD. Mechanical work for step-to-step transitions is a major determinant of the metabolic cost of human walking. *J Exp Biol*. 2002;205:3717-27.
22. Kuo AD, Donelan JM, Ruina A. Energetic consequences of walking like an inverted pendulum: step-to-step transitions. *Exerc Sport Sci Rev*. 2005;33:88-97.
23. Koolen T, Boer TD, Rebula J, Goswami A, Pratt J. Capturability-based analysis and control of legged locomotion, Part 1: Theory and application to three simple gait models. *Int J Rob Res*. 2012;31:1094-113.

24. Hong H, Kim S, Kim C, Lee S, Park S. Spring-like gait mechanics observed during walking in both young and older adults. *J Biomech.* 2013;46:77-82.
25. Kuo AD. Stabilization of lateral motion in passive dynamic walking. *Int J Robot Res.* 1999;18(9):917-930.
26. Roos PE, Dingwell JB. Influence of simulated neuromuscular noise on movement variability and fall risk in a 3D dynamic walking model. *J Biomech.* 2010;43(15):2929-2935.
27. Engelsberger J, Ott C, Albu-Schäffer A. Three-dimensional bipedal walking control using divergent component of motion. *Proceedings of. 2013 IEEE/RSJ International Conference on Intelligent Robots and Systems, Tokyo, Japan.* 2013;2600-2607.
28. D. García-Vallejo D, Schiehlen W. 3D-simulation of human walking by parameter optimization. *Arch Appl Mech.* 2012;82(4):533-556.
29. Yang QS, Qin JW, Law SS. A three-dimensional human walking model. *J Sound Vib.* 2015;357:437-456.
30. Liang H, Xie W, Zhang Z, Wei P, Cui C. A Three-Dimensional Mass-Spring Walking Model Could Describe The Ground Reaction Forces. *Mathematical Problems in Engineering.* 2021;2021:1-20.
31. Anderson FC, Pandy MG. Individual muscle contributions to support in normal walking. *Gait Posture.* 2003;17:159-69.
32. Buczek FL, Cooney KM, Walker MR, Rainbow MJ, Concha MC, Sanders JO. Performance of an inverted pendulum model directly applied to normal human gait. *Clin Biomech.* 2006;21:288-96.
33. Ellis RG, Sumner BJ, Kram R. Muscle contributions to propulsion and braking during walking and running: Insight from external force perturbations. *Gait Posture.* 2014;40:594-599.
34. Davidovits P. *Physics in Biology and Medicine.* 5th ed. London (UK): Academic Press; 2019.
35. Danion F, Varraine E, Bonnard M, Pailhous J. Stride variability in human gait: the effect of stride frequency and stride length. *Gait Posture.* 2003;18:69-77.
36. Alexander RMcN. The gaits of bipedal and quadrupedal animals. *Int J Robot Res.* 1984;3:49-59.
37. Turvey MT, Holt KG, Lafiandra ME, Fonseca ST. Can the Transitions to a from Running and the Metabolic Cost of Running Be Determined from the Kinetic Energy of Running? *J Mot Behav.* 1999;31(3):265-78.
38. Hanna A, Abernethy B, Neal Robert J, Burgess-Limerick R. Triggers for the Transitions Between Human Walking and Running. In *Energetics of Human Activity.* Sparrow W (ed). USA: Human Kinetics; 2000;124-64.
39. Raynor AJ, Yi CJ, Abernethy B, Jong QJ. Are transitions in human gait determined by mechanical, kinetic or energetic factors? *Hum Mov Sci.* 2002;21(5-6):785-805.
40. Prilutsky BI, Gregor RJ. Swing- and support-related muscle actions differently trigger human walk-run and run-walk transitions. *J Exp Biol.* 2001;204(13):2277-87.
41. Hreljac A, Imamura RT, Escamilla RF, Edward WB. When does a gait transition occur during human locomotion? *J Sports Sci Med.* 2007;6:36-43.
42. Abramowitz M, Stegun IA (eds). *Handbook of Mathematical Functions with Formulas, Graphs, and Mathematical Tables.* New York: Dover Publications; 1972.
43. Winter DA. *Biomechanics of Human Movement:* John Wiley Sons, Inc.; 1979.
44. Winter DA. *The biomechanics and motor control of human gait: Normal, Elderly and Pathological.* 2nd ed. Waterloo: Waterloo Biomechanics; 1991.
45. Patnaik L, Umanand L. Physical constraints, fundamental limits, and optimal locus of operating points for an inverted pendulum based actuated dynamic walker. *Bioinspir Biomim.* 2015;10:064001.

Formulation of a radiological scoring system to prognosticate patients with primary intracerebral haemorrhage

Krishna Kumar

Department of Neurosurgery, Government Thirumala Devaswom Medical College, Vandanam, Alappuzha, Kerala, India

 <https://orcid.org/0000-0002-4389-1697>

Corresponding author: drprkrishnan77@gmail.com

Harison Gopalan

Government Thirumala Devaswom Medical College, Vandanam, Alappuzha, Kerala, India

 <https://orcid.org/0000-0001-5346-6099>

Jayalakshmi Jayaprakash

Department of Internal Medicine, Government Thirumala Devaswom Medical College, Vandanam, Alappuzha, Kerala, India

 —

Keywords: radiological score, MIVL score, primary intracerebral haemorrhage

Received: 2022-08-23

Accepted: 2023-01-21

Published: 2023-03-30

How to Cite: Kumar K, Gopalan H, Jayaprakash J. Formulation of a radiological scoring system to prognosticate patients with primary intracerebral haemorrhage. Journal of Medical Science. 2023;92(1);e568. doi:10.20883/medical.e724



© 2023 by the author(s). This is an open access article distributed under the terms and conditions of the Creative Commons Attribution (CC BY-NC) licence. Published by Poznan University of Medical Sciences

 DOI: <https://doi.org/10.20883/medical.e724>

ABSTRACT

Background. Primary intracerebral haemorrhage is a neurological condition associated with high morbidity and mortality. Outcome prediction is necessary to allocate the available resources in such cases judiciously. Our study aims to identify the radiological predictors of in-hospital mortality based on a plain CT study of the brain at admission and to develop a prognostic scoring system based on them.

Material and methods. We collected the clinical and radiological data from 182 consecutive patients who presented with primary spontaneous ICH. Bivariate analysis of radiological predictors of in-hospital mortality was undertaken using unadjusted logistic regression. Those variables found to have significance were put into a multivariate logistic regression model. The Results of multivariate logistic regression were treated as a foundation for developing the scoring system.

Results. The mortality rate in our series was 23.6% (N = 43). After multivariate analysis, Midline shift (MLS), presence or absence of intraventricular haemorrhage (IVH), Volume of ICH and Location of haematoma were significant predictors of mortality. Based on the identified radiological variables, a five-score prognostic scoring system (AUROC = 0.925, 95% CI 0.887–0.964) was developed, with higher scores indicating higher mortality.

Conclusions. The established scoring system, MIVL, may help physicians to do better patient counselling regarding outcomes.

Introduction

Primary spontaneous intracerebral haemorrhage (PSICH) accounts for about 4–14% of all forms of stroke and carries a high mortality rate approach-

ing 40% [1–6]. Both medical and surgical treatments are available, but which modality would benefit an individual patient is yet to be clear [7, 8]. Clinical decisions regarding management

strategies are not often straightforward, given the ethical, moral and medical aspects involved in it. It is critical to strike the right balance between excessive but futile healthcare inputs on one side and dangerous self-fulfilling prophecies on the other. Such decisions assume paramount importance, especially when the resources are limited, to allocate them to the right patient with a high overall chance of survival. Literature is rife with several complex prognostic models, including clinical, biochemical, and radiological parameters but a scoring system based on radiological variables alone is lacking [9]. Therefore, in this study, we aim to define the radiological predictors of in-hospital mortality in PSICH based on information gathered from a plain CT scan of the brain obtained at admission and to develop a scoring system that can be adapted in such settings to enable easy exchange of objective prognostic information between healthcare professionals across various disciplines.

Materials and methods

After obtaining approval from the institutional ethics committee, we retrospectively analysed the data collected as a part of a single-centre prospective cohort study of primary ICH undertaken at our tertiary care teaching hospital. Patients who presented with PSICH to our hospital between May 2017 and May 2018 were recruited for the study. The patients or their responsible bystanders consented to the study. Basic demographic information and a detailed clinical history to reveal the chronology of events were collected. The Glasgow Coma Scale (GCS) score on admission and history of hypertension, diabetes mellitus, alcoholism and smoking were also recorded. For the study, the primary intracerebral haematoma was defined as spontaneous blood leakage into the supratentorial brain parenchyma, documented by a plain CT study of the brain. In-hospital mortality was defined as mortality occurring within the first 30 days of admission. Patients with infratentorial bleeds, age above 80 years, with multiple haemorrhages, presenting after 24 hrs of ictus and with secondary ICH due to any cause were excluded from the study.

A plain CT scan of the brain performed on admission was analysed, and the parameters

such as volume of haematoma, midline shift (MLS), intraventricular haemorrhage (IVH), presence or absence of hydrocephalus, side of haematoma and location of haematoma (deep/superficial) were noted. The volume of haematoma was measured by the method described by Kothari et al. [10] using the formula $ABC/2$, where A is the measure in the measurement of the most substantial haemorrhage dimension, B the diameter at 90 degrees to A, and C is the number of slices with haemorrhage multiplied by its thickness. For defining the location, the axial CT cut passing through the foramen of Monro was taken. First, a vertical line is drawn through the midline, and another line 2cm lateral to this line on either side is adjusted to scales. Next, two horizontal lines are drawn along this cut's most prominent anterior and posterior portion of the lateral ventricles. If the haematoma occupies the rectangle bounded by these four lines, it is classified as deep or zone 1. The primary outcome was in-hospital mortality, which was defined as death in the hospital during the current admission or within 30 days after. In-hospital mortality was considered a poor outcome, and the absence of this was defined as recovery the study.

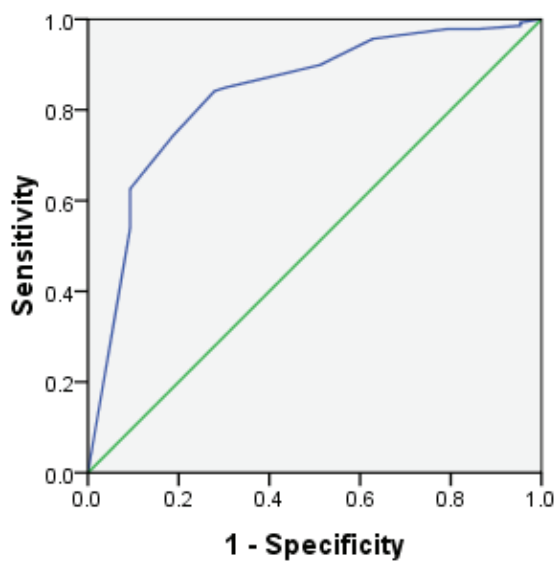
All data were analysed using SPSS software version 16.0 (SPSS Inc., Chicago, Illinois, USA). Continuous variables were stated as means with standard deviations, and categorical variables as percentages. The association between individual radiological parameters and outcome were first estimated using bivariate logistic regression analysis. Then, those radiological parameters showing statistical significance were analysed using a multivariate logistic regression model. Two continuous variables, hematoma volume and MLS were dichotomized using maximum sensitivity and specificity values obtained from the receiver operating curve (ROC). The regression coefficients of each factor in the multivariate logistic model were transformed into a risk score by dividing them by the smallest regression coefficient among the variables and then rounding the quotients to the nearest integer for developing the risk scoring system. Model performance consisting of the area under the receiver operating curve (AUROC) and Hosmer-Lemeshow goodness-of-fit test were further assessed. A *p*-value less than 0.05 was considered significant.

Results

The initial cohort included a total of 201 cases. After applying all the inclusion and exclusion criteria, 182 subjects were recruited for the study. Males constituted 56.6% (N = 103) of our subjects. The whole cohort had a mortality rate of 23.6% (N = 43). The mean age was 62.90 years (median 64.5 years, range 31 to 79 years). Most, 53.84% (N = 98), presented with headache and altered sensorium. Headache alone was the presenting symptom in 20.3% (N = 37) patients, while 25.8% (N = 47) were unconscious at presentation. Prominent risk factors identified were hypertension 112 (61.5%), smoking 108 (59.3%), diabetes mellitus 61 (33.5%), and alcohol intake 58 (31.9%) in that order. Mortality was high within the first 48 hours of ictus (N = 20, 46.5%), and their presenting GCS were also significantly low (7 vs 13, $P <$

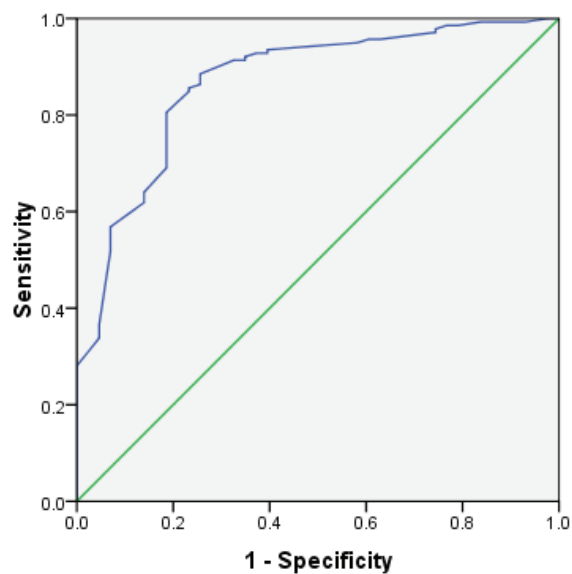
0.001). The mean hospital stay was 11 days. Most were managed along aggressive medical lines (88.4%, N = 161), while a surgical procedure was performed in 11.5% of patients (N = 21). Craniotomy and evacuation were done in 8.8% (N = 16) of patients, and external ventricular drainage alone in 2.7% (N = 5). A significant difference in outcome was not observed between the medical and surgical groups ($P = 0.119$).

The haematoma volume ranged from 4 ml to 230 ml (mean 45.5 ml). Patients with poor outcomes had a mean haematoma volume of 93.9 ml compared to 27.6 ml in those with recovery. The midline shift for the whole series ranged from 0 to 12 mm, with a mean of 2.8 mm. **Figures 1 and 2** show a ROC that was made to test the predictive accuracy of these variables (haematoma volume and MLS). IVH was present in 31.9% (N = 58) and hydrocephalus in 36% (N = 66) of subjects.



Diagonal segments are produced by ties.

Figure 1. ROC (Receiver operating curve) shows the accuracy of Midline shift for a favourable outcome



Diagonal segments are produced by ties.

Figure 2. ROC (Receiver operating curve) shows the accuracy of volume of haematoma for a favourable outcome.

Table 1. Results of bivariate Logistic regression analysis.

| Sl No | Radiological variable | P-value | OR | 95% confidence interval (lower-upper) |
|-------|------------------------------|---------|--------|---------------------------------------|
| 1 | Midline shift | 0.00 | 25.938 | 10.288–65.412 |
| 2 | Volume | 0.00 | 7.395 | 3.275–16.697 |
| 3 | Intraventricular haemorrhage | 0.00 | 6.988 | 2.541–19.214 |
| 4 | Hydrocephalus | 0.062 | 0.510 | 0.252–1.033 |
| 5 | Zone | 0.00 | 12.061 | 5.125–28.366 |
| 6 | Site | 0.826 | 0.926 | 0.466–1.839 |

Haematoma volume, MLS, IVH and location of haematoma attained statistical significance for in-hospital mortality on bivariate analysis (see **Table 1**). Haematoma volume and MLS were closely correlated with GCS. (Pearson correlation -0.663 and -0.612, respectively, $P < .001$). GCS was significantly low in patients with IVH and hydrocephalus ($P < .001$). On multivariate analysis MLS, the presence or absence of IVH, the volume of ICH and the location of haematoma were significant predictors of mortality (see **Table 2**).

The final risk prediction model contained four variables statistically significantly associated with in-hospital mortality in the multivariate

logistic regression analysis. The regression coefficients of all variables in the risk prediction model were transformed into risk scores, as demonstrated in Table 3. The risk scoring system, named MIVL, contained the following variables: 1) Midline shift (≤ 6 mm vs > 6 mm), 2) Intraventricular haemorrhage (present or absent), 3) Volume (≤ 30 ml vs > 30 ml), 4) Location of hematoma (deep vs superficial) as defined above. The sum of scores ranged from a minimum of 0 to a maximum of 5. No patient with a score of 0 died, while 18 (94.7%) patients with a score of 5 expired 30 days after admission (see **Figure 3**). The Hosmer-Lemeshow test yielded a P value of 0.438, indicating ade-

Table 2. OR for in-hospital mortality.

| Predictor variable | OR (95% CI) | P-value |
|------------------------------|------------------|---------|
| Intraventricular haemorrhage | | |
| Present | 6.7 (2.16–20.71) | 0.001 |
| Absent | – | |
| Volume | | |
| >30ml | 4.7 (1.4–15.1) | 0.009 |
| ≤ 30 ml | – | |
| Midline shift | | |
| >6mm | 14.5 (4.8–43.7) | 0.001 |
| ≤ 6 mm | – | |
| Zone | | |
| I | 4.7 (1.5–14.8) | 0.007 |
| II | – | |

Table 3. Determinants of the score.

| Variable | Regression coefficient | Risk score |
|------------------------------|------------------------|------------|
| Intraventricular haemorrhage | | |
| Absent | 0 | 0 |
| Present | 1.903 | 1 |
| Volume of haemorrhage | | |
| ≤ 30 ml | 0 | 0 |
| >30ml | 1.548 | 1 |
| Midline shift | | |
| ≤ 6 mm | 0 | 0 |
| >6mm | 2.680 | 2 |
| Zone of hematoma | | |
| Zone 2 | 0 | 0 |
| Zone 1 | 1.566 | 1 |

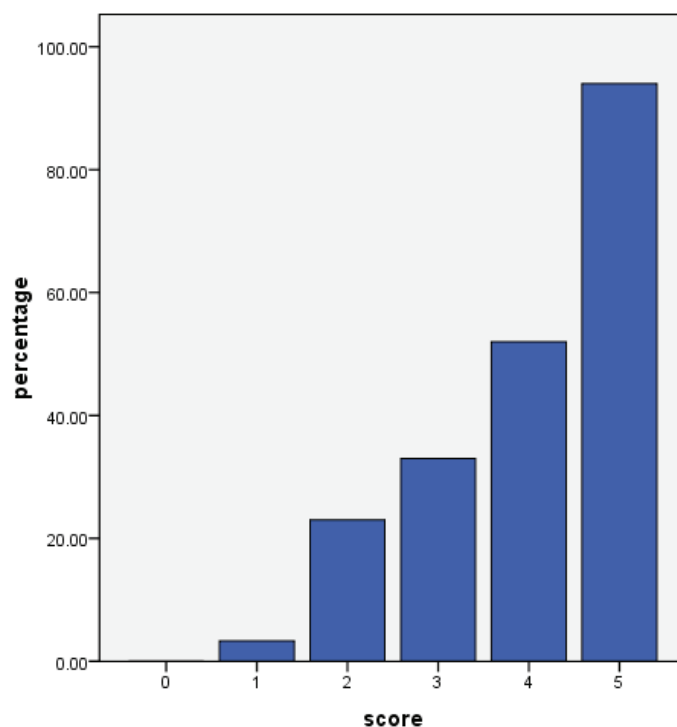


Figure 3. The Y-axis shows in-hospital mortality and the X-axis showing the MIVL score.

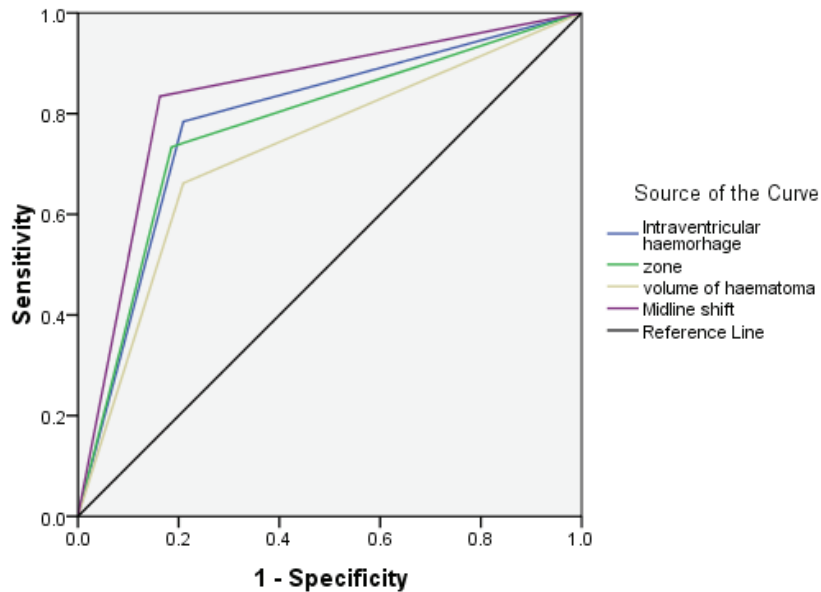


Figure 4. ROC curve for components of the score.

quate goodness-of-fit of the model. In the evaluation of the predictive accuracy of the model, the MIVL score was able to achieve an area under the curve (AUROC) of 0.925. **Figure 4** represents the ROC curve for components of score.

Discussion

Any prognostic scoring model must be simple and accurate, though it would be counterintuitive to assume to be both. In this study, we attempted to develop a simple scoring system based on radiological parameters only to prognosticate patients with primary spontaneous supratentorial intracerebral bleed. Clinical grading scales serve the purpose of providing consistency and standardisation of prognostication in neurological conditions. The intracerebral haemorrhage (ICH) score, one of the first available scores, is the most widely used for prognostication purposes to estimate 30-day mortality following spontaneous ICH [11]. The score is based on the location and volume of ICH, presence of IVH, GCS on admission and age of the patient. The score ranged from 0 (best outcome) to 6 (worst outcome). Thirty-day mortality rates for ICH scores 1, 2, 3 and 4 were 13%, 26%, 72% and 97%, respectively. In their cohort, no patient with a score of 0 died, and all patients with a score of 5 died. No patient had a score of 6 in their cohort.

Mc Cracken et al., in a review of 554 patients, have found that the ICH score did not accurately predict mortality [12]. Patient survival exceeded the ICH score predicted mortality regardless of the intervention. The score ranged from 0 to 11, and 85% of the patients with a FUNC score of 11 reached functional independence at 90 days [14]. Clinical and radiological variables are often combined in many models, which would, however, lead to a problem of collinearity because the radiological variables reflect the clinical condition rather than the cause.

The mass effect produced by the haematoma and associated oedema caused MLS and was a significant prognostic variable in our study. There was a good correlation between haematoma volume and MLS (Pearson's correlation 0.706, $P < 0.05$). Though it is reasonable to assume higher mortality to a higher degree of MLS, the literature does not uniformly endorse this. In several studies, MLS has not been a statistically significant predictor of outcome [15]. One reason is that many of these studies have included infratentorial haemorrhages also, where MLS may be absent. Infratentorial haemorrhages per se constitute a distinct cohort from treatment and prognostic points of view and hence excluded them from our study. The shift of midline structures is also closely linked to brain atrophy. An atrophied brain may tolerate more blood without producing much mass effect. Fogelholm et al.

demonstrated a significant relationship between MLS and outcome [16]. The shift of midline structures has been the most robust outcome predictor in our study and has been weighted more with a score of two points, which would mean that the prognostic implication of midline shift is more in spontaneous bleed.

IVH is consistently associated with poor outcomes across several studies. IVH was associated with a worse outcome in our study, with an OR of 6.7 ($P < 0.001$). Leira et al. [17] showed a 2.6 times chance of neurological deterioration following IVH. Blood is an irritant and can make the patient seizure-prone when collected in the ventricles. It can also obstruct the CSF pathways and produce hydrocephalus. Both these mechanisms augment the morbidity, along with the primary cause. Diringer et al. found that the shift of the pineal body and hydrocephalus were significant predictors of mortality [18]. Our cohort's hydrocephalus had no significant predictor on bivariate analysis (OR 0.51, 95% CI 0.252–1.033), which may result from IVH causing hydrocephalus and including both variables + in a single model will lead to the problem of collinearity. Ex vacuo hydrocephalus may accompany old age, so IVH-associated hydrocephalus can be difficult to distinguish. We have excluded hydrocephalus in our model due to these reasons.

The volume of haematoma is a significant prognosis predictor in several models. We have also identified volume as an important predictor of poor outcomes ($P < 0.001$). Haematoma volumes have been dichotomized into more than or less than 30 ml based on a trade-off between maximum sensitivity and specificity as predicted from ROC, enhancing its ease of usage. Though CT scanners could measure the volume of haematoma more accurately, we have used the ABC/2 method, considering the end users' ease of calculation. Moreover, this method has been found to be accurate with good inter-rater reliability.

Al-Mufti et al. researched various prognostic variables that could affect the outcome [19]. The most studied radiological predictors were the location, expansion, and volume of haematoma, swirl sign, spot sign, peri-haematoma oedema, IVH and hydrocephalus. Broderick et al. [20] have conducted a study of 30-day mortality based on ICH volume. For volumes more than 60cm³, they have reported 93% mortality for deep and 71%

mortality for lobar locations. The location of haematoma also attained statistical significance in our model, with a score of one attributed to deep locations. In a similar study, Flemming et al. [21] described 40 ml as a critical volume which would predict a bad outcome. We used the ROC curve and identified 39 ml as the optimum cut-off volume for poor outcome (sensitivity 79.6%, specificity 83%), while a generally accepted cut-off is set at 30 ml. A worse outcome has also been attributed to haematoma expansion, a volume increase of more than one-third [22].

Brain damage following ICH occurs in three stages [23]. Primary artery rupture and bleeding occur in the first stage, haematoma expansion in the second stage, and brain oedema in the third stage. Haematoma expansion occurs in the first six hours in about 30% of cases, accounting for the high mortality observed on the first day of ictus. After 24 hours, haematomas seldom enlarge [24]. We also observed that 46.5% of deaths occurred in the first 48 hours. By that time, the brunt of the brain damage might have occurred. This pathophysiological profile has clinical repercussions. It may be one reason early surgical intervention does not offer an advantage over aggressive medical counterparts regarding outcomes or functional independence. Some authors believe that surgical treatments are making a comeback [25], but we could not document any significant outcome advantage in our surgical group ($P = 0.119$). Though assuming that the outcomes may be worse for dominant side haemorrhages may be reasonable, we could not identify significance for a particular side. A higher frequency of putaminal haemorrhages was observed on the side of dominant A1 [26].

Different studies have attempted to elucidate prognostic information from radiological data in ICH. The leakage of contrast into the haematoma is called the spot sign [27] and is a grave prognostic marker. It is an indication of active haemorrhage. Delgado Almandoz et al. [28] have developed a spot sign scoring system to predict mortality and poor outcome. But this required a contrast CT scan, which is only sometimes taken as a first-line investigation. The swirl sign, which is classically described in epidural haematoma, can also be seen in intracerebral haemorrhages. This sign shows a low attenuated area with irregular density in the haematoma. If this sign is present, it is an independent predictor of death at one month

[29]. Li Q et al. [30] described the blend sign as the presence of two areas within the haematoma, one relatively hypoattenuating area with an adjacent hyperattenuating area with well-defined margins visible to the naked eye. There should be at least an 18-Hounsfield-unit difference between the two areas. This sign was observed only in 16.9% of patients, but if present, has got 95.5% specificity for predicting haematoma growth. Another sign described by Qi Li et al. is the black hole sign [31]. This is an area of hypoattenuation with clearly visible borders within an area of hyper attenuation with a difference of 28 Hounsfield units. The sign was specific for predicting haematoma growth and was present in 14.6% of patients. Of all the above radiological signs, the spot sign was the most reliable outcome predictor [32]. The heterogeneity of density of the haematoma itself is a marker of poor outcome [33]. However, the signs mentioned above are not present in all patients and hence cannot be uniformly applied to all patients.

Conclusion

In summary, based on radiological data alone, the MIVL score is an easy scoring system for risk stratification and prognostication of patients with supratentorial ICH. The score is simple and will enable an exchange of prognostic information between healthcare professionals across various disciplines, even if clinical data needs to be included, but not to be used as the best indicator of prognosis. The model has been primarily intended to be used in places where resources are limited to take appropriate decisions regarding referral, intensive care or operative interventions and patient counselling regarding the potential outcome. However, the relatively small number of patients in our cohort and its single institutional nature are major limitations of our study.

Acknowledgements

Statement of ethics

The Institutional Ethics Committee granted the ethical approval.

Authors contribution

KK, HG, and JJ prepared the concept and design. KK, HG, and JJ undertook the methodology and wrote the original draft. In addition, JJ did a critical review and final editing.

Acknowledgement

We want to acknowledge the scientific research committee of our institute for allowing us to conduct the study.

Conflict of interest statement

The authors declare no potential conflicts of interest concerning this article's research, authorship, or publication.

Funding sources

The authors received no financial support for the article's research, authorship, or publication.

References

1. Dennis MS. Outcome after brain hemorrhage. *Cerebrovasc Dis.* 2003;16(Suppl 1):9–13.
2. Daniel Agustin Godoy, Gustavo Piñero, Mario Di Napoli. Predicting Mortality in Spontaneous intracerebral hematoma. Can Modification to Original Score Improve the Prediction? *Stroke.* 2006;37:1038-1044.
3. Flaherty ML1, Haverbusch M, Sekar P, Kissela B, Kleindorfer D, Moomaw CJ, Sauerbeck L, Schneider A, Broderick JP, Woo D. Long-term mortality after intracerebral hemorrhage. *Neurology.* 2006 Apr 25;66(8):1182-6.
4. Bilbao G, Garibi J, Pomposo I, Pijoan JI, Carrasco A, Catalán G, González S. A prospective study of a series of 356 patients with supratentorial spontaneous intracerebral hematomas treated in a Neurosurgical Department. *Acta Neurochir (Wien).* 2005 Aug;147(8):823-9.
5. Rohit Bhatia, Hariom Singh, Shaily Singh, Madakaira V Padma, Kameshwar Prasad, Manjari Tripathi, Guresh Kumar, Mamta Bhushan Singh. A prospective study of in-hospital mortality and discharge outcome in spontaneous intracerebral hemorrhage. *Neuro India.* 2013;61:244-8.
6. Fogelholm R, Murros K, and Rissanen A, Avikainen S. Long term survival after primary intracerebral haemorrhage: a retrospective population based study. *J Neurol Neurosurg Psychiatry.* 2005 Nov;76(11):1534-8.
7. McKissock W, Richardson A, Taylor J. Primary intracerebral hemorrhage: A controlled trial of surgical and conservative treatment in 180 unselected cases. *Lancet.* 1961;2:221–6.
8. Batjer HH, Reisch JS, Allen BC, Plaizier LJ, Su CJ. Failure of surgery to improve outcome in hypertensive putaminal hemorrhage. A prospective randomized trial. *Arch Neurol.* 1990;47:1103–6.
9. Witsch J, Siegerink B, Nolte CH, Sprügel M, Steiner T, Endres M, Huttner HB. Prognostication after intracerebral hemorrhage: a review. *Neurol Res Pract.* 2021 May 3;3(1):22. doi: 10.1186/s42466-021-00120-5. PMID: 33934715; PMCID: PMC8091769.
10. Kothari RU, Brott T, Broderick JP, Barsan WG, Sauerbeck LR, and Zuccarello M, Khoury J: The ABCs of measuring intracerebral hemorrhage volumes. *Stroke.* 1996;27:1304-1305.
11. Hemphill JC, 3rd, Bonovich DC, Besmertis L, Manley GT, Johnston SC. The ICH score: a simple, reliable

- grading scale for intracerebral hemorrhage editorial comment: a simple, reliable grading scale for intracerebral hemorrhage. *Stroke*. 2001;32(4):891-897.
12. McCracken DJ, Lovasik BP, McCracken CE, Frerich JM, McDougal ME, Ratcliff JJ, Barrow DL, Pradilla G. The Intracerebral Hemorrhage Score: A Self-Fulfilling Prophecy? *Neurosurgery*. 2019 Mar 1;84(3):741-748. doi: 10.1093/neuros/nyy193. PMID: 29762777.
 13. Gregorio T, Pipa S, Cavaleiro P, Atanasio G, Albuquerque I, Chaves PC, Azevedo L. Prognostic models for intracerebral hemorrhage: Systematic review and meta-analysis. *BMC Med Res Methodol*. 2018;18, 145. <https://doi.org/10.1186/s12874-018-0613-8>.
 14. Rost NS, Smith EE, Chang Y, Snider RW, Chanderraj R, Schwab K, Rosand J. Prediction of functional outcome in patients with primary intracerebral hemorrhage: the FUNC score. *Stroke*. 2008;39(8):2304-2309 <https://doi.org/10.1161/STROKEAHA.107.512202>.
 15. Nag C, Das K, Ghosh M, Khandakar MR. Prediction of Clinical Outcome in Acute Hemorrhagic Stroke from a Single CT Scan on Admission. *N Am J Med Sci*. 2012 Oct;4(10):463-7. doi: 10.4103/1947-2714.101986.
 16. Fogelholm R, Murros K, Rissanen A, Avikainen S. Long term survival after primary intracerebral haemorrhage: a retrospective population based study. *J Neurol Neurosurg Psychiatry*. 2005 Nov;76(11):1534-8. doi: 10.1136/jnnp.2004.055145.
 17. Leira R, Dávalos A, Silva Y, Gil-Peralta A, Tejada J, Garcia M, Castillo J; Stroke Project, Cerebrovascular Diseases Group of the Spanish Neurological Society. Early neurologic deterioration in intracerebral hemorrhage: predictors and associated factors. *Neurology*. 2004 Aug 10;63(3):461-7. doi: 10.1212/01.wnl.0000133204.81153.ac.
 18. Diringner MN, Edwards DF, Zazulia AR. Hydrocephalus: a previously unrecognized predictor of poor outcome from supratentorial intracerebral hemorrhage. *Stroke*. 1998 Jul;29(7):1352-7. doi: 10.1161/01.str.29.7.1352.
 19. Al-Mufti F, Thabet AM, Singh T, El-Ghanem M, Amuluru K, Gandhi CD. Clinical and Radiographic Predictors of Intracerebral Hemorrhage Outcome. *Interv Neurol*. 2018 Feb;7(1-2):118-136. doi: 10.1159/000484571.
 20. Broderick JP, Brott TG, Duldner JE, Tomsick T, Huster G. Volume of intracerebral hemorrhage. A powerful and easy-to-use predictor of 30-day mortality. *Stroke*. 1993 Jul;24(7):987-93. doi: 10.1161/01.str.24.7.987.
 21. Flemming KD, Wijdicks EF, Li H. Can we predict poor outcome at presentation in patients with lobar hemorrhage? *Cerebrovasc Dis*. 2001;11(3):183-9. doi: 10.1159/000047636.
 22. Davis SM, Broderick J, Hennerici M, Brun NC, Diringner MN, Mayer SA, Begtrup K, Steiner T; Recombinant Activated Factor VII Intracerebral Hemorrhage Trial Investigators. Hematoma growth is a determinant of mortality and poor outcome after intracerebral hemorrhage. *Neurology*. 2006 Apr 25;66(8):1175-81. doi: 10.1212/01.wnl.0000208408.98482.99.
 23. Ferro JM. Update on intracerebral haemorrhage. *J Neurol*. 2006 Aug;253(8):985-99. doi: 10.1007/s00415-006-0201-4.
 24. Kazui S, Naritomi H, Yamamoto H, Sawada T, Yamaguchi T. Enlargement of spontaneous intracerebral hemorrhage. Incidence and time course. *Stroke*. 1996 Oct;27(10):1783-7. doi: 10.1161/01.str.27.10.1783.
 25. Menon G. Surgery for spontaneous intracerebral hemorrhage: Emerging trends. *Arch Med Health Sci [serial online]2017 [cited 2021 Dec 20]; 5:65-70*. Available from: <https://www.amhsjournal.org/text.asp?2017/5/1/65/208200>.
 26. Lee JH, Chang CH, Jung YJ, Kim JH. The Relationship Between the Direction of Putaminal Intracerebral Hemorrhage and Anterior Cerebral Artery Predominance. *World Neurosurg*. 2017 Nov;107:211-215. doi: 10.1016/j.wneu.2017.07.169.
 27. Becker KJ, Baxter AB, Bybee HM, Tirschwell DL, Abouelsaad T, Cohen WA. Extravasation of radiographic contrast is an independent predictor of death in primary intracerebral hemorrhage. *Stroke*. 1999;30(10):2025-32.
 28. Delgado Almandoz JE, Yoo AJ, Stone MJ, Schaefer PW, Goldstein JN, Rosand J, Oleinik A, Lev MH, Gonzalez RG, Romero JM. Systematic characterization of the computed tomography angiography spot sign in primary intracerebral hemorrhage identifies patients at highest risk for hematoma expansion: the spot sign score. *Stroke*. 2009 Sep;40(9):2994-3000. doi: 10.1161/STROKEAHA.109.554667.
 29. Selariu E, Zia E, Brizzi M, Abul-Kasim K. Swirl sign in intracerebral haemorrhage: definition, prevalence, reliability and prognostic value. *BMC Neurol*. 2012 Sep 26;12:109. doi: 10.1186/1471-2377-12-109.
 30. Li Q, Zhang G, Huang YJ, Dong MX, Lv FJ, Wei X, Chen JJ, Zhang LJ, Qin XY, Xie P. Blend Sign on Computed Tomography: Novel and Reliable Predictor for Early Hematoma Growth in Patients With Intracerebral Hemorrhage. *Stroke*. 2015 Aug;46(8):2119-23. doi: 10.1161/STROKEAHA.115.009185.
 31. Li Q, Zhang G, Xiong X, Wang XC, Yang WS, Li KW, Wei X, Xie P. Black Hole Sign: Novel Imaging Marker That Predicts Hematoma Growth in Patients With Intracerebral Hemorrhage. *Stroke*. 2016 Jul;47(7):1777-81. doi: 10.1161/STROKEAHA.116.013186.
 32. Sporns PB, Schwake M, Kemmling A, Minnerup J, Schwindt W, Niederstadt T, Schmidt R, Hanning U. Comparison of Spot Sign, Blend Sign and Black Hole Sign for Outcome Prediction in Patients with Intracerebral Hemorrhage. *J Stroke*. 2017 Sep;19(3):333-339. doi: 10.5853/jos.2016.02061.
 33. Barras CD, Tress BM, Christensen S, MacGregor L, Collins M, Desmond PM, Skolnick BE, Mayer SA, Broderick JP, Diringner MN, Steiner T, Davis SM. Density and shape as CT predictors of intracerebral hemorrhage growth. *Stroke*. 2009;40(4):1325-31.

Assessment of dietary habits among Polish women with Hashimoto's disease

Kinga Skoracka

Department of Gastroenterology, Dietetics and Internal Medicine, Poznan University of Medical Science, Poland

 <https://orcid.org/0000-0002-1593-1903>

Corresponding author: kingskoracka@gmail.com

Ewelina Swora-Cwynar

Department of Gastroenterology, Dietetics and Internal Medicine, Poznan University of Medical Science, Poland

 <https://orcid.org/0000-0002-6752-6002>

Aleksandra Królczyk

Department of Gastroenterology, Dietetics and Internal Medicine, Poznan University of Medical Science, Poland

 <https://orcid.org/0000-0001-5006-0421>

Małgorzata Kałużna

Department of Endocrinology, Metabolism and Internal Medicine Poznan University of Medical Sciences, Poland

 <https://orcid.org/0000-0002-2116-4384>

Katarzyna Ziemińska

Department of Endocrinology, Metabolism and Internal Medicine Poznan University of Medical Sciences, Poland

 <https://orcid.org/0000-0001-5377-8834>

Marek Ruchała

Department of Endocrinology, Metabolism and Internal Medicine Poznan University of Medical Sciences, Poland

 <https://orcid.org/0000-0001-9743-2405>

Agnieszka Dobrowolska

Department of Gastroenterology, Dietetics and Internal Medicine, Poznan University of Medical Science, Poland

 <https://orcid.org/0000-0002-3647-5070>

Iwona Krela-Kaźmierczak

Department of Gastroenterology, Dietetics and Internal Medicine, Poznan University of Medical Science, Poland

 <https://orcid.org/0000-0001-5122-8003>

 DOI: <https://doi.org/10.20883/medical.e735>

Keywords: Hashimoto's disease, diet, lifestyle, autoimmune thyroiditis (AIT), Hashimoto's thyroiditis

Received: 2022-09-11

Accepted: 2022-12-28

Published: 2023-03-30

How to Cite: Skoracka K, Swora-Cwynar E, Królczyk A, Kałużna M, Ziemińska K, Ruchała M, Dobrowolska A, Krela-Kaźmierczak I. Assessment of dietary habits among Polish women with Hashimoto's disease. *Journal of Medical Science*. 2023;92(1);e568. doi:10.20883/medical.e735



© 2023 by the author(s). This is an open access article distributed under the terms and conditions of the Creative Commons Attribution (CC BY-NC) license. Published by Poznan University of Medical Sciences

ABSTRACT

Introduction. Selected dietary components are crucial for a properly functioning thyroid gland. Therefore a healthy and balanced diet is crucial for treating patients with Hashimoto's disease.

Aim. This study aims to evaluate the dietary habits of women suffering from autoimmune thyroiditis.

Material and methods. A questionnaire study was conducted in a group of 58 women with Hashimoto's disease and among 42 women without autoimmune thyroiditis using the Food Frequency Questionnaire (FFQ-6). To assess compliance with the normal distribution, we used the Shapiro-Wilk test. The comparative assessment was made using the Student's t-test and Mann-Whitney test. The Chi-square test was used to assess the relationship between the response and the group. A p-value of less than 0.05 was considered significant.

Results. The study showed no significant differences in dietary habits between the two groups. Only 29% (n = 15) of women with HT declared daily consumption of fruits vs 31% (n = 12) in the control group (p = 0.3800), and only 2% (n = 1) declared consuming berries daily vs. 5% (n = 2), (p = 0.5270). The consump-

tion of the recommended several portions of vegetables per day was declared by only 22% (n = 11) of women with HT vs 28% (n = 11) in the control group (p = 0.3983). 42% (n = 24) of women with HT vs 38.5% (n = 16) of controls reported eating cruciferous vegetables several times a week (p = 0.8241). 14% (n = 8) of women with HT vs 19% (n = 8) of women in the control group declared daily consumption of green leafy vegetables (p = 0.3653). Most people in the study group consume nuts and seeds several times a month, and those in the control group several times a week. Most HT respondents also declare not to consume the recommended amount of fish.

Conclusions. The diet of patients with Hashimoto's disease does not differ significantly from that of non-Hashimoto's disease patients. Considering the study results and current scientific knowledge, it seems necessary to undertake educational activities for patients with Hashimoto's disease to increase patient awareness of the impact of diet on the course of the disease.

Introduction

Hashimoto's disease (HT, Hashimoto's Thyroiditis) is the most common chronic autoimmune disease in iodine-sufficient areas. HT is characterized by the presence of autoantibodies directed against thyroid peroxidase (anti-TPO) and thyroglobulin (anti-TG), elevated thyrotropic hormone (TSH) levels, and often reduced levels of free thyroxine (fT4) and sometimes free triiodothyronine (fT3). An ultrasound image of the thyroid gland shows lymphocytic T- and B-cell infiltration, fibrosis, and hypoechoic parenchyma [1, 2]. Occasionally, a thyroid goiter is also present, but in most cases a reduction in thyroid size is observed. Treatment of HT is mainly based on synthetic thyroid hormone therapy [3].

For the development of HT is responsible a complex autoimmune process involving thyroid cells through a chain reaction. Pathogenic mechanisms that may lead to the development of Hashimoto's disease include impaired function of regulatory T cells (Treg, T regulatory cells), which are responsible for inhibiting excessive anti-inflammatory response and protecting the organism from autoimmunity. Possible pathomechanism is also an increase in the activity of follicular helper T cells (Tfh) involved in stimulating the production of B lymphocytes, by increasing the production of interleukin-21 (IL-21). Furthermore, DNA fragments released after cell apoptosis and an altered microRNA profile are thought to initiate and perpetuate the autoimmune process. Infiltrating thyroid T and B lymphocytes show a cytotoxic effect on the cell, leading it to apoptosis and, consequently, to the production of antibodies and increased production of inflammatory cytokines [4].

Among the genes involved in the development of HT, the mainly mentioned are the tissue compatibility system (HLA, Human Leukocyte Antigen) and polymorphisms in the cytotoxic T-lymphocyte antigen 4 (CTLA-4) gene, as well as in the PTPN22, CD14, CD40 and IL2R genes [5]. However, Jabrocka-Hybel et al. in a study on 147 HT patients and 147 healthy individuals, showed that the genetic predisposition factors used for HT development, without taking into account environmental and personal factors, are not sufficient to predict the actual risk of HT [6].

Epidemiological observations show an increasing trend in the incidence of HT since the 1950s. Previously, few cases of the disease were reported, whereas today HT is the most common autoimmune disorder. These observations confirm that, in addition to genetic factors, environmental factors have a huge impact on the development of the disease. Environmental factors include dietary errors, including excessive iodine intake and selenium deficiency, infections, especially hepatitis C, excessive environmental hygiene, stress, certain drugs, cytokine therapies, and lithium salts [7, 8]. Factors predisposing to the development of HT also include the influence of oxidative stress, climate, age, and sex. The initiating effect of an autoimmune response in the thyroid gland has also been attributed to pregnancy [2, 7]. Interestingly, it has been observed that cigarette smoking and moderate alcohol consumption show a protective effect against the development of Hashimoto's disease [8].

In countries where mandatory iodine fortification of food has been introduced for the prevention of diseases caused by an insufficient iodine supply, the incidence of HT has increased, where-

as, in countries with an insufficient iodine supply, HT cases are observed less frequently [9].

Mechanisms explaining why excessive iodine intake may predispose to HT include modification of thyroglobulin at the epigenetic level, resulting in the production of a factor to which the immune system has not yet developed immune tolerance, and excessive induction of apoptosis of thyroid cells, resulting in the release of large numbers of T lymphocytes involved in the autoimmune response [8].

On the other hand insufficient dietary selenium supply is associated with a decrease in the activity of glutathione peroxidase (GPx), thioredoxin reductase (TRx), or iodothyronine deiodase (DIO). Decreased GPx activity is associated with increased production of hydrogen peroxide and thyroid peroxidase, resulting in the destruction of thyroid cells. GPx and TRx have antioxidant activity, so selenium deficiency contributes to a decrease in protective capacity against oxidative stress [8]. Deiodinases are responsible for the conversion of T4 to T3. Selenium can also regulate T lymphocytes, resulting in increased immune tolerance, and has an anti-inflammatory effect. Furthermore, selenium can inhibit the expression of HLA-DR molecules on thyrocytes, suppressing thyroid autoimmunity [9].

It is also worth paying attention to an adequate iron supply due to its significant role in the production of the thyroid hormones T3 and T4 – the enzyme TPO, which is involved in the synthesis of thyroid hormones, is only activated after heme binding [10]. Iron deficiency, which reduces the activity of the TPO enzyme, is more common in HT patients than in the healthy population [9]. Furthermore, it has been suggested that, through its effect on the immune system, also vitamin D may be involved in regulating thyroid function, but research in this area is conflicting [9].

Furthermore, there is an interest in elimination diets, e.g. gluten-free and lactose-free diets, among HT patients. Lactose intolerance is diagnosed in up to 75.9% of HT patients, and 5.9–22.5% of HT patients have positive CD-related autoantibodies [11].

Aim

The aim of this study was to assess eating habits in patients with HT.

Material and methods

We included 58 women with HT in the study group, and 42 women without HT, who were classified as controls. Data were collected from November 2019 to January 2021. A validated Food Frequency Questionnaire (FFQ-6) was used to assess dietary intake, allowing the collection of information on the frequency of consumption of 62 food groups, which simultaneously identifies the intake of 8 main food groups consumed over the preceding 12 months of questionnaire completion. The respondents could declare frequency of consumption by choosing one of the following answers: several times a day, every day, several times a week, several times a month, once a month or less often, never, or almost never.

The inclusion criteria for the study group were female sex and a diagnosis of Hashimoto's disease based on ultrasound and antibody testing. For the control group, the inclusion criteria were: female sex, and no Hashimoto's disease.

Before entering the study, each participant was asked to give written informed consent to participate in the study. Patients were informed that they could withdraw from the study at any stage. All data remained anonymous – each participant was given an anonymous number, which was used in analyses at further stages of the study.

The obtained results of the study were collected in the form of a database with the help of Microsoft Excel. Statistical analyses were carried out using Dell Statistica software. Qualitative data were presented in quantitative and percentage terms. The Shapiro-Wilk test was used to assess the concordance of the thyroid parameters studied with a normal distribution; a comparative assessment of the parameters and selected variables between the control group and the study group was performed using the Student's t-test and the Mann-Whitney test. The Chi-square test was used to assess the relationship between response and group. A p-value of less than 0.05 was considered significant.

The study was approved by the Bioethics Committee at the Poznan University of Medical Sciences (Poland) No. 69/19.

Results

A total of 100 women were enrolled in the study, where 58 women diagnosed with HT were included in the study group, and 42 women not suffering from HT were included in the control group. The mean age of the women in the study group was 31 ± 6.92 years and in the control group the mean age was 29 ± 6.47 years. The characteristics of the thyroid parameters of the study participants are shown in **Table 1**.

We found no statistically significant differences in diet between the group of female patients with Hashimoto's disease and the control group. When asked about the frequency of fruit consumption, the female participants most frequently answered that they consumed fruit several times a week – this answer was given by 44% of the study group and 33% of the control group, respectively, and daily consumption was declared by 29% of the study group and 31% of the control group. However, there was no correlation between responses and group ($p = 0.3800$). Detailed results are shown in **Figure 1**.

The majority of female patients in both groups reported consuming berries several times a month or once a month and less frequently. There was no correlation between responses and group ($p = 0.5270$). Detailed results are shown in **Figure 2**.

Most women in the study group declared to consume vegetables several times a week and daily, while in the control group it was daily and several times a day. There was no correlation between responses and group ($p = 0.3983$). The results are presented in **Figure 3**.

In both groups, most participants reported consuming vegetables several times a week and

several times a month. There was no correlation between responses and group ($p = 0.8241$). The results are shown in **Figure 4**.

Most women in the study group report consuming leafy vegetables several times a week, and those in the control group several times a month. There was no correlation between responses and group ($p = 0.3653$). The results are shown in **Figure 5**.

None of the respondents declared eating legumes several times a day. The most frequent answer in both groups was once a month or less often. There was no correlation between responses and group ($p = 0.8574$). The results are shown in **Figure 6**.

Most women with HT report consuming seeds and grains a few times a week, with the next most frequently chosen answers being a few times a month and never or almost never. In contrast, in the control group, the most frequently selected answer was a few times a month. There was no correlation between responses and group ($p = 0.3299$). The results are presented in **Figure 7**.

None of the respondents declared to eat oily fish several times a day or every day. The most frequent answer given in both groups was never or almost never. There was no correlation between responses and group ($p = 0.8995$). The results are shown in **Figure 8**.

Similarly, none of the respondents declared to consume lean fish several times a day or every day. The most frequent answer given was once a month or less often, and in the control group also several times a month. There was no correlation between responses and group ($p = 0.9679$). The results are shown in **Figure 9**.

Table 1. Comparison of thyroid panel parameters between groups.

| Parameter | Group | Mean | SD | p |
|------------------|---------|--------|--------|------------|
| TSH [uU/ml] | study | 2.76 | 3.42 | p = 0.7 |
| | control | 2.41 | 0.99 | |
| fT3 [pmol/l] | study | 4.89 | 0.77 | p = 0.05 |
| | control | 5.25 | 0.72 | |
| fT4 [pmol/l] | study | 17.04 | 3.41 | p = 0.002 |
| | control | 15.13 | 1.90 | |
| anty-TPO [IU/ml] | study | 155.86 | 149.50 | p < 0.0001 |
| | control | 9.32 | 2.59 | |
| anty-TG [IU/ml] | study | 348.45 | 531.25 | p < 0.0001 |
| | control | 15.24 | 11.91 | |

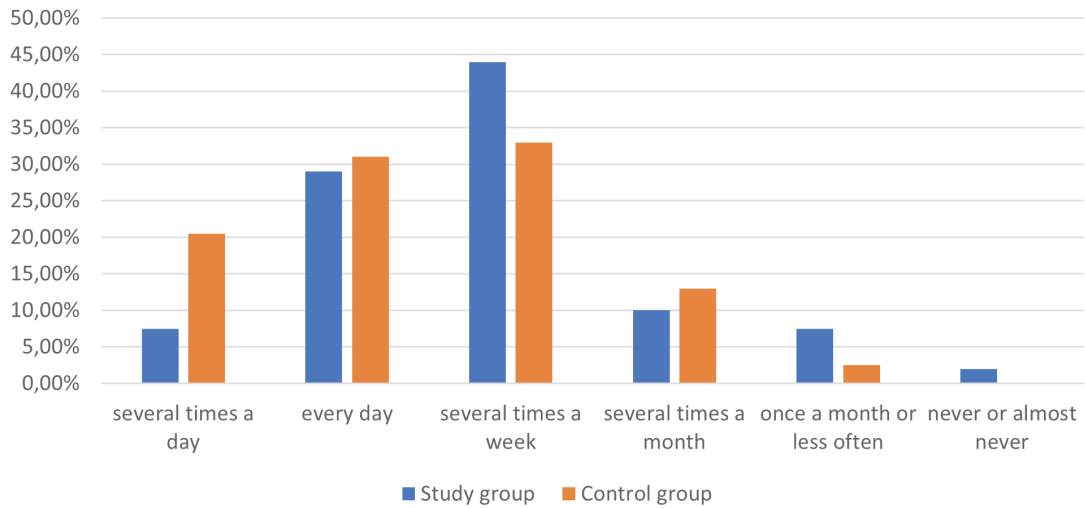


Figure 1. How often in the last 12 months have you drunk or eaten fruits, all types?

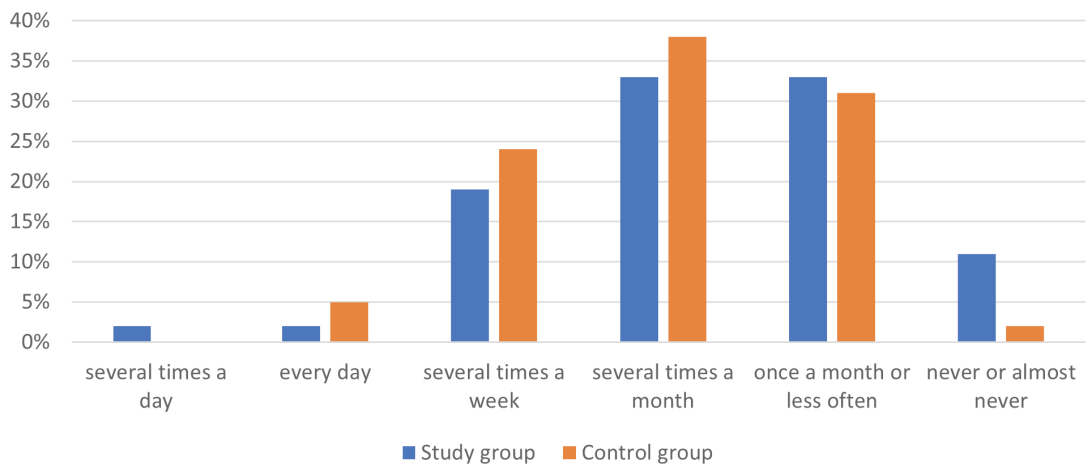


Figure 2. In the last 12 months, how often did you drink or eat berries: strawberries, raspberries, blackberries, blueberries, currants?

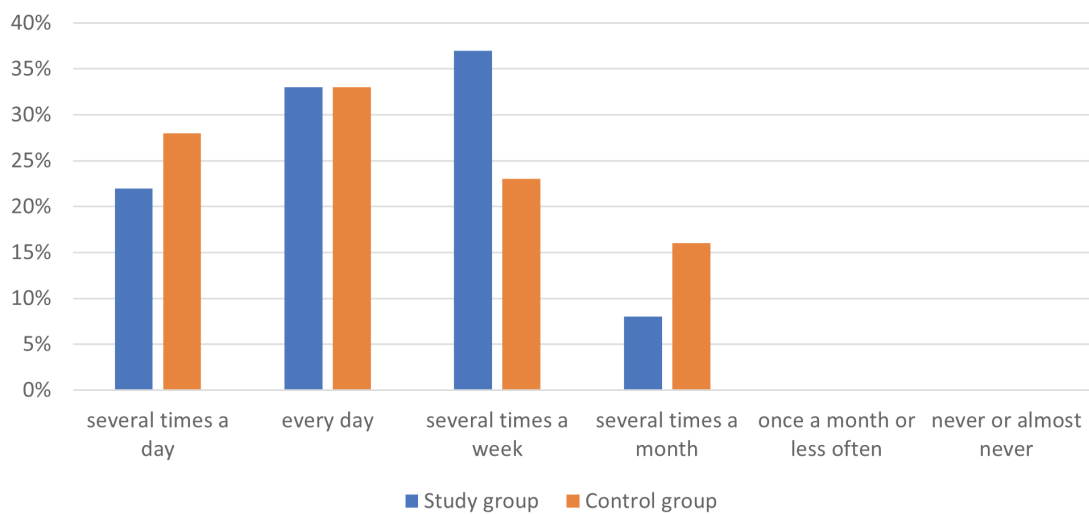


Figure 3. In the last 12 months, how often have you drunk or eaten vegetables, all types?

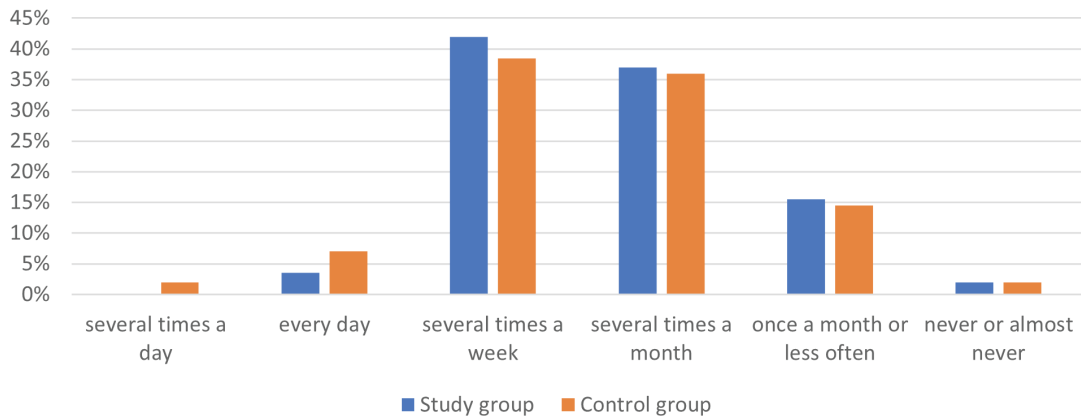


Figure 4. In the last 12 months, how often did you drink or eat cruciferous vegetables: white cabbage, Italian cabbage, red cabbage, Chinese cabbage, brussels sprouts, cauliflower, broccoli, kale?

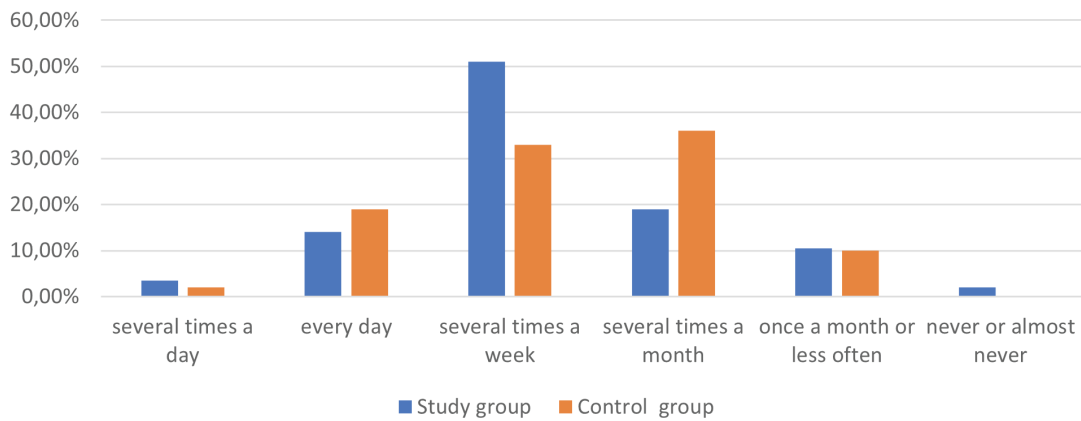


Figure 5. In the last 12 months, how often did you drink or eat leafy green vegetables: spinach, radicchio, butter lettuce, iceberg lettuce, romaine lettuce, rocket, leeks, celery, parsley leaves?

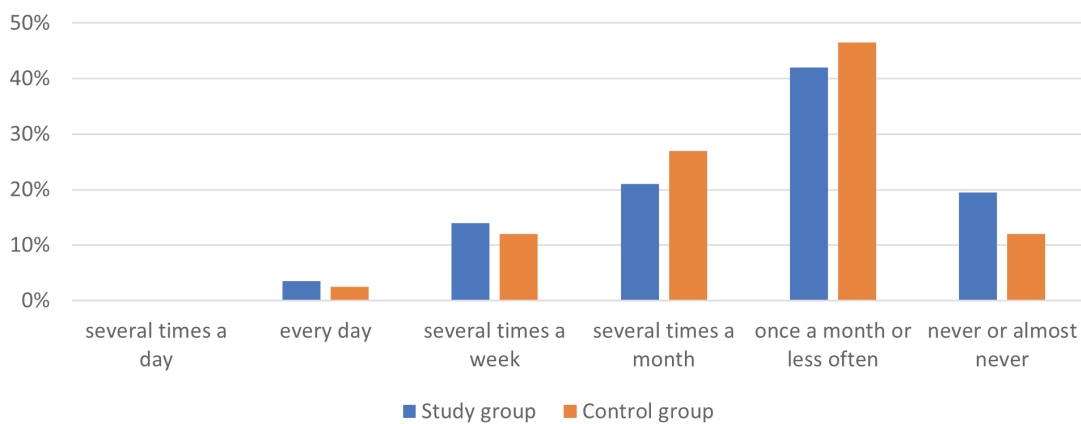


Figure 6. In the last 12 months, how often did you drink or eat dry pulses e.g. broad beans, beans, soya, peas, chickpeas, and in dishes e.g. pea soup, baked beans, hummus and other pastes?

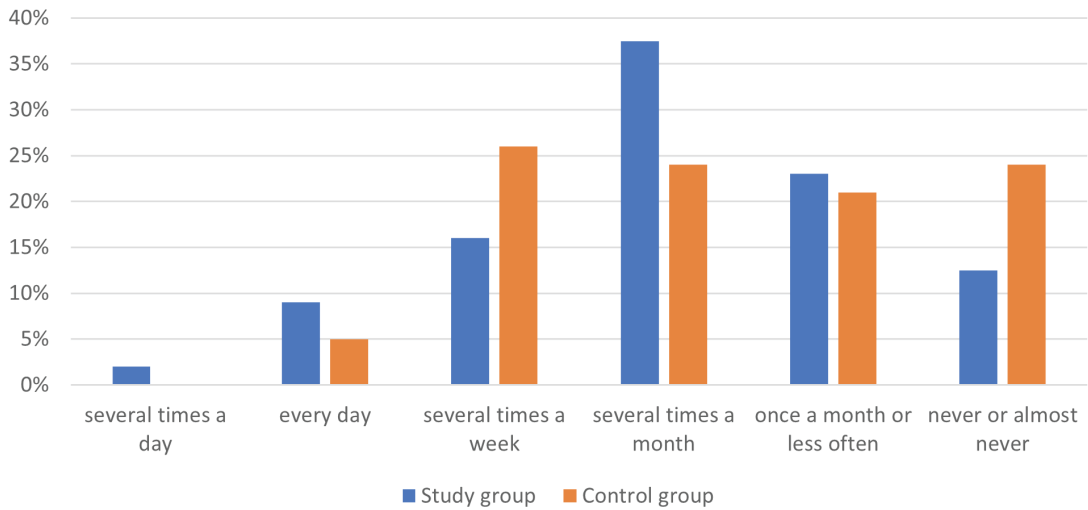


Figure 7. In the last 12 months, how often did you drink or eat grains, e.g. pumpkin, sesame, sunflower, wheat germ?

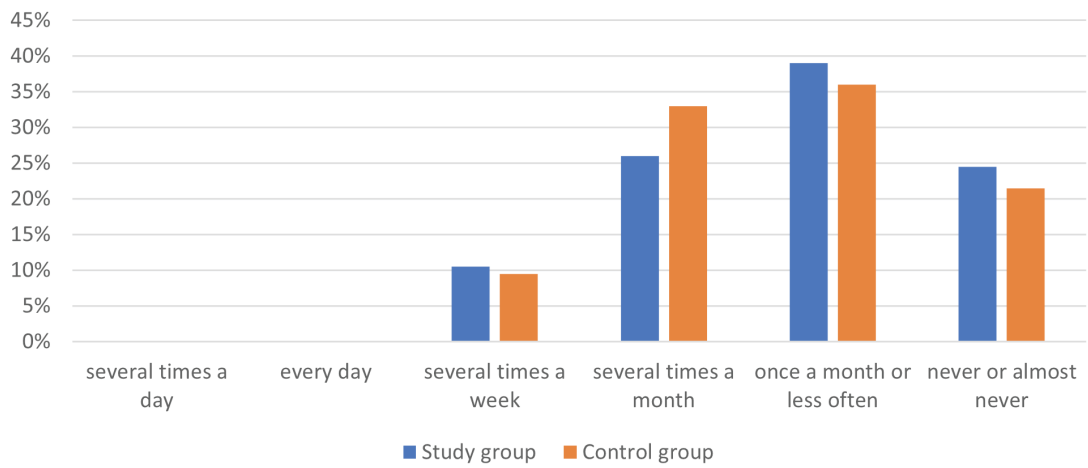


Figure 8. In the last 12 months, how often did you drink or eat oily fish, e.g. salmon, sardines, herring, mackerel, large carp, eel?

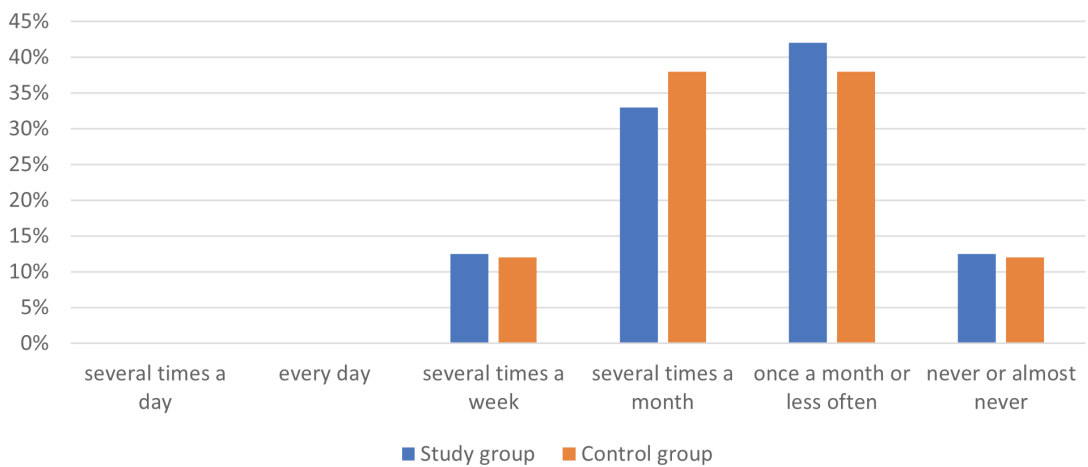


Figure 9. In the last 12 months, how often did you drink or eat lean fish, e.g. pollock, cod, perch, hake, carp up to 1 kg, tuna, panga, trout?

Discussion

An adequate diet seems to be an important part of the therapeutic management of patients with HT. However, our study showed no statistically significant differences between the diets of HT and control patients. Only 7.5% of women with HT declared that they consumed fruit several times a day, and 29% daily. Few subjects declared sufficient intake of berries, which have a high antioxidant potential – 2% of HT subjects declared consuming berries daily and 19% several times a week. In contrast, the consumption of the recommended several portions of vegetables per day was declared by only 22% of those with HT. Interestingly, no statistical differences were observed in the level of intake of cruciferous vegetables between the two groups. There is a popular myth that people with hypothyroidism should not consume cruciferous vegetables because of the goitrogens they contain, which can disrupt thyroid function by binding iodine used in the production of thyroid hormones. However, it should be emphasized that the consumption of cruciferous vegetables in moderation does not adversely affect the thyroid gland and that the adverse effects of goitrogens may only become apparent with a concomitant insufficient supply of iodine. Furthermore, heat

processing of food eliminates a significant proportion of goitrogenic substances [13].

It is therefore a positive result that, in the study, 43% of women with HT report eating cruciferous vegetables several times a week. Cruciferous vegetables are a rich source of bioactive substances with anticancer effects.

About half of women with HT declare that they consume green leafy vegetables several times a week, but less than 19% consume them daily. Legumes are most often consumed once a month or less often by 42% of the people in the study group and 46.5% of the control group. Only 2 people in the study group and 1 person in the control group declared to consume legumes daily.

In contrast, nuts and seeds are consumed several times a month by most people in the study group and several times a week by those in the control group.

The majority of HT respondents also declare not consuming the recommended amount of fish – almost 25% of female respondents answered that they never consume oily fish and 39% answered that they consume it once a month or less often. Similarly, lean fish – 33% of respondents consume it several times a month, 42% once a month or less often, and 13% never or almost never.

Table 2. Nutritional sources of dietary components important for proper thyroid functioning [12, 20].

| Nutrient | Dietary sources | Requirements for adult women |
|-----------|---|--|
| Iodine | milk and dairy products, fish and seafood and eggs iodised salt | 150 µg/day, 220 µg/day for pregnant women and 290 µg/day for breastfeeding women |
| Selenium | offal, especially kidney, sea food: shellfish and fish, milk and milk products, garlic, mushrooms, dry pulses | 55 µg/day, 60 µg/day for pregnant women and 70 µg/day for breastfeeding women |
| Iron | meat, fish, cereals, beans, nuts, egg yolks, dark green vegetables, potatoes and fortified foods | 18 mg/day for women aged 19–50 years, 10 mg/day after 50 years old, 27 mg/day for pregnant women and 10 mg/day for breastfeeding women |
| Zinc | meat, liver, rennet cheeses, brown bread, buckwheat, eggs | 8 mg/day for women, 11 mg/day for pregnant women and 12 mg/day for breastfeeding women |
| Vitamin D | fatty fish, eggs, milk and milk products, fortified margarine – only 20% of the body's vitamin D pool is obtained from the diet | 15 µg cholecalciferol/day at a sufficient intake level |
| Vitamin C | parsley, black currants, kiwi fruit, red pepper, cruciferous vegetables, strawberries, citrus fruits | 75 mg/day for women, 85 mg/day for pregnant women, and 120 mg/day for breastfeeding women |
| Vitamin E | wheat germ oil, sunflower oil, safflower oil, cereal products, nuts, vegetables, meat, and dairy products | 8 mg tocopherol/day, 10 mg/day for pregnant women, 11 mg/day for breastfeeding women |
| Vitamin A | β-carotene: carrots, parsley, spinach, kale, broccoli, apricots, peaches retinol: offal, especially in liver, eggs, rennet ripening cheese, butter and some sea fish | 700 µg retinol equivalent/day, 770 µg retinol equivalent/day for pregnant women, 1300 µg retinol equivalent/day for breastfeeding women |

Both green leafy vegetables and oily marine fish are part of the anti-inflammatory diet recommended for people with HT. Green leafy vegetables are a source of antioxidant micronutrients and oily marine fish are a source of highly anti-inflammatory omega-3 fatty acids. Also, lean fish is a source of iodine and selenium which are important dietary components for people with thyroid disease [13].

An interesting study was conducted by Omeljaniuk et al. on a group of 101 women aged 17–68 years with diagnosed Hashimoto's disease, living in the areas of Białystok, Kętrzyn and Zambrów. It was observed that the diets of the studied women were characterized by an insufficient energy supply, a low content of fats and dietary fiber, and, in turn, an excess of protein and digestible carbohydrates [14].

Kaličanin et al. in a study designed to demonstrate dietary differences between a group of 491 patients with HT and a group of 433 patients without thyroid disease, observed that patients with HT consumed higher amounts of animal fats and processed meat, as well as nuts compared to controls. In contrast, they were less likely to consume red meat, soft drinks, whole grain products, vegetable oil, olive oil, alcohol, fatty fish and fruit. Furthermore, researchers have shown that patients don't tend to change their eating habits after HT diagnosis [15].

A gluten-free diet has gained considerable popularity among people with HT. Celiac disease, an indication for adherence to a strict gluten-free diet, is diagnosed in HT patients up to 10 times more frequently than in the healthy population [11]. Some researchers suggest that gliadin, a component of gluten, triggers an immune system response that targets not only gliadin but also the thyroid gland [3]. Malabsorption is also a common symptom of celiac disease, and as a result, deficiencies of the key elements for thyroid function – iodine and selenium – can occur. Additionally, an improperly managed gluten-free diet is very often a deficiency diet [16].

Krysiak et al. conducted a study on a group of 34 women aged 20–45 years with newly diagnosed HT in a euthyroid state, not taking levothyroxine. The women were divided into two groups, group A and group B. Women in group A were put on a gluten-free diet for 6 months, while no dietary modifications were made in group B. After

6 months, it was observed that anti-TPO and anti-TG antibody levels decreased in women following the gluten-free diet. A slight increase in vitamin D3 levels was also observed compared to control subjects. The researchers suggest that a gluten-free diet may be of clinical benefit to euthyroid women with Hashimoto's thyroiditis, who are at high risk of developing hypothyroidism due to significantly elevated anti-thyroid antibodies [18].

On the other hand, Poblocki et al. on a group of 62 women with HT aged 18–55 years assessed the effect of a gluten-free diet on TSH, fT3, fT4, anti-TPO, and anti-TG levels after 3, 6 and 12 months. The women were taking levothyroxine and celiac disease was excluded. The researchers showed that eliminating gluten from the diet of HT patients led to lower TSH levels and increased fT4 levels compared to the control group, suggesting that a gluten-free diet may improve intestinal absorption of levothyroxine. However, no differences were seen in anti-TPO and anti-TG concentrations in both groups. The researchers also note that patients enrolled in the study group were educated on how to properly compose a healthy and balanced gluten-free diet by a qualified dietitian. Therefore, it is worth considering whether dietary education influenced the change of eating habits to healthier ones in patients from the study group [17].

In the light of current research, POLSPEN recommends the introduction of a gluten-free diet only in HT patients with coexisting coeliac disease. Thus, in the light of the current study, there is no indication to introduce a gluten-free diet in patients with HT. However, it is worth considering diagnostic testing for coeliac disease in HT patients due to the frequent co-occurrence of autoimmune diseases [19].

Also, lactose elimination is only recommended in patients with HT and coexisting lactose intolerance. Consumption of lactose by those with lactose intolerance reduces the bioavailability of levothyroxine [3]. Given the high prevalence of lactose intolerance, it is suggested that patients with HT, especially those presenting with specific symptoms, should be diagnosed for lactose intolerance [11].

The diet of people with HT should be based on the principles of healthy nutrition for the healthy population, but there is no universal diet for all HT patients. It is extremely important to individu-

alize dietary recommendations based on detailed health and nutritional history. Dietary factors affect thyroid function and hormone secretion mainly by influencing the hypothalamic-pituitary-thyroid-peripheral tissue axis. Diet can also influence inflammatory processes in the thyroid gland. The diet should therefore be rich in nutrient-dense foods to ensure proper synthesis and secretion of thyroid hormones, as well as in foods with high antioxidant and anti-inflammatory potential to give the diet an anti-inflammatory character. The diet shall be correctly composed in terms of energy, fatty acids, protein and carbohydrate content, as well as vitamins and minerals. Special attention should be paid to iodine, selenium, iron, as well as zinc, and vitamins A, D, E, and vitamin C [12].

Conclusions

The diet of patients with Hashimoto's disease does not differ significantly from that of non-Hashimoto's disease patients. Taking into account the results of the study and current scientific knowledge, we believe that it is advisable to undertake educational activities for patients with Hashimoto's disease in order to increase patient awareness of the impact of diet on the course of the disease.

Based on current scientific reports [3, 9, 11], the most important dietary recommendations for Hashimoto's patients are as follows:

1. Consume 4–5 regular, properly composed meals.
2. Ensure adequate intake of key vitamins and minerals: especially iodine, selenium, iron, vitamin D, as well as zinc, vitamin A, C and E.
3. Match the energy value of your diet to your lifestyle, health, sex, and age – both low-calorie and high-calorie diets can affect thyroid function by increasing TSH if the diet is too high in energy and decreasing fT3 levels if the diet is too low in energy.
4. Increase protein supply to 15–20% and in some cases up to 20–25% of daily energy intake.
5. Include sources of complex carbohydrates in the diet in the form of whole-grain and high-fibre products, especially with co-morbid carbohydrate imbalances and co-occurring con-

- stipation. Minimise the intake of simple sugars and eat more vegetables and fruit instead.
6. Ensure adequate quantity and quality of fats in the diet. Increase your intake of unsaturated fats from plant products, e.g. olive oil, rapeseed oil, linseed oil, nuts and seeds, and omega-3 fatty acids from oily marine fish.
7. Avoid elimination diets if not indicated.

Acknowledgements

Conflict of interest statement

The authors declare no conflict of interest.

Funding sources

There are no sources of funding to declare.

References

1. Mincer DL, Jialal I. Hashimoto Thyroiditis. In StatPearls. StatPearls Publishing: Treasure Island (FL) 2021.
2. Wu G, Zou D, Cai H, Liu, Y. Ultrasonography in the Diagnosis of Hashimoto's Thyroiditis. *Front Biosci (Landmark Ed)*. 2016;21:1006-1012. doi: 10.2741/4437.
3. Ratajczak AE, Moszak M, Grzymisławski, M. Dietary Recommendations for Hypothyroidism and Hashimoto's Disease. *Pielęgniarstwo i Zdrowie Publiczne / Nursing and Public Health*. 2017;7:305-311. doi: 10.17219/pzp/76716.
4. Ajjan RA, Weetman AP. The Pathogenesis of Hashimoto's Thyroiditis: Further Developments in Our Understanding. *Horm Metab Res*. 2015;47:702-710. doi: 10.1055/s-0035-1548832.
5. Jia X, Wang B, Yao Q, Li Q, Zhang, J. Variations in CD14 Gene Are Associated With Autoimmune Thyroid Diseases in the Chinese Population. *Front Endocrinol (Lausanne)* 2019;9:811. doi: 10.3389/fendo.2018.00811.
6. Jabrocka-Hybel A, Skalniak A, Piątkowski J, Turek-Jabrocka R, Vyhouskaya P, Ludwig-Słomczyńska A, Machłowska J, Kapusta P, Małeck M, Pach D, et al. How Much of the Predisposition to Hashimoto's Thyroiditis Can Be Explained Based on Previously Reported Associations? *J Endocrinol Invest*. 2018;41:1409-1416. doi: 10.1007/s40618-018-0910-4.
7. Hiromatsu Y, Satoh H, Amino, N. Hashimoto's Thyroiditis: History and Future Outlook. *Hormones (Athens)* 2013;12:12-18. doi: 10.1007/BF03401282.
8. Choroba Hashimoto – Aspekt Genetyczny i Środowiskowy – Luty – Forum Medycyny Rodzinnej. Available online: https://journals.viamedica.pl/forum_medicyny_rodzinnej/article/view/51240 (accessed on 8 June 2021).
9. Hu S, Rayman MP. Multiple Nutritional Factors and the Risk of Hashimoto's Thyroiditis. *Thyroid*. 2017;27:597-610. doi: 10.1089/thy.2016.0635.
10. Rayman MP. Multiple Nutritional Factors and Thyroid Disease, with Particular Reference to Autoimmune

- Thyroid Disease. *Proc Nutr Soc.* 2019;78:34-44. doi: 10.1017/S0029665118001192.
11. Ilnatowicz P, Drywień M, Wątor P, Wojsiat, J. The Importance of Nutritional Factors and Dietary Management of Hashimoto's Thyroiditis. *Ann Agric Environ Med.* 2020;27:184-193. doi: 10.26444/aaem/112331.
 12. Lachowicz K, Stachoń M, Pałkowska-Goździk E, Lange, E. Fizjologiczne aspekty postępowania dietetycznego w chorobie Hashimoto. *Kosmos.* 2019;68:201-214. doi: 10.36921/kos.2019_2545.
 13. Pastusiak K, Michałowska J, Bogdański, P. Postępowanie dietetyczne w chorobach tarczycy. *Forum Zaburzeń Metabolicznych.* 2017;8:155-160.
 14. Omeljaniuk WJ, Dziemianowicz M, Naliwajko SK, Bartosiuk E, Markiewicz-Zukowska R, Borawska MH. Ocena sposobu żywienia pacjentek z chorobą Hashimoto. *Bromatologia i Chemia Toksykologiczna.* 2011;44.
 15. Kaličanin D, Brčić L, Ljubetić K, Barić A, Gračan S, Brekalo M, Torlak Lovrić V, Kolčić I, Polašek O, Zemunik T, et al. Differences in Food Consumption between Patients with Hashimoto's Thyroiditis and Healthy Individuals. *Sci Rep.* 2020;10:10670. doi: 10.1038/s41598-020-67719-7.
 16. Lontiris MI, Mazokopakis EE. A concise review of Hashimoto thyroiditis (HT) and the importance of iodine, selenium, vitamin D and gluten on the autoimmunity and dietary management of HT patients. Points that need more investigation. *Hell J Nucl Med.* 2017 Jan-Apr;20(1):51-56. doi: 10.1967/s002449910507.
 17. Poblócki J, Pańka T, Szczuko M, Telesiński A, Syrenicz, A. Whether a Gluten-Free Diet Should Be Recommended in Chronic Autoimmune Thyroiditis or Not?—A 12-Month Follow-Up. *J Clin Med.* 2021;10:3240. doi: 10.3390/jcm10153240.
 18. Krysiak R, Szkróbka W, Okopień, B. The Effect of Gluten-Free Diet on Thyroid Autoimmunity in Drug-Naïve Women with Hashimoto's Thyroiditis: A Pilot Study. *Exp Clin Endocrinol Diabetes.* 2019;127:417-422. doi: 10.1055/a-0653-7108.
 19. Ch'ng CL, Jones MK, Kingham JG.C. Celiac Disease and Autoimmune Thyroid Disease. *Clin Med Res.* 2007;5:184-192. doi: 10.3121/cmr.2007.738.
 20. Jarosz M, Rychlik E, Stoś K, Wierzejska R, Wojtasik A, Charzewska J, Mojska H, Szponar L, Sajór I, Kłosiewicz-Latoszek L, et al. Normy żywienia dla populacji Polski. Instytut Żywności i Żywienia: Warszawa 2017.

Impact of autoimmune thyroiditis on primary hyperparathyroidism

Stefanos Chatzidakis

Department of Medicine, School of Medicine,
European University Cyprus

 <https://orcid.org/0000-0002-4652-397X>

Demetris Lamnisos

Department of Health Sciences, European University Cyprus

 <https://orcid.org/0000-0001-8535-6601>

Vasilis Constantinides

Department of Endocrine Surgery, Evangelistria
Medical Center, Engomi, Nicosia, Cyprus

 <https://orcid.org/0000-0002-0251-1037>

Angelos Kyriacou

Department of Medicine, School of Medicine,
European University Cyprus

 <https://orcid.org/0000-0003-2282-0192>

Aliki Economides

Department of Health Sciences, European University Cyprus
Thyroid & Endocrinology Center, Engomi, Nicosia, Cyprus

 <https://orcid.org/0000-0002-3965-1252>

Panayiotis A. Economides

Department of Medicine, School of Medicine,
European University Cyprus

Thyroid & Endocrinology Center, Engomi, Nicosia, Cyprus

 <https://orcid.org/0000-0002-5504-5113>

Corresponding author: P.Economides@euc.ac.cy

 DOI: <https://doi.org/10.20883/medical.e737>

Keywords: primary hyperparathyroidism, autoimmune thyroiditis, Hashimoto's thyroiditis, minimally invasive parathyroidectomy, surgical time, nephrolithiasis

Received: 2022-09-27

Accepted: 2023-01-02

Published: 2023-03-31

How to Cite: Chatzidakis S, Lamnisos D, Constantinides V, Kyriacou A, Economides A, Economides PA. Impact of autoimmune thyroiditis on primary hyperparathyroidism. Journal of Medical Science. 2023;92(1);e568. doi:10.20883/medical.e737



© 2023 by the author(s). This is an open access article distributed under the terms and conditions of the Creative Commons Attribution (CC BY-NC) license. Published by Poznan University of Medical Sciences

ABSTRACT

Aim. Primary hyperparathyroidism (PHPT) often coexists with thyroid diseases. Current guidelines advise preoperative ultrasound (US) examination of the thyroid gland for thyroid nodular disease or concomitant malignancy but not evaluation for autoimmune thyroiditis (AIT). The impact of autoimmune thyroiditis on the clinical presentation and intraoperative course of PHPT is not clear.

Material and methods. We retrospectively assessed the medical records of 21 patients with PHPT who underwent parathyroidectomy. Clinical, biochemical, ultrasonographic and intraoperative data were evaluated.

Results. There was a longer duration of parathyroidectomy in patients with AIT than in those without (113.3 min vs. 93.9 min, $P = 0.03$). A lower rate of kidney stones was noted in patients with autoimmune thyroiditis (44.4% vs. 0%, $P = 0.03$). Patients with AIT were more symptomatic, but this was not significant. There was no difference between the two groups in the prevalence of osteoporosis or thyroid nodular disease.

Conclusions. A significantly longer duration of parathyroidectomy was seen in PHPT patients with AIT. Patients with PHPT undergoing surgery should be investigated for autoimmune thyroiditis, as this may affect surgical planning.

Introduction

Primary hyperparathyroidism (PHPT) is characterized by elevated serum calcium levels along with elevated or paradoxically normal parathyroid hormone levels (PTH). It has varying incidence worldwide, ranging from 0.4 to 82 cases per 100,000 people [1]. When indicated, minimally invasive parathyroidectomy (MIP) is the surgical treatment of choice [2]. The American Association of Endocrine Surgeons (AAES) endorses the MIP approach due to its minimal operation length, fast recovery and rare intraoperative complications, and it provides a cure rate between 97% and 99% [2]. More than 85% of PHPT cases arise from solitary parathyroid adenomas, and the success of the operation depends on accurate imaging techniques that pinpoint the exact location of the adenoma, establish the probability that the adenoma is solitary or not and investigate the presence of concomitant thyroid nodular disease [2, 3].

Current guidelines suggest performing preoperative neck ultrasound to identify thyroid nodules and thyroid cancer [2, 4]. A study by M. Regal et al., showed that more than half of PHPT patients undergoing parathyroidectomy had concomitant thyroid disease [5]. Latina et al. showed that thyroid disease was present in 60% of PHPT patients, mostly thyroid nodular disease [6]. Even so, the current guidelines do not address preoperative screening for autoimmune thyroiditis, which is commonly present in patients with primary hyperparathyroidism.

Hashimoto's thyroiditis is the most common autoimmune thyroid disease and the most common cause of hypothyroidism in adults in the US, with an annual incidence worldwide of 0.3–1.5/1000 individuals/year and a much higher incidence [7]. It is characterized by chronic thyroid tissue inflammation, where the thyroid parenchyma is distorted by lymphocytic infiltration [7]. In a study by Ignjatovic et al., PHPT was more frequent in Hashimoto's thyroiditis patients, and it was postulated that chronically elevated TSH in the advanced stage of Hashimoto's thyroiditis may cause hyperplasia of the parathyroid gland [8].

Aim

The aim of this research study was to investigate the impact of autoimmune thyroiditis on PHPT

and to evaluate the association of these two diseases in terms of symptoms, biochemical variables, and surgical outcomes.

Material and methods

Patient Recruitment

This was a retrospective review of the medical and surgical records of 21 patients with PHPT in the Thyroid & Endocrinology Center in Nicosia, Cyprus, a referral center for thyroid, parathyroid and endocrine diseases [9]. Inclusion criteria were primary hyperparathyroidism and parathyroidectomy. Patients with secondary or tertiary hyperparathyroidism were excluded. All patients underwent parathyroidectomy between 2016 and 2020 by a single endocrine surgeon. Eighteen patients underwent minimally invasive parathyroidectomy. One patient underwent concomitant hemithyroidectomy, and another patient underwent concomitant total thyroidectomy. A third patient did not undergo primary surgery but underwent reoperation for persistent disease. These three patients were excluded from the analysis of procedure length. Patients who had two parathyroid adenomas were also excluded from the analysis of procedure length. Data recorded were sex, age, weight, height, presence of symptoms, number and locations of parathyroid adenomas, presence or absence of concomitant nodular thyroid disease, thyroid cancer or autoimmune thyroid disease, calcium, phosphorus, PTH, TSH, FT4, 25-OH Vit. D, presence or absence nephrolithiasis, and dual energy X-ray absorptiometry (DEXA). Surgical data included the size and locations of the adenomas and the duration of the operation.

All patients underwent thyroid and neck ultrasound (US) by a GE Logiq E9 system with a ML 6–15 MHz linear transducer by a single endocrinologist experienced in endocrine neck US [10]. The possible parathyroid adenomas identified on US were mapped onto a detailed diagram, denoting the location and dimensions of each adenoma [11]. The diagnosis of autoimmune thyroiditis was based on a combination of detailed history taking, ultrasound findings and the presence of thyroid autoantibodies. All patients underwent abdominal ultrasound examination to evaluate the presence or absence of kidney stones and dual-energy X-ray absorptiometry (DEXA) to

assess bone mineral density (BMD) of the lumbar spine and femoral head.

The following parameters were examined regarding the impact on PHPT: sex, age, BMI, eGFR, number of adenomas, preoperative US dimensions, postoperative dimensions and vascularity, Hashimoto's thyroiditis/Graves' disease, nodular thyroid disease, serum calcium, phosphate, PTH, TSH, FT4, calcitonin, bone mineral density, and presence or absence of clinical symptoms.

Statistical Analysis

The data are presented as mean and standard deviation (SD) for numerical variables and absolute and percentage frequencies for categorical variables. The comparison of continuous variables between the two groups was done by performing an independent samples t test. To compare categorical variables with two possible outcomes, such as sex; the presence of nephrolithiasis, cancer, or thyroid nodules; the number of parathyroid adenomas; and the presence or absence of symptoms, Fisher's exact test was performed. For categorical variables with three possible outcomes (bone mineral density status: normal, osteopenia, osteoporosis), Pearson's chi-square was performed. A two-sided value of $P < 0.05$ was considered statistically significant. Statistical analysis was performed using the statistical analysis software package IBM-SPSS 20.

The study was approved by the Cyprus National Bioethics Committee. Patients' personal information and identities were kept fully confidential throughout the study.

Results

Table 1 lists the demographic characteristics, laboratory values and clinical data. Nine patients (42.9%) did not have concomitant autoimmune thyroiditis (Group 1). Twelve patients (57.1%) had autoimmune thyroiditis (Group 2), of whom 11 had Hashimoto's thyroiditis and 1 had Graves' disease that had progressed to hypothyroidism. The mean age was 56.2 ± 10.5 (range from 32 to 76 years). Eighteen patients (85.7%) were female. Of the 21 patients, one patient (4.8%) had concomitant differentiated thyroid cancer, while 12 patients (57.1%) had thyroid nodules. Seventeen patients (81.0%) had a solitary adenoma, whereas the other 4 patients

(19.0%) had two. Four out of the 21 patients (19.0%) had nephrolithiasis or nephrocalcinosis. Fifteen patients (71.4%) reported symptoms of hyperparathyroidism, while 6 patients (28.6%) did not report any specific symptoms. The most common symptoms that were reported were bone pain, arthralgias, tiredness/fatigue and anxiety.

Preoperative serum calcium was $10.45 \text{ mg/dl} \pm 0.52$, while preoperative PTH and phosphorus were $124.6 \text{ pg/ml} \pm 65.8$ and $3.0 \text{ mg/dl} \pm 0.5$, respectively. Thyroid-stimulating hormone (TSH), 25-OH-vitamin D (calcidiol), and creatinine were $1.85 \text{ } \mu\text{IU/ml} \pm 0.93$, $26.8 \text{ ng/ml} \pm 10.08$ and 0.74 ± 0.12 , respectively. Six patients (28.6%) had normal bone mineral density, 10 patients had osteopenia (47.6%), and 5 patients (23.8%) had osteoporosis.

The mean age of Group 2 (autoimmune thyroiditis) was 59.2 ± 7.7 , whereas Group 1 (non-autoimmune thyroiditis) had a mean age of 52.2 ± 12.3 ($P = 0.15$). There were 3 male patients (33.3%) and 6 female patients (66%) in Group 1, while Group 2 had no male patients ($P = 0.06$). The mean eGFR in Group 2 was $85.89 \text{ mL/min/1.73 m}^2 \pm 12.63$, whereas in Group 1, the mean eGFR was $90.54 \pm 11.59 \text{ mL/min/1.73 m}^2$ ($P = 0.4$). In Group 1, 4 out of 9 patients (44%) had nephrocalcinosis or nephrolithiasis compared to none of the 12 patients in Group 2 ($P = 0.03$). There was no significant difference between the groups regarding the presence of clinical symptoms (55.6% vs. 83.3%, $P = 0.33$). Thyroid nodular disease was similarly common in both groups (66.6% vs. 50%, $P = 0.66$).

There were no statistically significant differences between the groups in the level of PTH, calcium, TSH, phosphorus, 25-OH-vitamin D or creatinine. The mean serum PTH was $155.0 \text{ pg/ml} \pm 89.3$ in Group 1 and $101.8 \text{ pg/ml} \pm 27.3$ in Group 2 ($P = 0.06$). The serum calcium in Group 1 was $10.42 \text{ mg/dl} \pm 0.57$ vs. $10.47 \text{ mg/dl} \pm 0.49$ in Group 2 ($P = 0.82$). Bone mineral density did not differ between the two groups ($P = 0.65$).

In all Group 1 patients, preoperative US imaging found that all the adenomas were situated where the surgeon localized them intraoperatively. In 1 of the 12 (8.3%) Group 2 patients, the adenoma was found to be at a different location than shown preoperatively and bore a second adenoma that had not been identified by US preoperatively.

Table 1. Demographic characteristics, laboratory values and clinical data

| Parameters | All Patients (n = 21) | Group 1 (n = 9) | Group 2 (Autoimmune Thyroiditis) (n = 12) | p value |
|--|--------------------------|--------------------|---|-------------------|
| Demographic Data | | | | |
| Age | 56.2 ± 10.5 | 52.2 ± 12.3 | 59.2 ± 7.7 | 0.15* |
| Male | 3 (14.3%) | 3 (33.3%) | 0 | 0.06 [§] |
| Female | 18 (85.7%) | 6 (66.6%) | 12 (100%) | |
| BMI kg/m ² | 26.8 ± 4.0 | 25.9 ± 3.5 | 27.5 ± 4.4 | 0.4* |
| eGFR ml/min/1.73 m ² | 87.89 ± 12.13 | 90.54 ± 11.59 | 85.89 ± 12.63 | 0.4* |
| Preoperative Ultrasonography | | | | |
| Thyroid Nodules (%) | 12 (57.1%) | 6 (66.6%) | 6 (50%) | 0.66 [§] |
| Number of Adenomas | | | | |
| Solitary Adenoma | 17 (81.0%) | 8 (88.9%) | 9 (75.0%) | 1 [§] |
| Two Adenomas | 4 (19.0%) | 1 (11.1%) | 3 (25.0%) | |
| Adenoma Size (cm) | 1.36 ± 0.61 | 1.49 ± 0.81 | 1.25 ± 0.40 | 0.39* |
| Abdominal Ultrasonography | | | | |
| Nephrolithiasis/Nephrocalcinosis (%) | 4 (19.0%) | 4 (44.4%) | 0 | 0.03 [§] |
| Clinical Symptoms | | | | |
| Symptomatic (%) | 15 (71.4%) | 5 (55.6%) | 10 (83.3%) | 0.33 [§] |
| Asymptomatic (%) | 6 (28.6%) | 4 (44.4%) | 2 (16.7%) | |
| Biochemical Laboratory Values | | | | |
| Serum PTH (pg/ml) | 124.6 ± 65.8 | 155.0 ± 89.3 | 101.8 ± 27.3 | 0.06* |
| Serum Ca (mg/dl) | 10.45 ± 0.52 | 10.42 ± 0.57 | 10.47 ± 0.49 | 0.82* |
| Serum Phosphorus (mg/dl) | 3.0 ± 0.5 | 2.90 ± 0.62 | 3.11 ± 0.33 | 0.37* |
| Serum TSH (μIU/ml) | 1.85 ± 0.93 | 2.27 ± 0.78 | 1.54 ± 0.94 | 0.07* |
| Serum 25-OH-Vitamin D (ng/ml) | 26.8 ± 10.08 | 30.32 ± 10.96 | 24.16 ± 8.90 | 0.17* |
| Serum Creatinine (mg/dl) | 0.74 ± 0.12 | 0.77 ± 0.15 | 0.72 ± 0.09 | 0.30* |
| BMD (DEXA) | | | | |
| Normal BMD (%) | 6 (28.6%) | 2 (22.2%) | 4 (33.3%) | 0.65 [†] |
| Osteopenia On Any Site (%) | 10 (47.6%) | 4 (44.4%) | 6 (50%) | |
| Osteoporosis On Any Site (%) | 5 (23.8%) | 3 (33.3%) | 2 (16.7%) | |
| Surgical Data | | | | |
| | All patients (n = 16) | Group 1 (n = 7) | Group 2 (Autoimmune Thyroiditis) (n = 9) | p value |
| Procedure Length (min) (Solitary adenomas) | 104.8 ± 18.5 | 93.9 ± 20.7 | 113.3 ± 11.5 | 0.03* |

Continuous variables expressed as mean ± SD, Categorical variable expressed as frequency and percentages

*Independent samples t test; [§]Fisher's exact test; [†]Pearson's chi-square

Procedure Length Results

After excluding from the procedure length analysis the patients who underwent concomitant thyroid surgery, reoperation for persistent disease and the patients with two parathyroid adenomas the mean duration of surgery of all the patients with solitary parathyroid adenoma (n = 16) was 104.8 min. ± 18.5 min. Group 1 had a mean duration of 93.9 min ± 20.7 min, whereas the mean duration in Group 2 was 113.3 min ± 11.5 min (P = 0.03).

Discussion

Our primary finding was that autoimmune thyroiditis increases the surgical time in patients with PHPT by an average of 19 min compared to the absence of autoimmune thyroiditis. As all but one of the patients in Group 2 had Hashimoto's thyroiditis, the effect on PHPT was primarily due to Hashimoto's thyroiditis. Thyroid pathologies, specifically Hashimoto's thyroiditis, are commonly found in patients with PHPT undergoing

parathyroidectomy. The incidence of Hashimoto's thyroiditis in patients undergoing parathyroidectomy has been reported to range from 2.2% to 42% [5, 12–17]. Our study, however, showed a higher rate (57.1%) of Hashimoto's thyroiditis in PHPT. Hashimoto's thyroiditis has been associated with a higher likelihood of transient complications during thyroidectomy, likely secondary to thyroid gland adherence to the surrounding tissues, increasing the risk of injury to the parathyroid glands and recurrent laryngeal nerves [18].

Current guidelines on preoperative work-up do not recommend screening for autoimmune thyroid disease prior to parathyroidectomy. Based on our research outcomes and the fact that Hashimoto's thyroiditis is a very prevalent disease, we can suggest that patients with PHPT scheduled to undergo parathyroidectomy be evaluated for autoimmune thyroiditis. As there is additional operative time needed in patients with autoimmune thyroiditis undergoing the MIP procedure, it is reasonable to suggest that in four-gland exploration procedures, the respective additional time would be disproportionately longer.

Our study found a high prevalence of concomitant thyroid disease in PHPT, either autoimmune thyroiditis or nodular thyroid disease or both. Wright et al. suggest that patients with thyroid pathologies undergoing surgery be investigated for parathyroid diseases and vice versa due to the high rate of coexistence of these two entities [19]. Similarly, the American Association of Endocrine Surgeons Guidelines for definite treatment of PHPT advises preoperative US screening of the thyroid gland to detect thyroid nodules and possible malignancies that can affect the course of the operation [2, 4, 19, 20]. These interventions are recommended on the grounds that unexpected concomitant thyroid pathology during parathyroidectomy would necessitate deviations from the preoperative surgical plan, increase postoperative complications, increase the discomfort caused to the patient and increase costs [3, 4, 19, 21].

Another important, unexpected finding of our study was that patients with autoimmune thyroiditis had significantly lower rates of kidney stones. Circulating thyroid hormones, more specifically hormones that alter the expression of certain ion channels and transporters, predispose patients to sodium equilibrium imbalances and are associated with alterations of the eGFR [22].

Patients with hypothyroidism can present with a significant reduction in GFR, which can be secondary to direct renal and systemic effects [22]. In our study, eGFR was lower in patients with AIT than in those without AIT, though this did not reach statistical significance. There is no clear explanation for the lower rate of kidney stones, but we assume that a lower GFR leads to lower calcium filtration to the kidney pelvis, therefore leading to less calcium aggregation and less nephrolithiasis or nephrocalcinosis.

Our study has several limitations. First, this was a retrospective study performed at a single center in Cyprus, and the small sampling size of only 21 patients inevitably led to sampling imprecision, which is common in endocrinological disease research but could have been mitigated if a larger sample had been available. Even so, to the best of our knowledge, this is the first study that has examined the intraoperative impact of autoimmune thyroid diseases in PHPT patients. As a second limitation, our study examined only patients with PHPT who underwent parathyroidectomy. Third, most patients with autoimmune thyroid disease had Hashimoto's thyroiditis, only one patient having Graves' disease. Considering this, a generalization to patients with Graves' disease cannot be made. Fourth, as US imaging was performed by a single examiner and operations were performed by a single surgeon, our results cannot be generalized.

In summary, our retrospective cohort study of 21 patients who underwent surgery for parathyroid adenomas showed a significantly longer duration of parathyroidectomy in PHPT patients with autoimmune thyroiditis. Patients with autoimmune thyroiditis had a significantly lower rate of kidney stones. Although not significant, patients with autoimmune thyroiditis were more symptomatic. Our results strongly suggest that patients with PHPT should undergo a complete investigation for autoimmune thyroiditis, as this may affect their surgical planning. More studies are needed to elucidate the clinical and surgical impact of autoimmune thyroid diseases on patients with PHPT.

Abbreviations

PHPT – primary hyperparathyroidism; AIT – autoimmune thyroiditis; PTH – parathyroid hormone levels; MIP – minimally invasive parathyroidism; US – ultrasound.

Acknowledgements

Conflict of interest statement

The authors declare no conflict of interest.

Funding sources

There are no sources of funding to declare.

References

1. Walker MD, Silverberg SJ. Primary hyperparathyroidism. *Nat Rev Endocrinol*. 2019;14(2):115-125. doi: 10.1038/nrendo.2017.104.
2. Wilhelm SM, Wang TS, Ruan DT, et al. The American Association of Endocrine Surgeons Guidelines for Definitive Management of Primary Hyperparathyroidism. *JAMA Surg*. 2016;151(10):959. doi: 10.1001/jamasurg.2016.2310.
3. Zheng Y, Xu S, Wang P, Chen L. Preoperative localization and minimally invasive management of primary hyperparathyroidism concomitant with thyroid disease. *J Zhejiang Univ Sci B*. 2007;8(9):626-631. doi: 10.1631/jzus.2007.B0626.
4. Ryan S, Courtney D, Moriariu J, Timon C. Surgical management of primary hyperparathyroidism. *Eur Arch Otorhinolaryngol*. 2017;274(12):4225-4232. doi: 10.1007/s00405-017-4776-4.
5. Regal M, Páramo C, Cano RL, et al. Coexistence of primary hyperparathyroidism and thyroid disease. *J Endocrinol Invest*. 1999;22(3):191-197. doi: 10.1007/BF03343540.
6. Latina A, Castellano E, Cesario F, Boriano A, Attanasio R, Borretta G. Unknown and Already Known Thyroid Abnormalities in Primary Hyperparathyroidism. *Endocr Pract*. 2018;24(7):628-633. doi: 10.4158/EP-2018-0016.
7. Ragusa F, Fallahi P, Elia G, et al. Hashimotos' thyroiditis: Epidemiology, pathogenesis, clinic and therapy. *Best Pract Res Clin Endocrinol Metab*. 2019;33(6):101367. doi: 10.1016/j.beem.2019.101367.
8. Ignjatovic VD, Matovic MD, Vukomanovic VR, Jankovic SM, Džodić RR. Is there a link between Hashimoto's thyroiditis and primary hyperparathyroidism? A study of serum parathormone and anti-TPO antibodies in 2267 patients. *Hell J Nucl Med*. 2013;16(2):86-90.
9. Hadjisavva IS, Dina R, Talias MA, Economides PA. Prevalence of Cancer in Patients with Thyroid Nodules in the Island of Cyprus: Predictive Value of Ultrasound Features and Thyroid Autoimmune Status. *Eur Thyroid J*. 2015;4(2):123-128. doi: 10.1159/000430438.
10. Papaioannou C, Lamnisis D, Kyriacou K, et al. Lymph Node Metastasis and Extrathyroidal Extension in Papillary Thyroid Microcarcinoma in Cyprus: Suspicious Subcentimeter Nodules Should Undergo FNA When Multifocality is Suspected. *J Thyroid Res*. 2020;2020;1-7. doi: 10.1155/2020/3567658.
11. Chisholm EJ, Economides P, Elmiyeh B, Pepper C, Dwivedi R, Rhys-Evans PH. Pictorial ultrasound reports combined with fine needle washout thyroglobulin assay to aid thyroid surgery. *The Laryngoscope*. 2011;121(6):1231-1232. doi: 10.1002/lary.21765.
12. Kutluturk K, Otan E, Yagci MA, Usta S, Aydin C, Unal B. Thyroid pathologies accompanying primary hyperparathyroidism: a high rate of papillary thyroid microcarcinoma. *Turk J Surg*. 2014;30(3):125-128. doi: 10.5152/UCD.2014.2685.
13. Heizmann O, Viehl CT, Schmid R, Müller-Brand J, Müller B, Oertli D. Impact of concomitant thyroid pathology on preoperative workup for primary hyperparathyroidism. *Eur J Med Res*. 2009;14(1):37. doi: 10.1186/2047-783X-14-1-37.
14. Bentrem DJ, Angelos P, Talamonti MS, Nayar R. Is Preoperative Investigation of the Thyroid Justified in Patients Undergoing Parathyroidectomy for Hyperparathyroidism? *Thyroid*. 2002;12(12):1109-1112. doi: 10.1089/105072502321085207.
15. Ryan S, Courtney D, Timon C. Co-existent thyroid disease in patients treated for primary hyperparathyroidism: implications for clinical management. *Eur Arch Otorhinolaryngol*. 2015;272(2):419-423. doi: 10.1007/s00405-014-3000-z.
16. Jovanovic MD, Zivaljevic VR, Diklic AD, Rovcanin BR, V. Zoric G, Paunovic IR. Surgical treatment of concomitant thyroid and parathyroid disorders: analysis of 4882 cases. *Eur Arch Otorhinolaryngol*. 2017;274(2):997-1004. doi: 10.1007/s00405-016-4303-z.
17. Gul K, Ozdemir D, Korukluoglu B, et al. Preoperative and Postoperative Evaluation of Thyroid Disease in Patients Undergoing Surgical Treatment of Primary Hyperparathyroidism. *Endocr Pract*. 2010;16(1):7-13. doi: 10.4158/EP09138.OR.
18. Ravikumar K, Muthukumar S, Sadacharan D, Suresh U, Sundarram T, Periyasamy S. The impact of thyroiditis on morbidity and safety in patients undergoing total thyroidectomy. *Indian J Endocrinol Metab*. 2018;22(4):494. doi: 10.4103/ijem.IJEM_209_17.
19. Wright M-C, Jensen K, Mohamed H, et al. Concomitant thyroid disease and primary hyperparathyroidism in patients undergoing parathyroidectomy or thyroidectomy. *Gland Surg*. 2017;6(4):368-374. doi: 10.21037/gs.2017.04.01.
20. Kyriacou A, Syed AA, Economides PA. Thyroid sonography as an extension of the bedside examination in hyperthyroidism. *J Med Sci*. 2020;89(4):e482. doi: 10.20883/medical.e482.
21. Castellano E, Benso P, Attanasio R, et al. Surgical Approach to Primary Hyperparathyroidism in Patients with Concomitant Thyroid Diseases: A Retrospective Single Center Study. *Int J Endocrinol*. 2020;2020;1-6. doi: 10.1155/2020/2182539.
22. Mariani LH, Berns JS. The Renal Manifestations of Thyroid Disease. *J Am Soc Nephrol*. 2012;23(1):22-26. doi: 10.1681/ASN.2010070766.

PD-L1 expression in Triple Negative Breast Cancer: a study of an Iraqi population

Gina James Keorges

Department of Pathology, College of medicine,
University of Duhok, Kurdistan Region, Iraq

 <https://orcid.org/0000-0002-3843-7035>

Corresponding author: gina.Keorges@uod.ac

Published: 2023-03-31

How to Cite: Keorges GJ. PD-L1 expression in Triple Negative Breast Cancer: a study of an Iraqi population. *Journal of Medical Science*. 2023;92(1);e806. doi:10.20883/medical.e806

 DOI: <https://doi.org/10.20883/medical.e806>

Keywords: expression, PD-L1, triple negative, breast cancer



© 2023 by the author(s). This is an open access article distributed under the terms and conditions of the Creative Commons Attribution (CC BY-NC) licence. Published by Poznan University of Medical Sciences

ABSTRACT

Introduction. Breast cancer is the second most common cause of cancer death in women. Breast cancer awareness has increased due to mammography screening.

Aim. The study aims to evaluate the prevalence of the anti-programmed death-ligand 1 (PD-L1) expression in triple-negative breast cancer (TNBC) cases and to correlate it with clinicopathological parameters.

Material and methods. This retrospective study investigates 44 triple-negative breast cancer cases. PD-L1 expression was measured by an immunohistochemical technique using Dako kits, PD-L1 IHC 22C3 pharm Dx on 44 paraffin block samples from Duhok Municipal Laboratories. If the specimen has a combined positive score (CPS) of 10 or higher, it expresses PD-L1. Age groups, grades, types, stages, and lymph node status are studied.

Results. The mean age of the 44 patients was 47.7 years. 54.5% of the patients were in the middle age group, 63.6% were in grade III, 88.6% had invasive ductal carcinoma, and 75% were negative for PD-L1. 63.6% of the patients had the nuclear protein Ki67 (Ki-67) less than 20. 70.5% of the patients were in stage T2, and 45.5% had N1 lymph node status. There is a significant association between PD-L1 and Ki67. All patients with positive PD-L1 had Ki67 more than 20, while only 15.2% of the patients with negative PD-L1 had Ki67 more than 20.

Conclusion. Most TNBC patients are middle age, have grade III, and 75% have negative PD-L1. There is a significant association between PD-L1 and Ki-67. All patients with positive PD-L1 have Ki67 of more than 20.

Introduction

Breast cancer is the most common type of cancer in women and the second most common cause of death from cancer in women [1]. In recent years, the use of mammography for screening has made more people aware of breast cancer [1]. The prognosis for breast cancer has improved dramatically as a result of treatments that target the estrogen receptor (ER), the progesterone receptor (PR), and the human epidermal growth fac-

tor receptor 2 (HER2) [2]. However, tumours that do not express ER, PR, or HER2 are called "triple-negative breast cancers" (TNBC). Triple-negative breast cancer (TNBC) affects only about 13 out of every 100,000 women diagnosed with breast cancer each year. It accounts for about 15% of all invasive breast cancers, has a poor prognosis, and cannot be treated well [3, 4]. The CD274 gene on chromosome 9 encodes a 40 kDa

transmembrane protein known as programmed death ligand-1 (PD-L1). Natural killer cells, macrophages, myeloid dendritic cells, B cells, epithelial cells, and vascular endothelial cells are all typical tissue cell types that contain it [5]. The PD-1 (Programmed death receptor 1)/PD-L1 signalling pathway aids in helping tumours evade the immune system, according to recent studies in various epithelial tumours, due to crosstalk between PD-1 on tumour-infiltrating lymphocytes (TIL) and PD-L1 in tumour cells [5]. Expression of PD-L1 on their cells is a crucial defence mechanism for tumours against the immune system [5]. Researchers have shown PD-L1 expression in many types of cancer, including melanoma, renal cell carcinoma, non-small cell lung cancer, colorectal cancer, gastric cancer, pancreatic cancer, and types of breast cancers [6]. Therapies that block PD-1/PD-L1 could be used to treat these tumours [6]. However, little information exists about how PD-L1 is expressed in breast cancer. There are different opinions about how PD-L1 expression might affect the outcome of breast cancer. Some studies say that PD-L1 is beneficial [7–9], while others suggest its detrimental role [10] or no effect at all [11]. The Ki67 protein is usually found only in growing cells [12]. During interphase, Ki67 is primarily found in the nucleolar cortex, but during mitosis, it moves to where the chromosomes are packed together [13, 14].

Aim

The study aims to evaluate the prevalence of PD-L1 expression in TNBC cases and to correlate it with clinicopathological parameters.

Material and methods

The study is a retrospective of 44 triple-negative breast cancer cases. The samples were collected as paraffin blocks from different laboratories in Duhok city. PD-L1 expression was assessed with an immunohistochemical method using Dako kits, PD-L1 IHC 22C3 pharm Dx. PD-L1 expression was determined by combined positive score (CPS), and the sample was considered positive if CPS was equal to or greater than 10 [15]. Patients who test PD-L1 positive are those whose

tumours have a combined positive score (CPS) of at least 10. A score ranging from 0 to 100 is obtained by dividing the total number of PD-L1-expressing tumour cells (TC), lymphocytes, and macrophages by the total number of alive TC. Study variables are; age, grades, types and stages of cancer and lymph node status. SPSS 22 was used for the statistical analysis. Frequencies and percentages were calculated for categorical data. Mean, median, and standard deviation were calculated for continuous data. Chi-square analysis was used to calculate the degree of correlation between two variables. A significant p-value is less than or equal to 0.05.

Results

The mean age of the patients was 47.7 years (47.7 ± 14). 54.5% of the patients were in the middle age group. 63.6% of the patients were in grade III, most (88.6%) had invasive ductal carcinoma, and 75% were negative for PD-L1. 63.6% of the patients had Ki-69 less than 20. 70.5% of the patients were in stage T2, and 45.5% had N1 lymph node status. **Table 1** shows the detailed data. There is no significant association between PD-L1 and age groups, grades, or types, as shown in **Table 2**. There is no significant association between PD-L1 status and stage. As shown in **Table 3**, there is also no significant association between PD-L1 status and lymph node status. As shown in **Table 4**, there is a significant association between PD-L1 status and the Ki-67 percentage score. 100% of patients with positive PD-L1 expression had Ki67 more than 20, while only 15.2% of patients with negative PD-L1 had Ki67 more than 20.

Discussion

Most triple-negative breast cancers are highly malignant tumours that affect young women. It accounts for 10%–20% of all breast cancers [16, 17]. Because they proliferate quickly, they are usually found at a late stage when they are diagnosed [3]. Chemotherapy drugs such as anthracyclines, taxanes, ixabepilone, and platinum-based drugs are currently used to treat these tumours, but no single drug works well in all tumours [18]. There is

Table 1. Distribution of patients by age groups, grades, types and PD-L1 status.

| | Variables | Frequency | Percentage |
|-------------------|-------------------------------|-----------|------------|
| Age (years) | Young adult (less than 30) | 12 | 27.3 |
| | Middle age (30-59) | 24 | 54.5 |
| | Old (60 and more) | 8 | 18.2 |
| Grade | I | 2 | 4.5 |
| | II | 14 | 31.8 |
| | III | 28 | 63.6 |
| Types | Adenoid | 1 | 2.3 |
| | Inflammatory breast carcinoma | 4 | 9.1 |
| | Invasive ductal carcinoma | 39 | 88.6 |
| PD-L1 | Negative | 33 | 75.0 |
| | Positive | 11 | 25.0 |
| Ki-67 | <20 | 28 | 63.6 |
| | >20 | 16 | 36.4 |
| Stages | T1 | 5 | 11.4 |
| | T2 | 31 | 70.5 |
| | T3 | 8 | 18.2 |
| Lymph node status | N0 | 13 | 29.5 |
| | N1 | 20 | 45.5 |
| | N2 | 9 | 20.5 |
| | N3 | 2 | 4.5 |

Table 2. Association between PD-L1 and (age groups, grades, types).

| Variables | PD-L1 | | P-value | |
|------------|-------------|------------|------------|-------|
| | Negative | Positive | | |
| Age groups | Young adult | 8; 24.3% | 4; 36.4% | 0.6 |
| | Middle age | 18; 54.5% | 6; 54.5% | |
| | Old | 7; 21.2% | 1; 9.1% | |
| | Total | 33; 100.0% | 11; 100.0% | |
| Grades | I | 2; 6.0% | 0; 0.0% | 0.31 |
| | II | 12; 36.4% | 2; 18.2% | |
| | III | 19; 57.6% | 9; 81.8% | |
| | Total | 33; 100.0% | 11; 100.0% | |
| Types | adenoid | 1; 3.1% | 0; 0.0% | 1.000 |
| | IDC | 32; 96.9% | 11; 100 % | |
| | Total | 33; 100% | 11; 100% | |

P-value \leq 0.05 (significant).

Table 3. Association between PD-L1 and (stages, lymph node status).

| | | PD-L1 | |
|-------------------|----|------------|------------|
| | | Negative | Positive |
| Stage | T1 | 3; 9.1% | 2; 18.2% |
| | T2 | 23; 69.7% | 8; 72.7% |
| | T3 | 7; 21.2% | 1; 9.1% |
| Total | | 33; 100.0% | 11; 100.0% |
| Lymph node status | N0 | 10; 30.3% | 3; 27.3% |
| | N1 | 12; 36.4% | 8; 72.7% |
| | N2 | 9; 27.3% | 0; 0.0% |
| | N3 | 2; 6.0% | 0; 0.0% |
| Total | | 33; 100.0% | 11; 100.0% |

P-value = 0.5 (not significant).

Table 4. Association between PD-L1 and Ki67.

| Variables | PD-L1 | | P-value |
|-----------|------------|------------|------------|
| | Negative | Positive | |
| Ki67 | <20 | 28; 84.8% | 0; 0.0% |
| | >20 | 5; 15.2% | 11; 100.0% |
| Total | 33; 100.0% | 11; 100.0% | 0.0001 |

P-value ≤ 0.05 (significant).

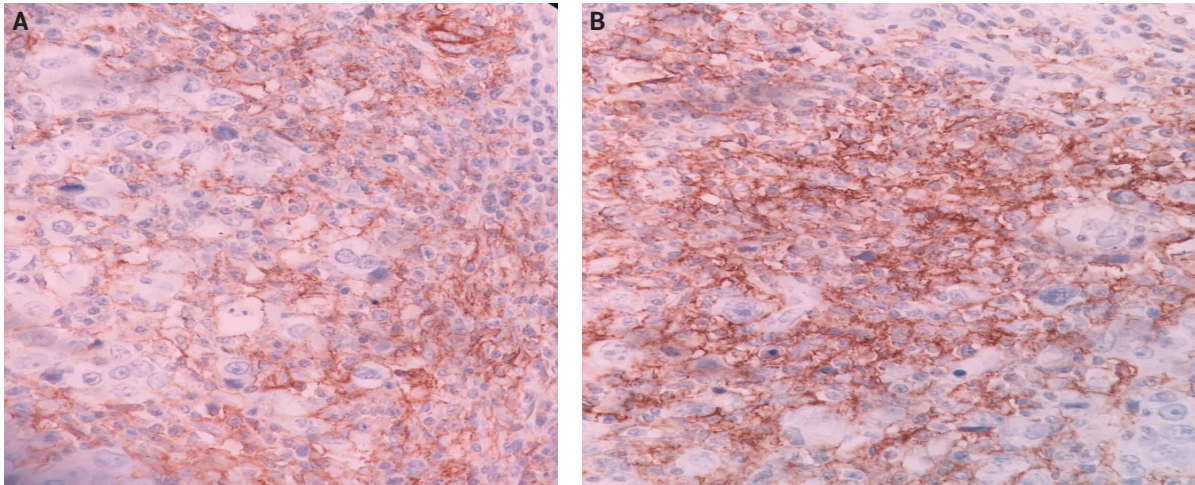


Figure 1. A) PD-L1 expression by tumour cells and associated inflammatory cells. B) PD-L1 expression by tumour cells.

much variation in how PD-L1 immunohistochemistry assays are performed and interpreted in the literature. H scores, 1% cut-offs, and graded scoring systems (0–3) are commonly used to measure PD-L1 expression in tumours [5, 11, 18, 19]. People have used 5% as a cut-off to see if PD-L1 is present in the tumour microenvironment [11, 19]. More extensive studies are needed to identify the optimal cut-off value and the antibody to use as a gold standard [20]. The presence of PD-L1 in tumours was observed to correlate with a higher Ki-67 proliferation index [$p = 0.017$]. Further life expectancy studies should confirm this finding [5, 7]. No correlation was observed between PD-L1 expression in the tumour or tumour microenvironment and age, tumour size, tumour grade, lymph node metastasis, the presence of Lymphovascular invasion (LVI) or Ductal Carcinoma In-situ (DCIS), recurrence, or metastatic status. However, PD-L1 expression in tumours has not been associated with these factors (age, tumour size, tumour grade, lymph node metastasis, the presence of Lymphovascular invasion (LVI) or Ductal Carcinoma In-situ (DCIS), recurrence, or metastatic status) in several studies [5, 7, 11, 19, 21]. Triple-negative breast

cancer is a tumour type with no targeted treatment; new treatment options are needed. PD-L1 in and around these aggressive tumours may be a reason to treat them with anti-PD-L1 therapies (PD-L1 monoclonal antibodies) [20].

Conclusion

Most TNBC patients are in the middle age group and have grade III. Therefore, this study's low prevalence of PD-L1 positivity may be related to the high CPS cut-off.

Acknowledgements

Conflict of interest statement

The authors declare no conflict of interest.

Funding sources

There are no sources of funding to declare.

References

1. Siegel RL, Miller KD, Jemal A. Cancer statistics, 2016. *CA Cancer J Clin.* 2016;66:7–30. doi: 10.3322/caac.21332.

2. Zhao Y, Wang R, Shi F, Wu J, Jiang F, Song Q. Diagnostic Efficacy of CT Examination on Early Detection of Lung Cancer during Pandemic of COVID-19. *Diagnostics (Basel)*. 2022 Sep 26;12(10):2317.
3. Ge J, Zuo W, Chen Y, Shao Z, Yu K. The advance of adjuvant treatment for triple-negative breast cancer. *Cancer Biol Med*. 2021 Aug 27;19(2):187–201.
4. https://www.agilent.com/cs/library/usermanuals/public/29389_22c3_pharmdx_tnbc_interpretation_manual_kn355.pdf.
5. Guan J, Lim KS, Mekhail T, Chang CC. Programmed Death Ligand-1 (PD-L1) expression in the Programmed Death Receptor-1 (PD-1)/PD-L1 blockade. *Arch Pathol Lab Med*. 2017;141:851–861.
6. Sabatier R, Finetti P, Mamessier E, Adelaide J, Chafanet M, Ali HR, Viens P, Caldas C, Birnbaum D, Bertucci F. Prognostic and predictive value of PD-L1 expression in breast cancer. *Oncotarget*. 2015;6:5449–5464.
7. Schalper KA, Velcheti V, Carvajal D, Wimberly H, Brown J, Puzstai L, Rimm DL. In situ tumor PD-L1 mRNA expression is associated with increased TILs and better outcome in breast carcinomas. *Clin Cancer Res*. 2014;20:2773–2782.
8. Baptista M, Sarian L, Derchain S, Pinto G, Vassallo J. Prognostic significance of PD-L1 and PD-L2 in breast cancer. *Hum Pathol*. 2016;47:78–84.
9. Qin T, Zeng YD, Qin G, Xu F, Lu JB, Fang WF, Xue C, Zhan JH, Zhang XK, Zheng QF, Peng RJ, Yuan ZY, Zhang L, Wang SS. High PD-L1 expression was associated with poor prognosis in 870 Chinese patients with breast cancer. *Oncotarget*. 2015;6:33972–33981.
10. Ali HR, Glont SE, Blows FM, Provenzano E, Dawson SJ, Liu B, Hiller L, Dunn J, Poole CJ, Bowden S, Earl HM, Pharoah PD, Caldas C. PD-L1 protein expression in breast cancer is rare, enriched in basal-like tumours and associated with infiltrating lymphocytes. *Ann Oncol*. 2015;26:1488–1493.
11. Chierico L, Rizzello L, Guan L, Joseph AS, Lewis A, Battaglia G. The role of the two splice variants and extranuclear pathway on Ki-67 regulation in non-cancer and cancer cells. *PLoS One*. 2017 Feb 10;12(2):e0171815.
12. Remnant L, Kochanova NY, Reid C, Cisneros-Soberanis F, Earnshaw WC. The intrinsically disorderly story of Ki-67. *Open Biol*. 2021 Aug;11(8):210120.
13. Hořejší B, Vinopal S, Sládková V, Dráberová E, Sulimenko V, Sulimenko T, Vosecká V, Philimonenko A, Hozák P, Katsetos CD, Dráber P. Nuclear γ -tubulin associates with nucleoli and interacts with tumor suppressor protein C53. *J Cell Physiol*. 2012 Jan;227(1):367–82.
14. Sales Gil R, Vagnarelli P. Ki-67: More Hidden behind a 'Classic Proliferation Marker'. *Trends Biochem Sci*. 2018 Oct;43(10):747–748.
15. https://www.agilent.com/cs/library/usermanuals/public/29389_22c3_pharmdx_tnbc_interpretation_manual_kn355.pdf.
16. Oakman C, Moretti E, Pacini G, Santarpia L, Di Leo A. Triple negative breast cancer: a heterogeneous subgroup defined by what it is not. *European J Cancer*. 2011;47:S370–S372.
17. McCart Reed AE, Kutasovic JR, Vargas AC, Jayanthan J, Al-Murrani A, Reid LE, Chambers R, Da Silva L, Melville L, Evans E, Porter A, Papadimos D, Thompson EW, Lakhani SR, Simpson PT. An epithelial to mesenchymal transition programme does not usually drive the phenotype of invasive lobular carcinomas. *J Pathol*. 2016 Mar;238(4):489–94.
18. Moy B, Rumble RB, Come SE, Davidson NE, Di Leo A, Gralow JR, Hortobagyi GN, Yee D, Smith IE, Chavez-MacGregor M, Nanda R, McArthur HL, Spring L, Reeder-Hayes KE, Ruddy KJ, Unger PS, Vinayak S, Irvin WJ Jr, Armaghani A, Danso MA, Dickson N, Turner SS, Perkins CL, Carey LA. Chemotherapy and Targeted Therapy for Patients With Human Epidermal Growth Factor Receptor 2-Negative Metastatic Breast Cancer That is Either Endocrine-Pretreated or Hormone Receptor-Negative: ASCO Guideline Update. *J Clin Oncol*. 2021 Dec 10;39(35):3938–3958.
19. Dill EA, Gru AA, Atkins KA, Friedman LA, Moore ME, Bullock TN, Cross JV, Dillon PM, Mills AM. PD-L1 expression and intratumoral heterogeneity across breast cancer subtypes and stages: an assessment of 245 primary and 40 metastatic tumors. *Am J Surg Pathol*. 2017;41:334–342.
20. Bae SB, Cho HD, Oh MH, Lee JH, Jang SH, Hong SA, Cho J, Kim SY, Han SW, Lee JE, Kim HJ, Lee HJ. Expression of Programmed Death Receptor Ligand 1 with high tumor-infiltrating lymphocytes is associated with better prognosis in breast cancer. *J Breast Cancer*. 2016;19:242–251.
21. Sun WY, Lee YK, Koo JS. Expression of PD-L1 in triple-negative breast cancer based on different immunohistochemical antibodies. *J Transl Med*. 2016;14:173.

Keep an eye on the crime – a new look at the forensic use of post-mortem eye examination to estimate time of death

Jacob van der Veer

Department of Forensic Medicine, Poznan
University of Medical Sciences, Poland



Szymon Rzepczyk

Department of Forensic Medicine, Poznan
University of Medical Sciences, Poland

<https://orcid.org/0000-0001-6330-1511>

Corresponding author: szymon.rzepczyk@interia.eu

Czesław Żaba

Department of Forensic Medicine, Poznan
University of Medical Sciences, Poland

<https://orcid.org/0000-0001-7522-4568>

Keywords: time of death, eye examination, post-mortem interval, forensic medicine, post-mortem examination

Received: 2022-10-11

Accepted: 2023-01-09

Published: 2023-02-16

How to Cite: van der Veer J, Rzepczyk S, Żaba C. Keep an eye on the crime – a new look at the forensic use of post-mortem eye examination to estimate time of death. *Journal of Medical Science*. 2023;92(1);e753. doi:10.20883/medical.e753



© 2023 by the author(s). This is an open access article distributed under the terms and conditions of the Creative Commons Attribution (CC BY-NC) licence. Published by Poznan University of Medical Sciences

DOI: <https://doi.org/10.20883/medical.e753>

ABSTRACT

Determining the time of death plays a crucial role in a forensic post-mortem examination. Many methods for the time of death (TOD) determination have been developed. However, most are not applicable during the first hours after death and produce large post-mortem interval (PMI) ranges. Eye examination makes it possible to precisely determine the time of death during the initial period after death with half-hour accuracy. In recent years methods for estimating the time of death by measuring the changes in the eye have made great strides. Those methods use the changes in the reaction to drugs and macroscopically visible morphological changes. Experimental studies also produced equations that can estimate the post-mortem interval using biochemical, electrochemical and thermal changes within the eye.

Introduction

Forensic eye examination has long played a key role in post-mortem diagnostics [1]. Its location makes it easy to collect samples which are used for, among other things, toxicological analysis [2]. Studies have shown that some xenobiotics (e.g. alcohol) penetrate the blood-retinal barrier allowing their detection when a blood sample is impossible to obtain [3]. In recent years methods for determining the time of death (TOD) using eye

examination have been developed. Accurately estimated TOD is crucial in forensic medicine, both to criminal (finding suspects, verifying alibi) and civil law (timelines for multiple deaths and inheritance) [4–6]. Known methods for determining TOD using post-mortem changes in remains (algor mortis, rigour mortis, and livor mortis) are imprecise and are uncertain during the first 4–6 h after death due to effect of environmental factors (e.g. temperature and humidity) [6, 7]. An in-depth

eye examination allows for determining TOD accurately with even half-hour accuracy [4].

Pharmacological methods

The oldest and least precise methods rely on measuring the change in pupil diameter before and 10 minutes after applying 2% pilocarpine or 1% atropine drops to the eye [8, 9]. Depending on source, the reaction can be observed up to 15 h [9] or even 21 h [8] post-mortem. The determination may either observe if the reaction has occurred or measure the change and apply it to an experimentally obtained linear regression equation that estimates post-mortem interval (PMI) [8, 9]. Changes are expressed in millimetres and estimated PMI in hours. Equations have limited applicability as they can only be used up to 8 h after death (see **Table 1**) [9]. Some studies challenge the efficacy of using atropine, pilocarpine or combined atropine and pilocarpine drops in TOD determination [10].

Morphological changes

Due to post-mortem degeneration of the endothelial barrier and changes in cornea hydration, it becomes opaque [11]. Weather conditions influence when full opacity is reached: high humidity and temperature accelerate process [12]. Due to this effect, full opacity is reached from 24 h (high temperature and humidity) to over 36 h (low temperature) [12]. Historically this method was subjective and required visual cornea assessment, but in recent years AI algorithms to estimate PMI based on pictures have been developed [13, 14]. Algorithms automatically identify corneal and non-corneal areas of interest in a picture and calculate values of colour and texture required

to produce a prediction [13, 14]. For example, a computer program that classified subjects into six-hour time intervals from 0 to 72 h had an accuracy of <3 h when used <36 h post-mortem and 6-8 h when used >36 h post-mortem (see **Table 1**) [14]. In addition, there have been attempts to use measurements of corneal thickness or opacity of the non-corneal areas of the eye to predict PMI [11, 15]. Also, changes occurring in the lens after death can be used to predict PMI in the range of 24-96 h [16]. For this purpose, the assessment of opacity and sphericity changes and histological examination of the prepared lens are used [16].

The use of optical coherence tomography (OCT) in the post-mortem examination of the eye creates new possibilities for determining PMI by the possibility of assessing almost all anatomical structures of the eye [15]. The analysis of changes co-occurring in most of the anatomical structures of the eye (sclera, cornea, anterior chamber, retina) in the first 72 hours after death and looking for typical signs (Nioi-Napoli sign – waves on the posterior part of the cornea) could allow providing the approximate PMI in a non-invasive way in future [15]. The corneal OCT examination provides the most information on the time of death, but it is affected by the position of the eyelids post mortem and environmental factors [17].

Biochemical changes

Potassium concentration in the vitreous humour (VH) is a biochemical marker with the strongest correlation with PMI [18]. After death transport of potassium stops, and ion leaks out from inside cells into VH in a linear manner up to 100 h post-mortem [18]. The usefulness of this biomarker is limited to 120 h. Many factors limit efficacy by influencing potassium concentration: age, method and manner of death, ambient tem-

Table 1 Comparison of methods of assessing the time of death(TOD) with the use of eye examination.

| | Pilocarpine 1% / Atropine 2% | Corneal opacity algorithms | VH Potassium concentration | Eye temperature |
|-----------------------------|--------------------------------------|---------------------------------|----------------------------|-----------------|
| Application (h post-mortem) | 15-21 ^a 8 ^b | 72 | 120 | 10 |
| Accuracy (h) | 2.5 ^b | <3 (PMI < 36) 6-8 (PMI > 36) | 1-10 ^c | 0.5 |

a – For nominal results; b – For equation (pilocarpine 2%); c – Dependent on the PMI.

perature, renal insufficiency, carbon monoxide or methanol poisoning [18, 19]. This method has been investigated extensively. Therefore, there are many equations available to calculate PMI [19, 20]. Scientific literature provides multiple linear and nonlinear equations that also include coefficients for ambient temperature [20]. Accuracy can be one h for short PMI and up to 10 h with PMI 110 h [21]. It is also postulated to use the PMI determination method to assess changes in potassium concentration in the VH of the eye over a more extended period using a nonlinear model adjusted to ambient temperature and age [19]. Attempts to use other ions to estimate PMI during the first hours after death have not produced conclusive results yet and require further investigations [20, 22]. The changes in sodium and chlorine ion levels can barely be used for PMI estimation in the initial time after death. However, there are noticeable decreases days after death [23]. The concentrations of sodium and chloride ions in the VH are closely related to the electrolyte balance before death and influenced by the environment (especially in bodies immersed in water) [23]. The electrolyte balance and environmental factors should be accounted for when assessing changes in their concentration after death as they may be used to predict the cause of death (e.g. differentiation between freshwater and saltwater drowning, electrolyte derangements before death) [23]. Changes in the concentrations of magnesium, calcium and phosphorus ions in the vitreous body after death were also noted, but their use in PMI assessment requires further research [20, 24]. The studies showed no differences between the concentrations of ions between the eyeballs of the corpse and an imperceptible effect of the technique of collecting the VH sample on the results of the examination, which makes the collection of a small amount of VH from one eye sufficient material for analysis [25].

Lactate and hypoxanthine have been identified as potential biomarkers for estimating TOD. However, limited attempts are yet to produce some definite results. Post-mortem lactate diffuses through the retina, gradually increasing its VH concentration [26]. Based on experimental research, a linear regression equation was created that correlated lactate to time post-mortem, which suggests a reverse equation is also possible [26]. Depending on the source, hypoxan-

thine increases in VH linearly up to 120 h [18] or nonlinearly [27]. A double source of hypoxanthine may trigger the above: degradation of AMP and diffusion [18]. Perimortem ambient temperature affects changes in lactate and hypoxanthine. High temperature accelerates increase, while low slows it down [28]. Currently, research studies are also conducted using the identification of peptides and changes in their concentrations using mass spectrometry to determine the PMI [29].

Eye temperature measurements

Determining TOD based on the core temperature measured, e.g. in the anus, is well known and has been used in forensic medicine for years [8, 30]. However, numerous limitations influence the method's accuracy [6]. Among them are the influence of body weight, clothes worn, and body position [7]. Moreover, core temperature measurement in the anus is contraindicated in exceptional cases, e.g. in the event of sexual assault [5]. Additionally, accuracy is limited during the first 4-6 hours post-mortem [5, 6, 31] and results from the temperature plateau effect (TPE) that appears right after death [31]. TPE is the body maintaining a constant core temperature or its slight decrease within error margins [7]. It is caused by tissue residual anaerobic metabolism and the ability to store heat [6, 31]. Moreover, core post-mortem temperature may also be influenced by pre-mortem conditions, e.g. hypothermia or some drugs [31]. A novel method to address TPE is measuring temperature within the eyeball. It is possible due to the homogeneous structure of the eye filled with VH, of which temperature corresponds to the temperature within the skull [7]. Corneal temperature is highly dependent on ambient temperature. Therefore it is not considered in TOD determination [5]. Studies have shown no temperature plateau in VH in the first hours after death. On the contrary, the temperature drops within minutes after death [7], thus allowing a supplement method of core temperature measurement when its usage is limited, i.e. during the first hours after death [6]. Studies on animal (canine, swine) and human models show this method to have 30 min accuracy (see **Table 1**) [4, 5, 7, 32]. Furthermore, measurement is minimally invasive and does not leave noticeable marks on the body, requiring

a thin probe to be inserted approximately 20 mm into the eyeball [5, 6]. Another advantage of this approach is the complete lack of interference from deceased bodyweight and clothes, although the possible effect of haircoat requires additional investigation [4, 5]. New models and calculators that allow for fast and precise determination of TOD with the accuracy of minutes have been developed recently [33, 34].

Conclusions

Accurate TOD determination plays a key role during investigations and court proceedings; for example, assessing the reliability of testimonies, confirming or disproving alibis and ascertaining timelines of deaths. Unfortunately, classical methods for TOD determination had limited applicability during the first few hours after death and limited accuracy. Developing novel methods based on eye examination could help solve those problems. Additional studies on larger data sets are necessary to fine-tune equations and computational models. The efficacy of using multiple methods to produce even more accurate predictions should also be assessed.

Acknowledgements

Conflict of interest statement

The authors declare no conflict of interest.

Funding sources

There are no sources of funding to declare.

References

1. Ang JL, Collis S, Dhillon B, Cackett P. The Eye in Forensic Medicine: A Narrative Review. *Asia Pac J Ophthalmol (Phila)*. 2021 Sep 14;10(5):486-494. doi: 10.1097/APO.0000000000000426. PMID: 34524140.
2. Szeremeta M, Mironiuk E, Janica M, Drobuliakova P, Lomperta K, Szczepk M, Niemcunowicz-Janica A. Vitreous humour as an alternative material for the determination of alcohol concentration in human corpses. *Arch Med Sadowej Kryminol*. 2018;68(2):108-118. English. doi: 10.5114/amsik.2018.77923. PMID: 30509023.
3. Bévalot F, Cartiser N, Bottinelli C, Fanton L, Guitton J. Vitreous humor analysis for the detection of xenobiotics in forensic toxicology: a review. *Forensic Toxicol*. 2016;34:12-40. doi: 10.1007/s11419-015-0294-5. Epub. 2015 Oct 28. PMID: 26793276; PMCID: PMC4705140.
4. Kaliszan M. First practical applications of eye temperature measurements for estimation of the time of death in casework. Report of three cases. *Forensic Sci Int*. 2012 Jun 10;219(1-3):e13-5. doi: 10.1016/j.forsciint.2011.11.027. Epub. 2011 Dec 23. PMID: 22196913.
5. Kaliszan M. Studies on time of death estimation in the early post mortem period -- application of a method based on eyeball temperature measurement to human bodies. *Leg Med (Tokyo)*. 2013 Sep;15(5):278-82. doi: 10.1016/j.legalmed.2013.06.003. Epub. 2013 Jul 20. PMID: 23879937.
6. Kaliszan M, Wujtewicz M. Eye temperature measured after death in human bodies as an alternative method of time of death estimation in the early post mortem period. A successive study on new series of cases with exactly known time of death. *Leg Med (Tokyo)*. 2019 May;38:10-13. doi: 10.1016/j.legalmed.2019.03.004. Epub. 2019 Mar 18. PMID: 30901685.
7. Kaliszan M, Hauser R, Buczyński J, Jankowski Z, Raczynska K, Kernbach-Wighton G. The potential use of the eye temperature decrease in determining the time of death in the early postmortem period: studies in pigs. *Am J Forensic Med Pathol*. 2010 Jun;31(2):162-4. doi: 10.1097/PAF.0b013e3181d8e2e7. PMID: 20308872.
8. Raszeja S, Nasiłowski W, Markiewicz J. *Medycyna sądowa: podręcznik dla studentów*. Warszawa: Państw. Zakład Wydawnictw Lekarskich; 1993.
9. Larpkrajang S, Worasuwannarak W, Peonim V, Udnoon J, Srisont S. The use of pilocarpine eye drops for estimating the time since death. *J Forensic Leg Med*. 2016 Apr;39:100-3. doi: 10.1016/j.jflm.2016.01.008. Epub. 2016 Jan 21. PMID: 26874433.
10. Orrico M, Melotti R, Mantovani A, Avesani B, De Marco R, De Leo D. Criminal investigations: pupil pharmacological reactivity as method for assessing time since death is fallacious. *Am J Forensic Med Pathol*. 2008 Dec;29(4):304-8. doi: 10.1097/PAF.0b013e3181847e10. PMID: 19259014.
11. Cantürk İ., Çelik S., Şahin M.F., Yağmur F., Kara S., Karabiber F. Investigation of opacity development in the human eye for estimation of the postmortem interval. *Biocybern. Biomed. Eng*. 2017;37:559-565. doi: 10.1016/j.bbe.2017.02.001.
12. De-Giorgio F, Grassi S, d'Aloja E, Pascali VL. Post-mortem ocular changes and time since death: Scoping review and future perspective. *Leg Med (Tokyo)*. 2021 May;50:101862. doi: 10.1016/j.legalmed.2021.101862. Epub. 2021 Feb 12. PMID: 33610931.
13. Cantürk İ, Özyılmaz L. A computational approach to estimate postmortem interval using opacity development of eye for human subjects. *Comput Biol Med*. 2018 Jul 1;98:93-99. doi: 10.1016/j.combiomed.2018.04.023. Epub. 2018 May 17. PMID: 29778926.
14. Zheng J, Huo D, Wen H, Shang Q, Sun W, Xu Z. Corneal-Smart Phone: A novel method to intelligently estimate postmortem interval. *J Forensic Sci*. 2021 Jan;66(1):356-364. doi: 10.1111/1556-4029.14611. Epub. 2020 Oct 28. PMID: 33112427.

15. Nioi M, Napoli PE, Demontis R, Locci E, Fossarello M, d'Aloja E. Postmortem Ocular Findings in the Optical Coherence Tomography Era: A Proof of Concept Study Based on Six Forensic Cases. *Diagnostics (Basel)*. 2021 Feb 28;11(3):413. doi: 10.3390/diagnostics11030413. PMID: 33670928; PMCID: PMC7997319.
16. Prieto-Bonete G, Perez-Carceles MD, Luna A. Morphological and histological changes in eye lens: Possible application for estimating postmortem interval. *Leg Med (Tokyo)*. 2015 Nov;17(6):437-42. doi: 10.1016/j.legalmed.2015.09.002. Epub. 2015 Sep 14. PMID: 26593986.
17. Nioi M, Napoli PE, Demontis R, Chighine A, De-Giorgio F, Grassi S, Scordia V, Fossarello M, d'Aloja E. The Influence of Eyelid Position and Environmental Conditions on the Corneal Changes in Early Postmortem Interval: A Prospective, Multicentric OCT Study. *Diagnostics*. 2022;12(9):2169. <https://doi.org/10.3390/diagnostics12092169>.
18. Madea B. Methods for determining time of death. *Forensic Sci Med Pathol*. 2016 Dec;12(4):451-485. doi: 10.1007/s12024-016-9776-y. Epub. 2016 Jun 4. PMID: 27259559.
19. Zilg B, Bernard S, Alkass K, Berg S, Druid H. A new model for the estimation of time of death from vitreous potassium levels corrected for age and temperature. *Forensic Sci Int*. 2015 Sep;254:158-66. doi: 10.1016/j.forsciint.2015.07.020. Epub. 2015 Jul 17. PMID: 26232848.
20. Pigaiani N, Bertaso A, De Palo EF, Bortolotti F, Tagliaro F. Vitreous humor endogenous compounds analysis for post-mortem forensic investigation. *Forensic Sci Int*. 2020 May;310:110235. doi: 10.1016/j.forsciint.2020.110235. Epub. 2020 Mar 4. PMID: 32169668.
21. Madea B, Rödiger A. Time of death dependent criteria in vitreous humor: accuracy of estimating the time since death. *Forensic Sci Int*. 2006 Dec 20;164(2-3):87-92. doi: 10.1016/j.forsciint.2005.12.002. Epub. 2006 Jan 24. PMID: 16439082.
22. Siddamsetty AK, Verma SK, Kohli A, Puri D, Singh A. Estimation of time since death from electrolyte, glucose and calcium analysis of postmortem vitreous humour in semi-arid climate. *Med Sci Law*. 2014 Jul;54(3):158-66. doi: 10.1177/0025802413506424. PMID: 24166687.
23. Zilg B, Alkass K, Berg S, Druid H. Interpretation of postmortem vitreous concentrations of sodium and chloride. *Forensic Sci Int*. 2016 Jun;263:107-113. doi: 10.1016/j.forsciint.2016.04.006. Epub. 2016 Apr 11. PMID: 27105154.
24. Yang M, Li H, Yang T, Ding Z, Wu S, Qiu X, Liu Q. A Study on the Estimation of Postmortem Interval Based on Environmental Temperature and Concentrations of Substance in Vitreous Humor. *J Forensic Sci*. 2018 May;63(3):745-751. doi: 10.1111/1556-4029.13615. Epub. 2017 Aug 17. PMID: 28833136.
25. Zilg B, Alkass K, Kronstrand R, Berg S, Druid H. A Rapid Method for Postmortem Vitreous Chemistry-Deadside Analysis. *Biomolecules*. 2021 Dec 27;12(1):32. doi: 10.3390/biom12010032. PMID: 35053180; PMCID: PMC8773483.
26. Bertaso A, De Palo EF, Cirielli V, Tagliaro F. Lactate determination in human vitreous humour by capillary electrophoresis and time of death investigation. *Electrophoresis*. 2020 Jun;41(12):1039-1044. doi: 10.1002/elps.201900462. Epub. 2020 May 12. PMID: 32180233.
27. Cordeiro C, Ordóñez-Mayán L, Lendoiro E, Febrero-Bande M, Vieira DN, Muñoz-Barús JI. A reliable method for estimating the postmortem interval from the biochemistry of the vitreous humor, temperature and body weight. *Forensic Sci Int*. 2019 Feb;295:157-168. doi: 10.1016/j.forsciint.2018.12.007. Epub. 2018 Dec 17. Erratum in: *Forensic Sci Int*. 2019 Aug;301:446. PMID: 30611119.
28. Go A, Shim G, Park J, Hwang J, Nam M, Jeong H, Chung H. Analysis of hypoxanthine and lactic acid levels in vitreous humor for the estimation of post-mortem interval (PMI) using LC-MS/MS. *Forensic Sci Int*. 2019 Jun;299:135-141. doi: 10.1016/j.forsciint.2019.03.024. Epub. 2019 Apr 1. PMID: 31003185.
29. Boroumand M, Grassi VM, Castagnola F, De-Giorgio F, d'Aloja E, Vetrugno G, et al. Estimation of post-mortem interval using top-down HPLC-MS analysis of peptide fragments in vitreous humour: A pilot study. *Int J Mass Spectrom*. 2023 Jan;483:116952. doi: 10.1016/j.ijms.2022.116952.
30. Di Maio VJM, Di Maio DJ, Świątek B, Przybylski Z, Jurek T, Maksymowicz K, et al. *Medycyna sądowa*. Wrocław: Edra Urban & Partner; 2018.
31. Smart JL, Kaliszan M. The post mortem temperature plateau and its role in the estimation of time of death. A review. *Leg Med (Tokyo)*. 2012 Mar;14(2):55-62. doi: 10.1016/j.legalmed.2011.11.002. Epub. 2012 Jan 28. PMID: 22285645.
32. Listos P, Gryzinska M, Batkowska J. Post-mortem decrease in temperature in the orbit of dogs for use in determining time of death. *Slov Vet Res*. 2016;53(2):85-90.
33. Smart JL, Kaliszan M. Use of a finite element model of heat transport in the human eye to predict time of death. *J Forensic Sci*. 2013 Jan;58 Suppl 1:S69-77. doi: 10.1111/1556-4029.12022. Epub. 2012 Nov 26. PMID: 23181434.
34. Smart JL. Use of postmortem temperature decay response surface plots of heat transport in the human eye to predict time of death. *J Forensic Sci*. 2014 Mar;59(2):390-8. doi: 10.1111/1556-4029.12333. PMID: 24745075.

Journal of Medical Science (JMS) is a PEER-REVIEWED, OPEN ACCESS journal that publishes original research articles and reviews which cover all aspects of clinical and basic science research. The journal particularly encourages submissions on the latest achievements of world medicine and related disciplines. JMS is published quarterly by Poznan University of Medical Sciences.

ONLINE SUBMISSION:

Manuscripts should be submitted to the Editorial Office by an e-mail attachment: nowinylekarskie@ump.edu.pl. You do not need to mail any paper copies of your manuscript.

All submissions should be prepared with the following files:

- Cover Letter
- Manuscript
- Tables
- Figures
- Supplementary Online Material

COVER LETTER: *Manuscripts* must be accompanied by a *cover letter* from the author who will be responsible for correspondence regarding the manuscript as well as for communications among authors regarding revisions and approval of proofs. The cover letter should contain the following elements: (1) the full title of the manuscript, (2) the category of the manuscript being submitted (e.g. Original Article, Brief Report), (3) the statement that the manuscript has not been published and is not under consideration for publication in any other journal, (4) the statement that all authors approved the manuscript and its submission to the journal, and (5) a list of at least two referees.

MANUSCRIPT: Journal of Medical Science publishes Original Articles, Brief Reports, Review articles, Mini-Reviews, Images in Clinical Medicine and The Rationale and Design and Methods of New Studies. From 2014, only articles in English will be considered for publication. They should be organized as follows: Title page, Abstract, Introduction, Materials and Methods, Results, Discussion, Acknowledgments, Conflict of Interest, References and Figure Legends. All manuscripts should be typed in Arial or Times New Roman font and double spaced with a 2,5 cm (1 inch) margin on all sides. They should be saved in DOC, DOCX, ODT, RTF or TXT format. Pages should be numbered consecutively, beginning with the title page.

Ethical Guidelines

Authors should follow the principles outlined in the Declaration of Helsinki of the World Medical Association (www.wma.net). The manuscript should contain a statement that the work has been approved by the relevant institutional review boards or ethics committees and that all human participants gave informed consent to the work. This statement should appear in the Material and Methods section. Identifying information, including patients' names, initials, or hospital numbers, should not be published in written descriptions, illustrations, and pedigrees. Studies involving experiments with animals must be conducted with approval by the local animal care committee and state that their care was in accordance with institution and international guidelines.

Authorship:

According to the International Committee on Medical Journal Ethics (ICMJE), an author is defined as one who has made substantial contributions to the conception and development of a manuscript. Authorship should be based on all of the following: 1) substantial contributions to conception and design, data analysis and interpretation; 2) article drafting or critical advice for important intellectual content; and 3) final approval of the version to be published. All other contributors should be listed as acknowledgments. All submissions are expected to comply with the above definition.

Conflict of Interest

The manuscript should contain a conflict of interest statement from each author. Authors should disclose all financial and personal relationships that could influence their work or declare the absence of any conflict of interest. Author's conflict of interest should be included under Acknowledgements section.

Abbreviations

Abbreviations should be defined at first mention, by putting abbreviation between brackets after the full text. Ensure consistency of abbreviations throughout the article. Avoid using them in the title and abstract. Abbreviations may be used in tables and figures if they are defined in the table footnotes and figure legends.

Trade names

For products used in experiments or methods (particularly those referred to by a trade name), give the manufacturer's full name and location (in parentheses). When possible, use generic names of drugs.

Title page

The first page of the manuscript should contain the title of the article, authors' full names without degrees or titles, authors' institutional affiliations including city and country and a running title, not exceeding 40 letters and spaces. The first page should also include the full postal address, e-mail address, and telephone and fax numbers of the corresponding author.

Abstract

The abstract should not exceed 250 words and should be structured into separate sections: Background, Methods, Results and Conclusions. It should concisely state the significant findings without reference to the rest of the paper. The abstract should be followed by a list of 3 to 6 Key words. They should reflect the central topic of the article (avoid words already used in the title).

The following categories of articles can be proposed to the Journal of Medical Science:

ORIGINAL RESEARCH

Original articles: Manuscripts in this category describe the results of original research conducted in the broad area of life science and medicine. The manuscript should be presented in the format of Abstract (250-word limit), Keywords, Introduction, Material and Methods, Results, Discussion, Perspectives, Acknowledgments and References. In the Discussion section, statements regarding the importance and *novelty of the study* should be presented. In addition, the limitations of the study should be articulated. The abstract must be structured and include: Objectives, Material and Methods, Results and Conclusions. Manuscripts cannot exceed 3500 words in length (excluding title page, abstract and references) and contain no more than a combination of 8 tables and/or figures. The number of references should not exceed 45.

Brief Reports: Manuscripts in this category may present results of studies involving small sample sizes, introduce new methodologies, describe preliminary findings or replication studies. The manuscript must follow the same format requirements as full length manuscripts. Brief reports should be up to 2000 words (excluding title page, abstract and references) and can include up to 3 tables and/or figures. The number of references should not exceed 25.

REVIEW ARTICLES

Review articles: These articles should describe recent advances in areas within the Journal's scope. Review articles cannot exceed 5000 words length (excluding title page, abstract and references) and contain no more than a combination of 10 tables and/or figures. Authors are encouraged to restrict figures and tables to essential data that cannot be described in the text. The number of references should not exceed 80.

A THOUSAND WORDS ABOUT... is a form of Mini-Reviews. Manuscripts in this category should focus on *latest achievements of life science and medicine*. Manuscripts should be up to 1000 words in length (excluding title page, abstract and references) and contain up to 5 tables and/or figures and up to 25 most relevant references. The number of authors is limited to no more than 3.

OTHER SUBMISSIONS

Invited Editorials: Editorials are authoritative commentaries on topics of current interest or that relate to articles published in the same issue. Manuscripts should be up to 1500 words in length. The number of references should not exceed 10. The number of authors is limited to no more than 2.

Images in Clinical Medicine: Manuscripts in this category should contain one distinct image from life science or medicine. Only original and high-quality images are considered for publication. The description of the image (up to 250 words) should present relevant information like short description of the patient's history, clinical findings and course, imaging techniques or molecular biology techniques (e.g. blotting techniques or immunostaining). All labeled structures in the image should be described and explained in the legend. The number of references should not exceed 5. The number of authors is limited to no more than 5.

The Rationale, Design and Methods of New Studies: Manuscripts in this category should provide information regarding the grants awarded by different founding agencies, e.g. National Health Institute, European Union, National Science Center or National Center for Research and Development. The manuscript should be presented in the format of Research Project Objectives, Research Plan and Basic Concept, Research Methodology, Measurable Effects and Expected Results. The article should also contain general information about the grant: grant title, keywords (up to five), name of the principal investigator and co-investigators, founding source with the grant number, *Ethical Committee permission number*, code in clinical trials (if applicable). Only grant projects in the amount over 100,000 Euro can be presented. Manuscripts should be up to 2000 words in length (excluding references) and can include up to 5 tables and/ or figures. The abstract should not exceed 150 words. The number of authors is limited to the Principal Investigator and Co-investigators.

Acknowledgements

Under acknowledgements please specify contributors to the article other than the authors accredited. List here those individuals who provided help during the research (e.g., providing language help, writing assistance or proof reading the article, etc.). Also acknowledge all sources of support (grants from government agencies, private foundations, etc.). The names of funding organizations should be written in full.

References

All manuscripts should use the 'Vancouver' style for references. References should be numbered consecutively in the order in which they appear in the text **and listed at the end of the paper.** References cited only in Figures/Tables should be listed in the end. Reference citations in the text should be identified by Arabic numbers in square brackets. Some examples:

- This result was later contradicted by Smith and Murray [3].
- Smith [8] has argued that...
- Multiple clinical trials [4–6, 9] show...

Journal names should be abbreviated according to Index Medicus. If available always provide Digital Object Identifier (DOI) or PubMed Identifier (PMID) for every reference.

Some examples

Standard journal articles

1. Petrova NV, Kashirskaya NY, Vasilyeva TA, Kondratyeva EI, Marakhonov AV, Macek Jr M, Ginter EK, Kutsev SI, Zinchenko RA. Characteristics of the L138Ins (p.Leu138dup) mutation in Russian cystic fibrosis patients. *JMS* [Internet]. 2020 Mar 31;89(1):e383. doi: 10.20883/medical.383.

Books

Personal author(s)

1. Rang HP, Dale MM, Ritter JM, Moore PK. *Pharmacology*. 5th ed. Edinburgh: Churchill Livingstone; 2003.

Editor(s) or compiler(s) as authors

2. Beers MH, Porter RS, Jones TV, Kaplan JL, Berkwitz M (editors). *The Merck manual of diagnosis and therapy*. 18th ed. Whitehouse Station (NJ): Merck Research Laboratories; 2006.

Chapter in the book

1. Phillips SJ, Whisnant JP. Hypertension and stroke. In: Laragh JH, Brenner BM, editors. *Hypertension: pathophysiology, diagnosis, and management*. 2nd ed. New York: Raven Press; 1995. p. 465–478.

TABLES: Tables should be typed on sheets separate from the text (each table on a separate sheet). They should be numbered consecutively with Arabic numerals. Tables should always be cited in text (e.g. table 2) in consecutive numerical order. Each table should include a compulsory, concise explanatory title and an explanatory legend. Footnotes to tables should be typed below the table body and referred to by superscript lowercase letters. No vertical rules should be used. Tables should not duplicate results presented elsewhere in the manuscript (e.g. in figures).

FIGURES: All illustrations, graphs, drawings, or photographs are referred to as figures and must be uploaded as separate files when submitting a manuscript. Figures should be numbered in sequence with Arabic numerals. They should always be cited in text (e.g. figure 3) in consecutive numerical order. Figures for publication must only be submitted in high-resolution TIFF or EPS format (*minimum 300 dpi resolution*). Each figure should be self-explanatory without reference to the text and have a concise but descriptive legend. All symbols and abbreviations used in the figure must be defined, unless they are common abbreviations or have already been defined in the text. Figure Legends must be included after the reference section of the Main Text.

Color figures: Figures and photographs will be reproduced in full colour in the online edition of the journal. In the paper edition, all figures and photographs will be reproduced as black-and-white.

SUPPLEMENTARY ONLINE MATERIAL: Authors may submit supplementary material for their articles to be posted in the electronic version of the journal. To be accepted for posting, supplementary materials must be essential to the scientific integrity and excellence of the paper. The supplementary material is subject to the same editorial standards and peer-review procedures as the print publication.

Review Process

All manuscripts are reviewed by the Editor-in-Chief or one of the members of the Editorial Board, who may decide to reject the paper or send it for external peer review. Manuscripts accepted for peer review will be blind reviewed by at least two experts in the field. After peer review, the Editor-in-Chief will study the paper together with reviewer comments to make one of the following decisions: accept, accept pending minor revision, accept pending major revision, or reject. Authors will receive comments on the manuscript regardless of the decision. In the event that a manuscript is accepted pending revision, the author will be responsible for completing the revision within 60 days.

Copyright

The copyright to the submitted manuscript is held by the Author(s), who grants the Journal of Medical Science (JMS) a nonexclusive licence to use, reproduce, and distribute the work, including for commercial purposes.